


2000-01-01

## Electroanalysis Using Differential Pulse Methods and Stripping Techniques.

Enda Howard

*Technological University Dublin*

Follow this and additional works at: <https://arrow.tudublin.ie/scienmas>

 Part of the [Chemistry Commons](#), [Computer Sciences Commons](#), and the [Electro-Mechanical Systems Commons](#)

---

### Recommended Citation

Howard, E. (2000). *Electroanalysis using differential pulse methods and stripping techniques*. Masters dissertation. Technological University Dublin. doi:10.21427/D7CS42

This Theses, Masters is brought to you for free and open access by the Science at ARROW@TU Dublin. It has been accepted for inclusion in Masters by an authorized administrator of ARROW@TU Dublin. For more information, please contact [arrow.admin@tudublin.ie](mailto:arrow.admin@tudublin.ie), [aisling.coyne@tudublin.ie](mailto:aisling.coyne@tudublin.ie), [vera.kilshaw@tudublin.ie](mailto:vera.kilshaw@tudublin.ie).

# Electroanalysis using Differential Pulse Methods and Stripping Techniques

by

Enda Howard,

A thesis presented to the Dublin Institute of Technology for the award of MPhil, prepared under the supervision of Dr. John Cassidy, School of Chemistry, Faculty of Science.

January 2000

To my Parents

I certify that this thesis which I now submit for examination for award of MPhil is entirely my own work and has not been taken from the work of others save and to the extent that such work has been cited and acknowledged within the text of my work.

This thesis was prepared according to the regulations for postgraduate studies by research of the Dublin Institute of Technology and has not been submitted in whole or in part for an award in any other Institute or University.

The Institute has permission to keep, to lend or to copy this thesis in whole or in part, on condition that any such use of the material of the thesis be duly acknowledged.

Signature Enda Howard date 7/7/00  
Candidate

### *Acknowledgements*

This thesis details the research that I carried out between January 1998 and September 1999 at D.I.T. Kevin Street under the supervision of Dr. John Cassidy. I will always look back on this time with fond memories and I would like to take advantage of this opportunity to thank those who assisted me throughout this time and made the whole project an enjoyable experience. Firstly, I would like to acknowledge the contribution of Dr. Cassidy to this work and sincerely thank him for his dedication, patience, willingness to lighten the load whenever possible and for his friendly manner of supervision.

I am also grateful to the lecturing and technical staff of the Chemistry Department and my fellow postgraduate students for their assistance and friendship. Thank you for helping whenever possible and making me feel welcome from day one.

Finally, I would like to thank my parents for their support and encouragement, not only in my education but in every aspect of my life. Thank you for always being there.

# TABLE OF CONTENTS

<b>Abstract</b>	<b>4</b>
<b>1 INTRODUCTION</b>	<b>5</b>
1.1 <b>References</b>	<b>12</b>
<b>2 ELECTROANALYSIS USING DIFFERENTIAL PULSE METHODS AT MICROELECTRODES</b>	
2.1 <b>Introduction</b>	<b>13</b>
2.2 <b>Theory</b>	<b>16</b>
2.3 <b>Experimental</b>	<b>19</b>
2.3.1 Instrumentation, Cells, Electrodes and Chemicals	19
2.3.2 Fabrication of Microelectrodes	19
2.4 <b>Results and Discussion</b>	<b>23</b>
2.4.1 Determination of Microelectrode radius	23
2.4.2 Characterisation of the microelectrode response to a Differential Pulse Waveform	23
2.4.3 Comparison of experimental and theoretical results	25
2.4.4 Differential Pulse Voltammetry at low concentrations	28
2.4.5 Limitations of Model 2	31
2.4.6 Differential Pulse study at larger electrodes	31
2.4.7 Electroanalysis with Microelectrodes using Microsoft Excel Solver	41
2.5 <b>Conclusions</b>	<b>47</b>
2.6 <b>References</b>	<b>50</b>

<b>3</b>	<b>DIFFERENTIAL PULSE VOLTAMMETRY AT A ROTATING DISK ELECTRODE</b>	
<b>3.1</b>	<b>Introduction</b>	<b>51</b>
<b>3.2</b>	<b>Theory</b>	<b>53</b>
<b>3.3</b>	<b>Experimental Procedure</b>	<b>56</b>
<b>3.4</b>	<b>Results and Discussion</b>	<b>56</b>
3.4.1	Determination of the active electrochemical area of the electrode	56
3.4.2	Characterisation of RDE response to a differential pulse waveform	57
3.4.3	Generation of theoretical data sets	60
3.4.4	Evaluation of the correlation between experimental and theoretical data	65
3.4.5	Determination of the limits of detection and limits of quantitation	67
3.4.5	Detailed study of the background current	69
<b>3.5</b>	<b>Conclusion</b>	<b>82</b>
<b>3.6</b>	<b>References</b>	<b>84</b>
<b>4</b>	<b>COMPARISON AND CRITICAL EVALUATION OF THE RELATIVE SUITABILITY OF GFAAS AND ASV TECHNIQUES FOR THE DETERMINATION OF LEAD IN POTABLE WATER</b>	
<b>4.1</b>	<b>Introduction</b>	<b>86</b>
<b>4.2</b>	<b>Theory</b>	<b>89</b>
4.2.1	Anodic Stripping Voltammetry	89
4.2.2	Graphite Furnace Atomic Absorption Spectroscopy	91
<b>4.3</b>	<b>Experimental</b>	<b>94</b>
4.3.1	Instrumentation	94
4.3.2	Reagents	95
4.3.3	Labware Selection and Cleaning	95
4.3.4	Sample Preparation	96
4.3.5	Sample Collection	96

<b>4.4</b>	<b>Comparison of DPASV and GFAAS methods for the determination of lead in potable water</b>	<b>97</b>
4.4.1	Lead analysis in potable water by DPASV	113
4.4.2	Lead analysis in potable water by GFAAS	124
<b>4.5</b>	<b>Practical Considerations</b>	<b>134</b>
<b>4.6</b>	<b>Conclusions</b>	<b>134</b>
<b>4.7</b>	<b>References</b>	<b>136</b>
<b>5</b>	<b>DETERMINATION OF TRACE LEVELS OF LEAD AND CADMIUM IN SEAWATER BY DPASV AND GFAAS</b>	
<b>5.1</b>	<b>Introduction</b>	<b>137</b>
<b>5.2</b>	<b>Theory</b>	<b>138</b>
5.2.1	Matrix Modification	138
5.2.2	Background Correction	139
<b>5.3</b>	<b>Experimental</b>	<b>139</b>
<b>5.4</b>	<b>Comparison of Methods for the determination of lead and cadmium in seawater</b>	<b>142</b>
5.4.1	Optimisation of the analysis of lead and cadmium in seawater by DPASV	143
5.4.2	Evaluation of the performance of the DPASV method for the analysis of lead and cadmium in seawater by DPASV	149
5.4.3	Optimisation of the analysis of lead and cadmium in seawater by GFAAS	156
<b>5.5</b>	<b>Conclusions</b>	<b>162</b>
<b>5.7</b>	<b>References</b>	<b>163</b>
	<b>Appendix A</b>	<b>164</b>



## Electroanalysis using Differential Pulse Methods and Stripping Techniques

Application of a differential pulse waveform to a microelectrode or a rotating disk electrode results in a peaked response for amperometric redox reactions. Based on these observations models were proposed and tested for these methods. Simulations of the models were carried out by inputting the relevant equations into Microsoft Excel. The microelectrode study revealed a good correlation between one model and the numerical derivative of the current following a linear sweep potential waveform. Experimentally the derivative can be obtained numerically following a linear sweep. The alternative differential pulse waveform requires more sophisticated equipment and the response can be affected by slow kinetics. The limit of detection for the rotating disk electrode system was  $2.3 \times 10^{-5} \text{M}$  with a limit of quantitation of  $7.68 \times 10^{-5} \text{M}$  for the  $[\text{Fe}(\text{CN})_6]^{+}$  system.

The use of curve fitting for the analysis and interpretation of voltammetric data obtained while working with microelectrodes was investigated. Microsoft Excel Solver was the curve fitting package used for this study. This technique was applied to the determination of unknown concentrations of ferrocyanide and the most satisfactory recovery of concentrations was found when both the values of the formal potential ( $E^0$ ) and concentration ( $C$ ) were varied to match the experimental results with an equation characterising the current potential curve for a reversible couple. In this case recoveries of  $100\% \pm 5\%$  were obtained for the concentration range  $5 \times 10^{-4} \text{M}$  to  $1 \times 10^{-2} \text{M}$ . It was also found that Solver was unable to fit the equation when the sum of squared residuals was  $< 2 \times 10^{-9}$ .

Methods were developed for the analysis of heavy metals in potable and seawaters by anodic stripping voltammetry. It was found in both cases that the anodic stripping methods compared well with the established method of graphite furnace atomic absorbance spectroscopy under the validation criteria of calibration curve linearity, accuracy, precision, limit of detection, limit of quantitation and specificity.

# *Chapter 1*

## *Introduction*

Chemistry plays a major role in our environment. It is common for the public to draw attention to the presence of synthetic chemicals in the environment and their creators for current pollution problems. It passes unrecognised that most of the environmental problems of past centuries and decades, such as the biological contamination of drinking water, were solved only when the methods of science in general and chemistry in particular were applied to them. The phenomenal rise in human life expectancy and in the material quality of life that has come about in recent decades is due in no small measure to chemicals and chemistry.

Nevertheless, it is true that chemicals, as defined in the broadest sense, lie at the heart of most of today's environmental problems. The by-products of the chemicals used to improve our health and standard of living have in some instances returned to haunt us by degrading our health and that of plants and animals. In short, our conquest of widespread biological pollution and the increase in our standards of health and material wealth in developed countries has been achieved at the expense of the widespread, low level chemical pollution of the earth.

Low level chemical pollution might appear a small price to pay for the increased quality of life afforded by these synthetic products, but in many cases the potency of these contaminants is such that the presence of trace levels may be sufficient to cause long term, widespread and sometimes irreversible damage.

Recently a number of leading world scientists voiced their concerns about the impact of human activities on our environment by releasing the "World Scientists' Warning to Humanity"[1]. In this document we are warned that, "Human beings and the natural world are on a collision course. Human activities inflict harsh and often irreversible damage on the environment and on critical resources. If not checked, many of our

current practices put at risk the future that we wish for human society and the plant and animal kingdoms, and may so alter the natural world that it will be unable to sustain life in the manner that we know [1].”

Historically, it was assumed implicitly or explicitly that chemicals emitted into the environment would be assimilated by nature, either the natural system would convert them into harmless, naturally occurring substances, or the chemicals would be diluted to such an extent they would pose no threat to life. The attitude towards environmental pollution in the early and middle decades of the twentieth century was characterised by the common attitude that, “The solution to pollution is dilution.” However in the 1960s and 1970s it became clear that some substances are not assimilated and are in fact persistent, that is, they are unaltered by the action of light, water, air or microorganisms for very long periods of time. Examples of these persistent substances include pesticides such as dichlorodiphenyltrichloroethane (DDT), the refrigerants chlorofluorocarbons (CFCs), polychlorinated biphenyls (PCBs) and heavy metals.

In the 1940s and 1950s, the chemical industries in North America and Western Europe produced large quantities of many new pesticides, especially insecticides. The active ingredients in most of these pesticides were organochlorines, many of which share several notable properties:

- (I) Stability against decomposition or degradation in the environment
- (II) Very low solubility in water, unless oxygen or nitrogen is also present in the molecules
- (III) High solubility in hydrocarbon-like environments, such as the fatty material in living matter

The low solubility of these pesticides in water may lead one to assume that they pose little threat to the aquatic environment. Consider the example of the compound hexachlorobenzene (HCB). Although very soluble in organic media such as liquid hydrocarbons, it is almost insoluble in water, only 0.0062 milligrams of HCB dissolve in one litre of water. But the pollution of the aquatic environment is not merely a

question of the concentration of pollutants in the solution state. Much greater amounts of these substances are bound to the surfaces of the organic particulate matter suspended in the water or present in the muddy sediments at the bottom of rivers and lakes. From these sources, as well as from the amounts actually dissolved in the water, organochlorines enter both plants and animals living in the natural waters. Many organochlorines have been detected in living matter at levels exceeding those in the solution state by thousands and even millions of times. Many organochlorine insecticides have been removed from use as a consequence. Unfortunately however due to their stability they will continue to constitute a problem for many years to come. Possibly the first instance of widespread public concern regarding the levels of pollutants in the environment and their effect on the health of both wildlife and humans revolved around the widespread use of DDT in the 1940s, 1950s and 1960s. DDT or para-dichlorodiphenyltrichloroethane, was first discovered to be an insecticide in 1939 by Paul Muller, a chemist working for the Swiss company Geigy on the development of various chemicals to fight agricultural insects. Muller was awarded the Nobel Prize for medicine and physiology in 1948 in recognition of the many civilian lives that DDT saved after the war. In 1945 it was hailed as “miraculous” by Winston Churchill because of its use in the war effort. It was very effective against mosquitoes that carry malaria and yellow fever, against body lice that can transmit typhus, and against plague-carrying fleas. The World Health Organisation estimated that malaria reduction programs, one component of which was the use of DDT, saved the lives of more than five million people.

However DDT was widely overused, particularly in the agricultural sector, which consumed 80% of its production. As a result, its environmental concentration rose rapidly and it began to affect the reproductive abilities of birds which indirectly incorporated it into their bodies through the consumption of DDT laden earthworms. In 1962 DDT was deemed an “elixir of death” by the writer Rachel Carson in her book *Silent Spring*, because of its role in reducing the populations of certain birds such as the American robin and the bald eagle. The DDT intake of the bald eagle was particularly high because of its position at the top of the food chain. Carson’s book stimulated widespread concerns in the public about DDT and other pesticides. The plight of the

bald eagle was of gravest concern, the American public not wanting to see their national emblem consigned to the history books.

DDT persistence in the environment is due to its low vapour pressure and its consequent slow rate of evaporation, to its low reactivity with respect to light and to chemicals in the environment, and to its very low solubility in water. The biomagnification of DDT along some of the Great Lakes is shown in Figure 1.1. Comparing the herring gulls high level of DDT with those of the fish in the chain leading up to it gives a clear idea of the scale of the bioaccumulation. A study of the protected waters around Long Island Sound in the United States found that the concentration of DDT in the seawater was approximately 3 ppt, but it reaches 0.04 ppm in the plankton, 0.5 ppm in the fat of minnows and 2 ppm in the needlefish that swim in these waters, and 25 ppm in the cormorants and osprey that feed on the fish. The result is a bioaccumulation factor of about ten million. Furthermore a recent government study in the United States found that the average adult body contained DDT at a concentration of 3 ppm. Fortunately DDT is only lethal to humans in extremely large dosages. However, a recent study by Mary Wolff of Mount Sinai Hospital in New York appears to suggest that the higher the levels of dichlorodiphenyldichloroethane (DDE), a metabolite of DDT in a woman's blood the more likely she is to contract breast cancer.

Another class of toxic materials is that of heavy metals. Heavy metals have a density of  $> 6 \text{ g / cm}^3$  and occur naturally in rocks but concentrations are frequently elevated as a result of contamination. Sources of heavy metals include metalliferous mining, metal smelting, corrosion of metals in use and fossil consumption. Heavy metals differ from the toxic organic compounds discussed above in that they are completely nondegradable, they are practically indestructible and as a result they accumulate in the environment.

Although mercury vapour is highly toxic, the heavy metals mercury, lead, cadmium and arsenic are not particularly toxic as the condensed free elements. However, all four are dangerous in the form of their cations and when bonded to short chains of carbon atoms. Biochemically, the mechanism of their toxic action arises from the strong affinity of the metal cations for sulphur. Thus sulphhydryl groups, -SH, which occur commonly in the

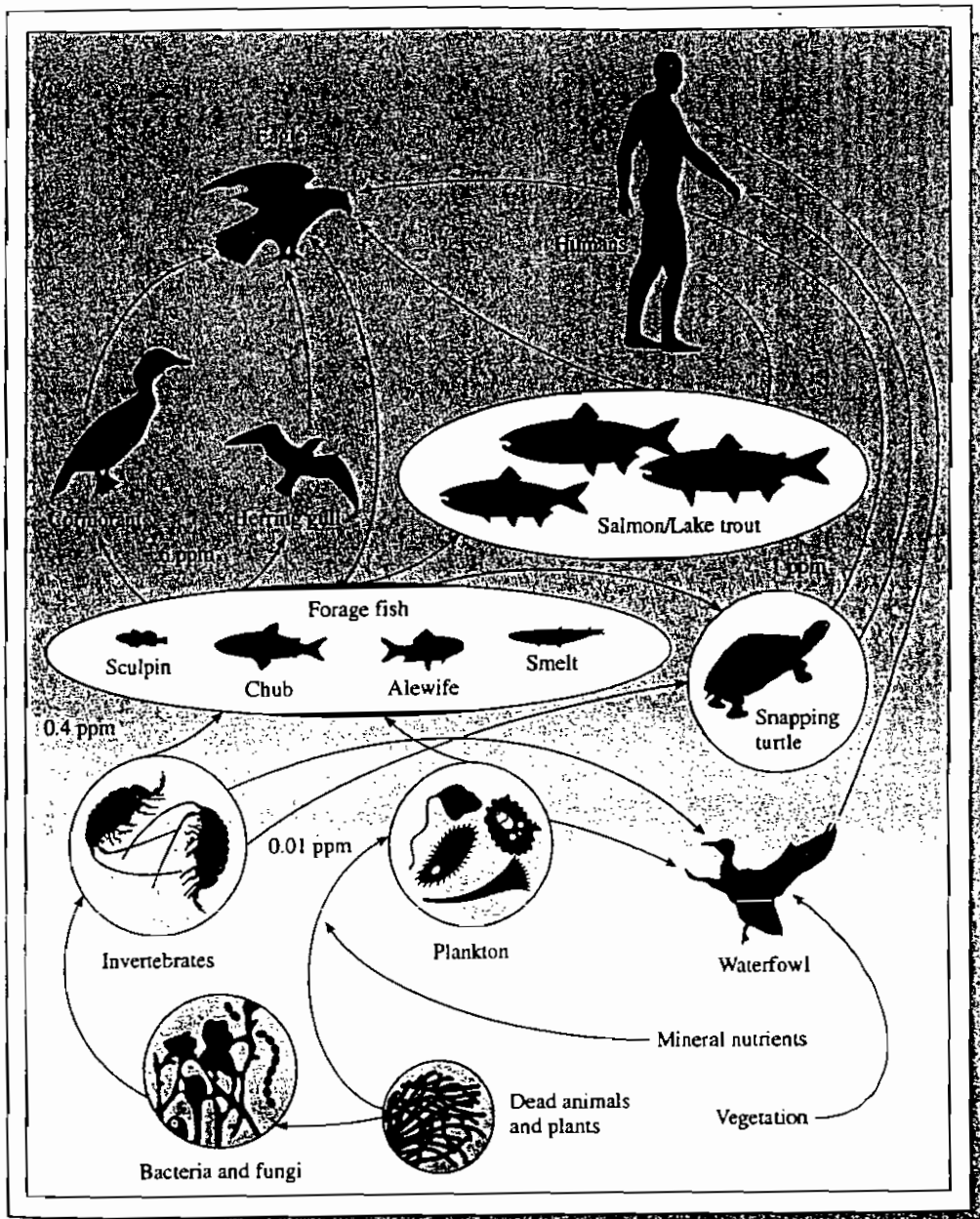


Fig. 1.1 Simplified food web for the Great Lakes with typical DDT concentrations for some species [2].

enzymes that control the speed of critical metabolic reactions in the human body, readily attach themselves to ingested heavy metal cations or molecules that contain the metals. Because the resultant metal-sulphur bonding affects the entire enzyme it cannot act normally and human health is adversely affected, sometimes fatally.

Heavy metals enter the human body through contaminated drinking water, from certain types of food, particularly fish and in some instances from particulate matter in the air we breathe. Many aquatic organisms bioconcentrate heavy metals, for example, oysters and mussels can contain levels of mercury and cadmium that are one hundred thousand times greater than those in the water in which they live. There have been many cases of widespread heavy metal poisoning and large scale soil and water contamination remains a problem in the Czech Republic, the River Danube and in Poland. Classic cases are those of Minimata in Japan where ingestion of seafood laden with mercury caused many deaths.

The above examples illustrate clearly that pollutants in our environment inevitably make their way into the human body and can have adverse affects. It is also clear that these pollutants pose a threat to human health when present only at trace levels due to their persistence and tendencies to bioaccumulate.

Public concern and scientific information has lead to new legislation, the trend of which has been to lower the maximum permissible levels of known toxins and to limit their use. Examples include the introduction of legislation encouraging the use of unleaded petrol, with the result that unleaded petrol accounted for 89% of the total petrol sales in Ireland in the first quarter of 1999. Also new legislation governing the quality of drinking water in the European Union, introduced in 1999, reduces the permissible levels of heavy metals and other substances likely to damage public health by considerable amounts relative to existing legislation.

The importance of obtaining reliable and accurate information about these toxins was stressed by the Minister of State at the Department of the Environment and Local Government, Mr. Dan Wallace at the launch of *Environment in Focus*, a discussion document presented by the EPA. He said that, "Environment policy making should be

based on sound information. Good information can help to change behaviour in society, and influence in a positive way the impact on the environment of our modern lifestyles. Above all, to secure change, we should be making sure that the right information is communicated to the right people.” He added, “Indicators are critical in this regard. As the EPA points out in *Environment in Focus*, indicators translate and deliver concise, scientifically credible information in a manner that can be readily understood and used by decision makers at all levels. They can clarify a mass of data, and highlight whether and to what extent we are moving towards sustainability. By identifying and quantifying trends, we can assess the success rates and the relevance of our policies, and better target our responses.”

The above examples illustrate that monitoring of toxins in the environment is essential to ensuring the quality of public health. Furthermore, the introduction of new legislation regulates these monitoring procedures and ensures that strict standards are met. Effective monitoring of a given toxin requires that the means exist to detect and accurately quantify it in the matrix of interest. In some cases new legislation has reduced the maximum permissible levels set down in previous legislation to the extent that the revised permissible level approaches the limit of detection of the analytical method of choice. Also new compounds are being classified as toxic on a regular basis. Monitoring of these new compounds is a prerequisite to understanding their transport between media and their effect on the environment. Accurate monitoring allows sound decisions regarding the classification and handling of these new compounds to be made. Methods must be devised for their detection and monitoring. One of the challenges facing the analytical chemist as we approach the end of this millennium is to develop novel methods capable of detecting these toxins in a wide range of matrices at sensitivities superior to those of current methods. Failure to meet this challenge could adversely affect the quality of public health in the future.

The purpose of this work is to develop and characterise novel electroanalytical methodologies with a view to lowering limits of detection and to critically compare electrochemical and spectroscopic methods for ppb lead analysis in potable and sea water.



## 1.1 References

1. Reprint available:- Union of Concerned Scientists, 26 Church Street, Cambridge, MA 02238.
2. Baird, C., *Environmental Chemistry*, 2<sup>nd</sup> Ed., W.H. Freeman and Company, New York, 1995.

## *Chapter 2*

### *Electroanalysis using Differential Pulse Methods at Microelectrodes*

#### **2.1 Introduction**

Although the advantageous properties of very small electrodes were recognised for many years, research in this area did not become popular until the late 1970s. Advances made in the field of electronics, especially in the measurement of very small currents, and the advent of microstructural materials provided the tools that were necessary to build and use electrodes of small dimensions. These electrodes became known as microelectrodes.

Microelectrodes are working electrodes which are constructed to have a very small surface area. Generally one of their dimensions do not exceed  $20\mu\text{m}$  and because of their small size they exhibit very different voltammetric properties than do electrodes of conventional size. They can be made by embedding a platinum wire (generally of radius 1, 5 or  $10\mu\text{m}$ ) or carbon fibre ( $8\mu\text{m}$ ) in glass or epoxy and exposing the cross sectional disk to solution. Electrodes constructed in this form are referred to as planar

disk microelectrodes. Cylindrical and other geometries have also been employed, however this work is restricted to planar disk geometries.

Microelectrodes have a number of advantages over the larger conventional electrodes, the majority of which can be attributed to their small electrochemical area [1,2,3]. Only extremely small currents are involved when using microelectrodes and currents as low as  $10^{-17}$ A can be measured with relative ease [3]. There may also be no need to introduce an auxiliary electrode as a 'current sink' as the current may not be large enough to have a disruptive effect on the reference electrode. It is therefore possible to operate microelectrodes in a two electrode cell configuration [4]. This avoids the expense and complications associated with a three electrode potentiostat system which is required for operation of conventional electrodes. Also there is no need to deliberately add supporting electrolyte, which is essential at conventional electrodes to minimise the phenomenon of migration. The small currents drawn by microelectrodes together with their small dimensions allow them to be used for *in vivo* analysis [5,6,7] i.e. they can be used to make chemical measurements inside the living brain. Some very interesting information concerning drug-induced changes of chemical compounds in the mammalian brain has been obtained by using microelectrodes [8]. Yet another advantage associated with a microelectrode compared to its larger area counterpart is that it has a greater faradaic to double layer charging current ratio yielding lower detection limits. This is due to the presence of so called "edge effects" which result because of non-linear diffusion to the electrode surface. This non-linear diffusion is due to the build up of a hemispherical diffusion layer at the microelectrode surface in contrast to a planar diffusion layer build up at a macroelectrode. Decreasing the size of

electrodes also gives an enhanced signal to noise ratio and hence lower detection limits making them more desirable as analytical tools [1]. Finally microelectrodes have great potential for very fast measurements since the timescale of double layer charging currents is proportional to the electrode area. Therefore the smaller the electrode the shorter the charging current time and it is the charging current time that determines the shortest time at which meaningful measures of faradaic current can be measured.

Unfortunately microelectrodes also have some disadvantages associated with their small dimensions. Practical problems of polishing and manipulation arise because the electrode surface is not visible with the naked eye and as a rule the microelectrodes tend to be quite fragile. Another difficulty associated with microelectrodes is the requirement for a low noise means of current measurement and while the effect of double layer charging is diminished compared to that at a macroelectrode, it is still present. However the main disadvantage is that use of a microelectrode in a direct mode potential sweep results in a sigmoidal output, which is difficult to interpret at low analyte concentrations. The aim of this work is to characterise the response from the application of a differential pulse voltammetric waveform to a microelectrode.

## 2.2 Theory

The following assumptions were made in postulating the theory for differential pulse voltammetry at a planar disk microelectrode [5] and are the basis for Model 1.

- a) The Cottrell equation may be used for characterisation of the current response at short time periods following the pulse.
- b) The current due to the potential ramp follows the traditional microelectrode behaviour with a potential dependent component.
- c) The above two currents, a) and b), are additive for an electrochemically reversible reduction, thus;

$$i_1 = \frac{nFAC\sqrt{D}}{\sqrt{\pi\delta}} \left[ \frac{(1-\sigma^2)\varepsilon_1}{(1+\varepsilon_1)(1+\sigma^2\varepsilon_1)} \right] \quad (2.1)$$

where,

$$\sigma^2 = \exp\left(\frac{nF\Delta E}{RT}\right) \quad (2.2)$$

$$i_2 = \frac{4nFrDC}{1+\varepsilon_1} \quad (2.3)$$

where,

$$\underline{\varepsilon_1 = \exp\left(\frac{nF(E_1 - E^{0'})}{RT}\right)} \quad (2.4)$$

$$\underline{i_3 = \frac{4nFrDC}{1 + \varepsilon_2}} \quad (2.5)$$

where,

$$\underline{\varepsilon_2 = \exp\left(\frac{nF(E_2 - E^{0'})}{RT}\right)} \quad (2.6)$$

Where  $i_1$  is the current contribution from the pulse alone,  $i_2$  is the current due to the potential ramp before the pulse is applied, taking the limiting steady state current to be;

$$i_l = 4nFrDC \quad (2.7)$$

where  $r$  is the electrode radius,  $n$  is the number of electrons involved,  $F$  is the Faraday constant and  $D$  and  $C$  are the diffusion coefficient and the concentration of the electroactive species respectively.  $i_3$  is the current due to the potential ramp at a time  $(\delta+\tau)$ , if the pulse was not applied.  $E_1$  is the potential prior to pulse (at a time  $\tau$ ),  $E_2$  is the potential defined by the potential ramp if the pulse was not applied (at a time  $\delta+\tau$ ).

$\tau$  is the time at which the current is sampled before the pulse is applied and  $(\delta+\tau)$  is the time at which the current is sampled after the pulse is applied.  $\Delta E$  is the pulse

amplitude and all other symbols have their usual meaning. The instrumental differential output is represented as follows by the sum of the current due to the underlying ramp at time  $(\delta+\tau)$ ,  $i_3$ , and the current due to the pulse  $i_1$ , less the current before the pulse  $i_2$ .

$$\partial i = i_1 + i_3 - i_2 \quad (2.8)$$

In practice during the timescale of the experiment the diffusion layer thickness was found to be of the same order of magnitude as the diameter of the microelectrode. This facilitated the presence of “edge effects” which leads to a steady state current being reached within the pulse width ( $\delta$ ). By modifying the theory the differential current may be calculated as follows using Model 2.

$$\underline{\hat{\alpha}^* = i_4 - i_2} \quad (2.9)$$

$$\text{where, } \underline{i_4 = \frac{4nFrDC}{1 + \varepsilon_3}} \quad (2.10)$$

$$\text{and } \underline{\varepsilon_3 = \exp\left(\frac{nF(E_2 + \Delta E - E^{0'})}{RT}\right)} \quad (2.11)$$

where  $i_4$  is the steady state current following the pulse and  $i_2$  is the current due to the ramp potential before the pulse is applied. This modified theory allows for steady state current to occur before and after the pulse.

Model 1 applies for larger microelectrodes while Model 2 applies for smaller microelectrodes under conditions of longer pulse widths.

## 2.3 Experimental

### 2.3.1 Instrumentation, Cells, Electrodes and Chemicals

The potentiostat used throughout this work was an Edt Model ECP 100 and a J.J. Lloyd X-Y chart recorder Model PL3 was used to chart the response. A three electrode system consisting of a carbon rod auxiliary, a saturated calomel reference electrode and an EG&G Parc platinum planar disk microelectrode was employed. All chemicals used were of reagent grade and all solutions were made up using deionised water. Fresh solutions of potassium ferrocyanide were prepared daily and the electrochemical cell was blackened to minimise exposure of the ferrocyanide to light. Solutions were degassed by bubbling with nitrogen for at least 15 minutes prior to recording any data and a positive nitrogen pressure was maintained over the cell during analyses. A Pasco Scientific CI-6510 analogue to digital converter was used to collect and store the data digitally and the simulations were carried out using a program written in Microsoft



Excel. The microelectrode of radius  $\approx 5\mu\text{m}$  was supplied by EG&G Princeton and microelectrodes of larger radii were fabricated in our laboratory.

### 2.3.2 Fabrication of Microelectrodes

The specifications of the conducting wires used for the fabrication of the microelectrodes are as follows:

1. Insulated platinum wire:	Supplier	Goodfellow
	Diameter	0.025mm
	Insulation	PTFE
	Insulation thickness	0.0004mm
	Purity	99.999%
2. Insulated copper wire:	Supplier	RS Components
	Diameter	0.2mm

Electrical contact between the 25  $\mu\text{m}$  platinum wire and the more rigid copper wire was achieved through solder. This assembly was then embedded in an insulating material taking the form of a heat sealed glass which collapses around the platinum with a cross section of the platinum wire being exposed.

Before electrical contact could be made between the platinum and copper wires the PTFE insulating coating had to be removed. At first it was thought that the PTFE was too stable to dissolve off and that due to the small dimensions of the platinum wire it

would not be capable of withstanding the temperatures necessary to incinerate the coating. For these reasons it was decided that the only option available was to scrape the coating from the surface of the metal with the aid of a sharp blade using a microscope to observe the procedure. This proved very difficult, the blade tending to sever the wire if too much force was applied. It was decided to investigate further the possibilities of incinerating or dissolving the coating. On consulting the Merck Index the properties of PTFE were found to be as follows:

Melting point: 327°C

Reverts to gaseous monomer at temperatures > 400°C

No solvent has been found which will dissolve the polymer at moderate temperatures

It was also found that platinum has a melting point of 1127°C and based on this data it was decided that the most convenient method of removing the PTFE was to heat the insulated platinum to a temperature above 400°C but much less than 1127°C. This temperature range was achievable in a bunsen flame. An ohmmeter was used to check that the insulator had been removed.

The 0.2mm copper wire was also insulated, however due to its larger dimensions it was possible to remove its insulation coating by scraping with a blade. Only the insulation within approx. 2cm from each end was removed. One end was to be connected to the platinum wire and the other end would facilitate connection to the potentiostat.

Due to its dimensions the platinum wire was quite fragile and initial attempts to make a connection to the more rigid wire by a series of windings proved unsuccessful as the platinum tended to break very easily. A magnifying glass was employed throughout this process to aid visibility. A number of different methods of making a connection were investigated and the most successful of these involved threading the platinum wire through a pre prepared loop at one end of the copper wire. This loop was then collapsed on the thread of platinum wire and the joint sealed with a coating of a silver conductive paint. Having allowed the paint to dry the connection was tested with an ohmmeter, a resistance of zero ohms indicating a good electrical contact between the platinum and copper wires. This method reduced the length of platinum wire required as it was not necessary to wind the platinum around the copper.

Having achieved a good contact it was necessary to encase the wire assembly in a protective housing so it could be used in an experimental arrangement. Initially a glass pasteur pipette was used as housing for the wires. The copper wire was introduced into the pipette at the narrow end and pulled through until the tip of the platinum wire was at the end of the narrow tip of the pipette. This end of the pipette was then introduced into a bunsen flame and heat sealed. During heating the pipette was manually rotated to prevent curvature along the longitudinal axis of the tube. The copper wire at the other opening of the pipette was secured with an epoxy resin (Araldite) to both seal the tube and firmly secure the wire connections within the pipette.

Unfortunately the heat sealing process was difficult to control and open to numerous problems. These included incomplete sealing of the tube, distortion of the glass tubing

and blackening of the platinum wire. Even in the case where perfect sealing was achieved the cross sectional area of the electrode was relatively small making it fragile and difficult to polish. It was decided to explore other possibilities for housing the wire assembly.

It was found that placing the platinum/copper wire assembly in a length of rubber tubing which was then filled with an epoxy resin by means of a syringe produced a sturdy electrode with a pre determinable cross-sectional area.

## 2.4 Results and Discussion

### 2.4.1 Determination of the microelectrode radius

From the limiting current ( $i_L$ ) of the voltammetric response obtained by scanning the potential of a platinum microelectrode in a solution of  $5 \times 10^{-3} \text{M}$  ferrocyanide in a solution of  $0.1 \text{M}$  KCl, the electrode radius was found from equation (2.7). Taking  $i_L$  to be  $5.60 \times 10^{-9} \text{A}$ , and the diffusion coefficient ( $D$ ) for  $[\text{Fe}(\text{CN})_6]^{4-}$  to be  $6.5 \times 10^{-6} \text{cm}^2 \text{sec}^{-1}$  [9] the electrode radius ( $r$ ) was calculated as  $4.46 \times 10^{-6} \text{m}$ . This is smaller than the nominal radius of  $5 \times 10^{-6} \text{m}$  but the discrepancy is attributed to polishing.

### 2.4.2 Characterisation of the microelectrode response to a Differential Pulse

Waveform

Figure 2.1 shows the response obtained by the application of a differential pulse waveform to a platinum microelectrode of radius  $4.46\mu\text{m}$  in a solution of  $5\text{mM}$   $[\text{Fe}(\text{CN})_6]^{4-}$ . It can be seen that the peak current heights increase with increasing pulse amplitude but at the expense of return to baseline. The baseline shifts directly with pulse height. Closer investigation revealed that the increase in peak current height was linear with pulse amplitude over a limited range. The effect of varying the differential pulse waveform period (taken here to be the time between pulse applications) was also investigated. It was found that long differential pulse waveform periods ( $> 1.0\text{sec.}$ ) resulted in stepped responses with ill defined peaks

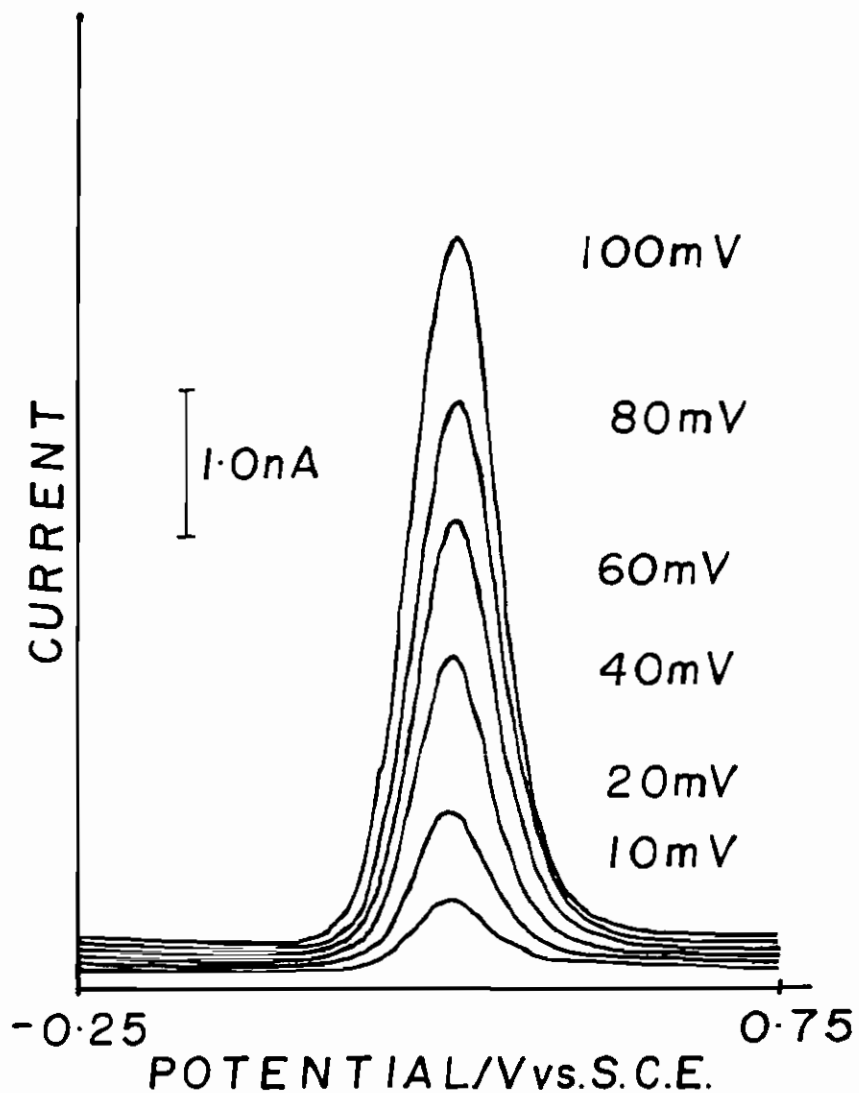


Fig. 2.1 Differential pulse output for a microelectrode in a solution of 5mM  $[\text{Fe}(\text{CN})_6]^{4-}$  in 0.1M KCl. Instrumental time constant = 1 sec., sweep rate = 10mV/sec. Differential pulse waveform period = 1.0 sec. Pulse width =  $55 \times 10^{-3}$  sec. Pulse amplitudes are shown in the figure.

while shorter differential pulse waveform periods resulted in smoother traces with well defined peaks. This can be explained by the fact that the potentiostat samples the current twice during each waveform period. Therefore as the differential pulse waveform period is decreased the number of pulses applied per unit time increases and the current is sampled more regularly giving smoother traces. The magnitude of the differential pulse waveform period was found to have negligible effect on peak current heights. It can be seen that the baseline shifts with pulse amplitude which is due to double layer charging.

#### 2.4.3 Comparison of experimental and theoretical results

Figure 2.2 compares the experimental results obtained from the numerical derivative of a sigmoidal experimental plot, Fig.2.2(a), and the response from the application of a differential pulse waveform to the same electrode, Fig.2.2(b). The numerical derivative was obtained using Excel. Also included are simulated plots using eq.(2.8) Fig.2.2(c), and eq.(2.9), Fig.2.2(d). It is immediately obvious that Model 1 (eq.2.8), does not correlate well with either of the experimental traces whereas Model 2 (eq.2.9) correlates well with both experimental traces.

Table 2.1 lists the peak current heights corresponding to each of the experimental methods and simulations over a range of pulse amplitudes. In the case of the differential pulse waveform the correlation between experimental peak current heights and those predicted by Model 2 occurs only over a narrow pulse amplitude range. However it can be seen that the peak current heights obtained by numerically differentiating the

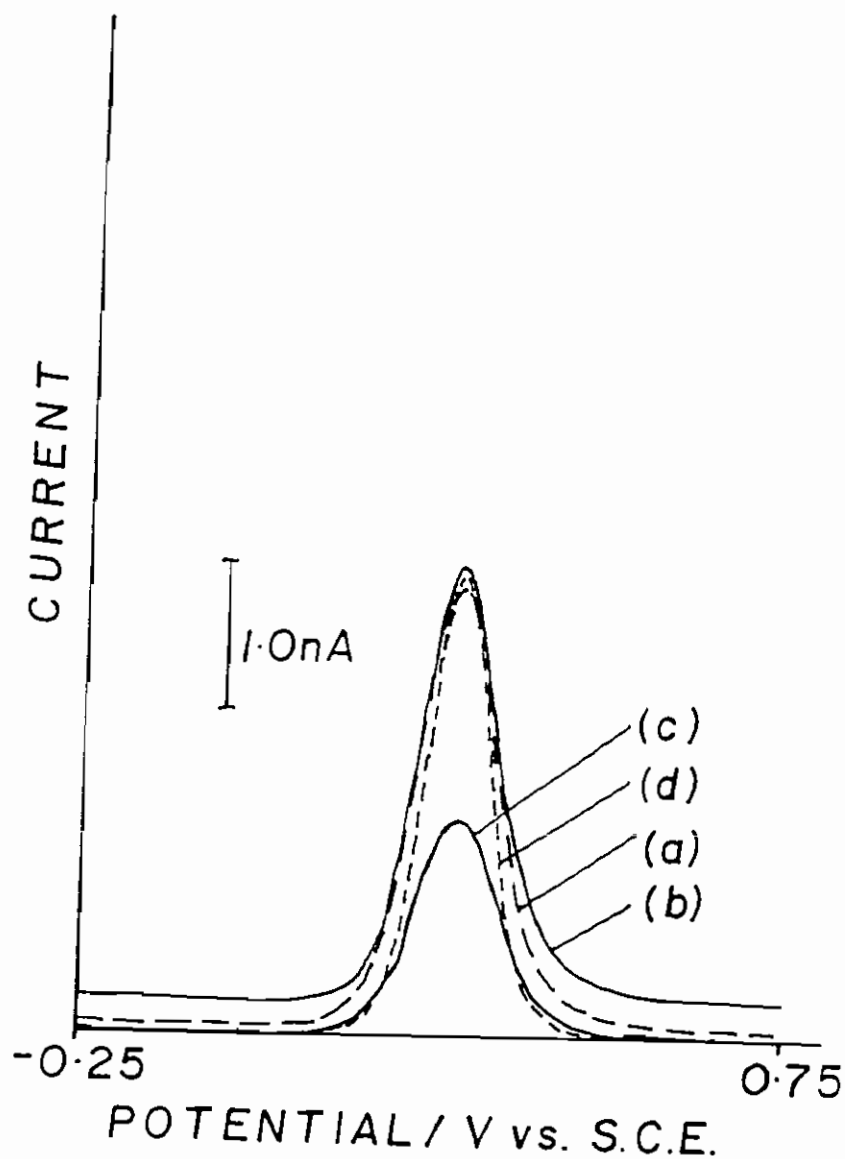


Fig. 2.2 (a) Numerical point by point derivative of a linear sweep response for 5mM  $[\text{Fe}(\text{CN})_6]^{4-}$  in 0.1M KCl at a microelectrode ( $r = 4.46 \times 10^{-6} \text{m}$ ) where the sweep rate was 10mV/sec. Points which gave a pulse height of 60mV were chosen. (b) Experimental differential pulse output ( $\Delta E = 60 \text{mV}$ ), sweep rate = 10mV/sec., time constant = 1 sec. (c) Model 1, (eq. (2.8)) calculated using the parameters as above. (d) Model 2, (eq. 2.9)) calculated using the parameters as above.



sigmoidal experimental plot correlate well with those predicted by Model 2 over the complete range of pulse amplitudes studied. It is therefore possible to enjoy the advantage of a peaked response which is well defined (Model 2) over a wide range of pulse amplitudes without having to invest in new and sophisticated equipment, the only system requirements being a linear ramp waveform generator, a data acquisition unit and a computer with relevant software, all of which are commonplace in any electrochemistry laboratory.

Table 2.1: Comparison of the various theoretical models with the experimental data. Conditions as in Fig.2.2.

Pulse Amplitude (mV)	Differential Pulse Peak Height (nA)	Peak Heights from Model 1 (nA)	Peak Heights from Model 2 (nA)	Numerical Derivative Peak Heights (nA)
100	4.98	1.45	4.29	4.23
80	3.80	1.29	3.76	3.61
60	2.98	1.05	3.05	2.90
40	1.85	0.76	2.19	2.09
20	0.65	0.43	1.14	1.09

The results for peak current heights from Model 2 and peak current values from the numerical derivative of a linear sweep correlate well. The reason for slight differences may be because of the fast sweep rate used (10mV/sec.). However the experimental differential pulse response deviates from Model 2, indicating that there may be some contribution to the response from the pulse and that a steady state has not occurred in the timescale of the pulse width. This may be due to slow electron transfer kinetics on such a short time scale or a combination of slow electron transfer kinetics and diffusion control.

#### 2.4.4 Differential Pulse Voltammetry at low concentrations

A distinct advantage of applying a differential pulse to a microelectrode can be seen at lower concentrations. This is evident in figure 2.3 where the response is shown both for direct current and the differential current following the application of a differential pulse. The direct current response is very difficult to interpret and therefore almost useless in providing analytical information. However for the differential pulse response there is useful information to be gained as a peak is clearly seen at the potential at which the electrochemical reaction in question is known to occur. This has the effect of lowering the limits of detection relative to the direct current experiments. Also a peaked response is more desirable as a baseline can be drawn enabling peak current heights to be easily determined. This is in stark contrast to the difficulties encountered when attempting to measure limiting current from a direct current microelectrode experiment at sub-millimolar concentrations. Figure 2.4 shows the response obtained when a differential pulse waveform was applied to a microelectrode of radius  $4.46\mu\text{m}$  at a range of  $[\text{Fe}(\text{CN})_6]^{4-}$  concentrations. The peaked response can be clearly seen and is well defined at concentrations as low as  $5 \times 10^{-9}\text{M}$ . At smaller concentrations the peaks become very broad and approach the baseline making them difficult to interpret. In contrast no useful information can be obtained from the sigmoidal response at a concentration of  $5 \times 10^{-5}\text{M}$   $[\text{Fe}(\text{CN})_6]^{4-}$  as can be seen in Fig. 2.3.

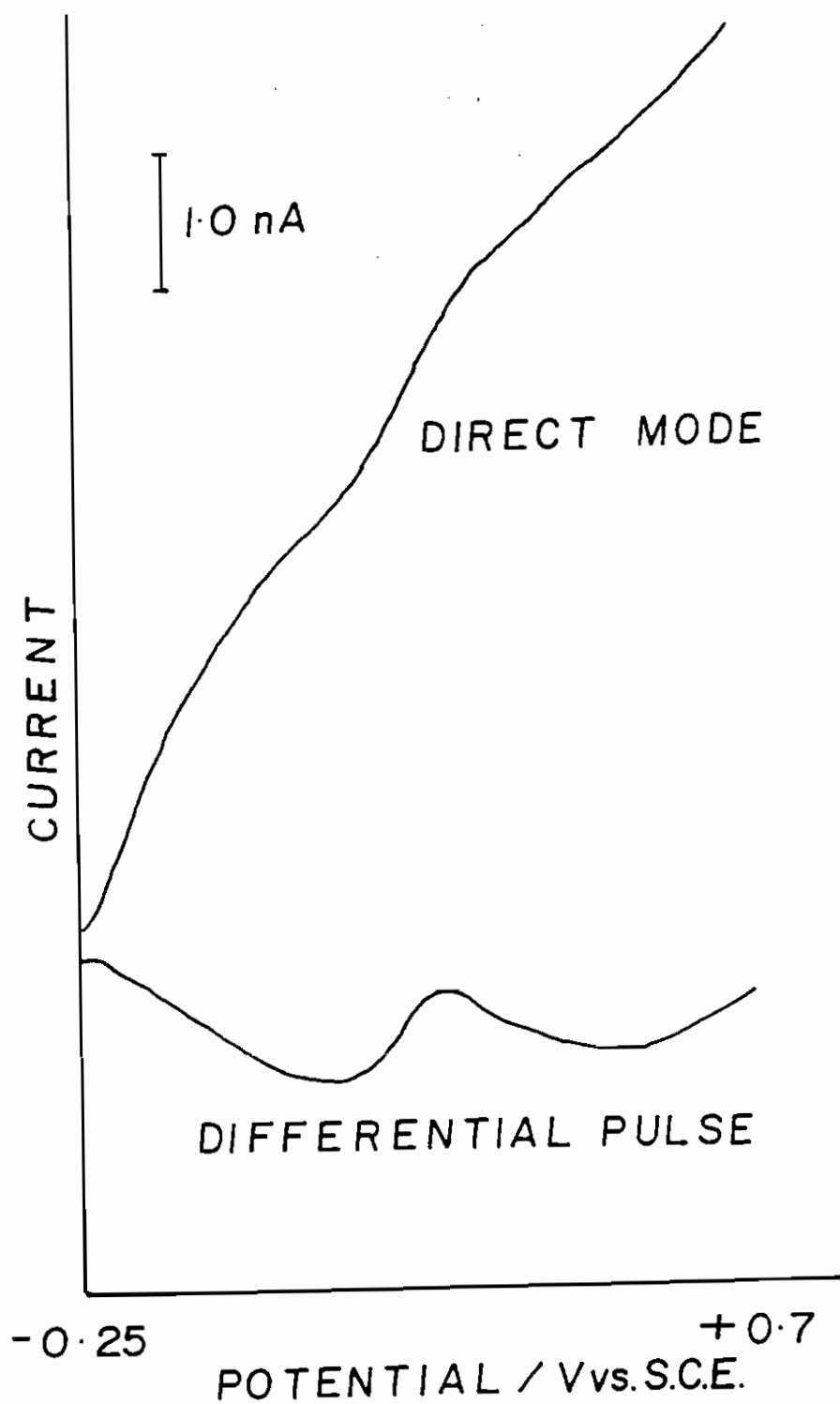


Fig. 2.3. Comparison of the responses produced by the application of a linear sweep and a differential pulse waveform at a microelectrode in a solution of  $5 \times 10^{-5} \text{M}$   $[\text{Fe}(\text{CN})_6]^{4-}$  in 0.1M KCl. Platinum microelectrode of radius  $4.46 \times 10^{-6} \text{m}$ , scan rate in both cases was  $10 \text{mV sec}^{-1}$  and in the case of the differential pulse the time constant = 1.0 sec. Differential pulse waveform period = 1.0 sec, pulse width =  $55 \times 10^{-3} \text{sec}$  and the pulse amplitude = 100m V.

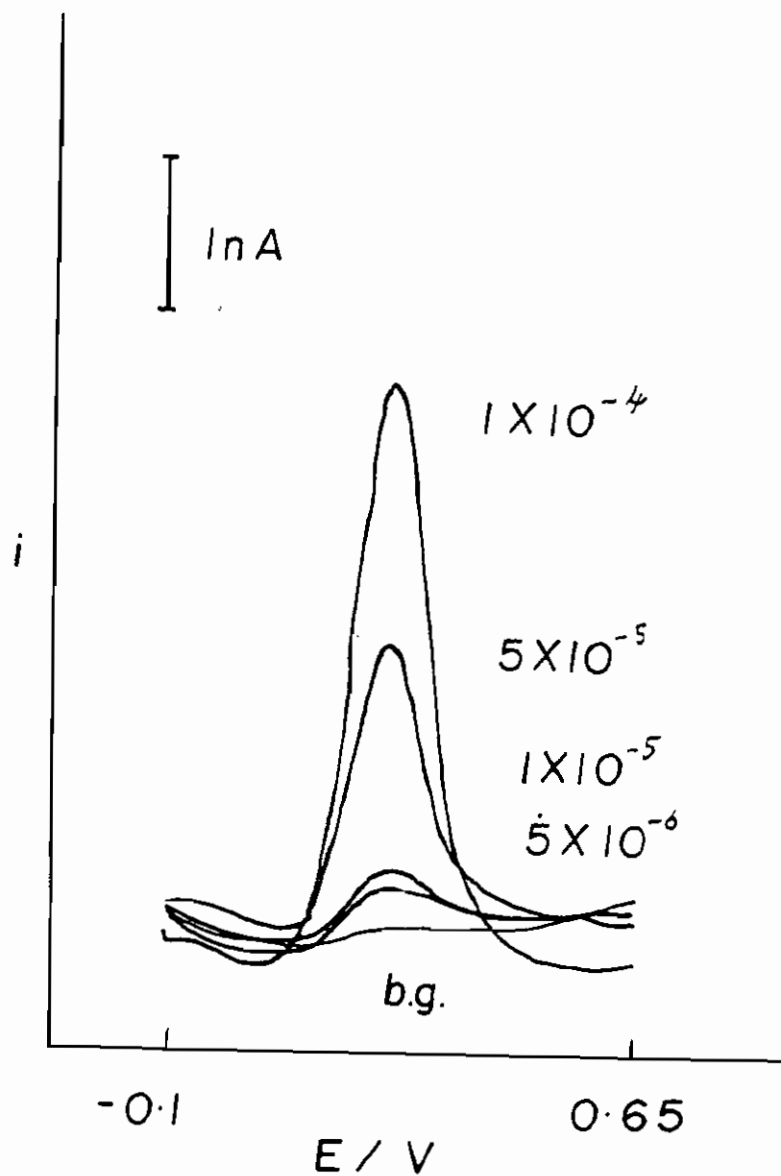


Figure 2.4 Experimental differential pulse response for a range of ferrocyanide concentrations, listed in the figure in moles  $\text{dm}^{-3}$ . The curve labeled  $\text{b.g.}$  is the background scan and the other conditions are as in Figure 2.3

#### 2.4.5 Limitations of Model 2

As stated earlier Model 2 is based on the fact that a steady state current is reached within the pulse width due to the presence of edge effects which in turn are due to the thickness of the diffusion layer being of the same order of magnitude as the electrode diameter. It is clear that the extent to which Model 2 can be applied to a given experimental arrangement depends directly on the relative magnitudes of the electrode diameter and the diffusion layer thickness. The diffusion layer thickness ( $d$ ) is approximated by the equation  $d = (\pi Dt)^{1/2} = 1.06 \times 10^{-5} \text{m}$  where  $t = \text{pulse width} = 55 \text{ms}$  and  $D = \text{diffusion coefficient} = 6.5 \times 10^{-6} \text{cm}^2 \text{sec}^{-1}$ . Therefore the thickness of the diffusion layer ( $d$ ) is independent of the electrode radius. The previous discussion concerned a situation where the electrode diameter ( $9.92 \mu\text{m}$ ) and the diffusion layer thickness ( $10.60 \mu\text{m}$ ) were of the same order of magnitude and it was found that Model 2 was applicable. It was decided to test the limitations of this model by running a similar set of experiments at a microelectrode of radius  $\approx 25 \mu\text{m}$  i.e. where the electrode diameter and diffusion layer thickness are no longer of the same order. The following is a discussion of the results obtained.

#### 2.4.6 Differential Pulse study at larger microelectrodes

Using the same technique employed previously (Section 2.4.1) the radius of this electrode was found to be  $24.3 \mu\text{m}$ . Again the variation from the nominal radius of

25.0 $\mu\text{m}$  can be attributed to distortions introduced into the electrode surface during polishing. To facilitate a comparison between the responses produced by the two microelectrodes a corresponding set of experimental and theoretical data was collected for the larger electrode as had been collected at the smaller electrode. Table 2.2 compares the peak current heights recorded by the experimental methods at a microelectrode of radius 24.3 $\mu\text{m}$  with the peak current heights predicted by the various theoretical treatments.

Table 2.2: Comparison of the various theoretical models with the experimental data.

Conditions as in fig. 2.2 (microelectrode radius = 24.32 $\mu\text{m}$ )

Pulse Amplitude (mV)	Peak Heights from Model 1(nA)	Peak Heights from Model 2(nA)	Numerical Derivative Peak Heights(nA)	Differential Pulse Peak Height (nA)
100	36.98	21.90	22.62	77.33
80	31.90	19.21	19.88	65.83
60	26.03	15.55	16.07	49.17
40	20.16	11.11	11.31	32.83
20	9.84	6.03	6.07	13.00

As was the case with the microelectrode of radius 4.46 $\mu\text{m}$  the peak current heights predicted by Model 2 and those predicted by the numerical derivative of the linear sweep correlate well over the complete range of pulse amplitudes studied and again the slight differences can be attributed to the fast sweep rate (10mV/sec.) at which the linear sweep was recorded. However, the most striking feature of this data table is that the experimental differential pulse response fails to correlate with the data obtained by any

of the other methods, in fact they differ by at least a factor of two. This discrepancy can be explained as follows.

During each differential pulse waveform period the current is sampled twice by the potentiostat, just before the pulse is applied and again 5ms before the pulse ends. These sampling times are a specification of the potentiostat used and cannot be altered. Also the pulse width is fixed by the potentiostat to have a value of 60ms. The instrumental output is the difference between these two current samples for every differential pulse waveform period. The current sampled before the application of the pulse is the current due to the underlying linear ramp waveform (i.e. the current that would have existed if the pulse had not been applied) and the current sampled at the end of the pulse is the current due to the pulse.

Figure 2.5 is a schematic of the current response produced by the application of a differential pulse waveform. Before the pulse is applied the instantaneous current is determined solely by the linear sweep waveform with no contribution from the pulse. On application of a pulse the current increases sharply before decaying during the pulse lifetime. On termination of the pulse the current decreases sharply before gradually returning to a value governed by the underlying ramp i.e. the value it would have attained if the pulse had not been applied before application of the next pulse.

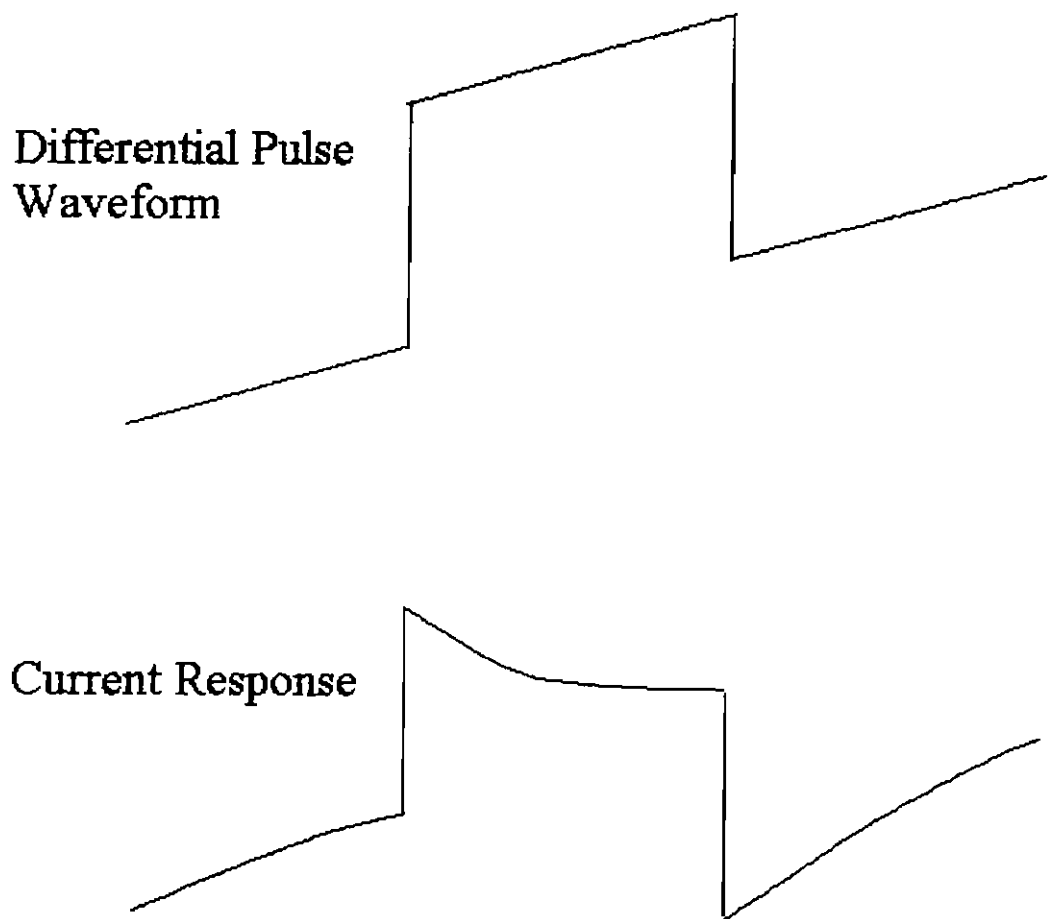


Fig. 2.5 Schematic showing the typical current response following the application of a differential pulse waveform.



Consider the case where the current fails to return to the value determined by the underlying ramp prior to the application of the next pulse i.e. the current does not reach steady state after the pulse. (Note: Model 2 assumes a steady state current with fast kinetics is reached both during and after the pulse). The instrumental output therefore does not accurately represent the current contribution from the pulse and will be greater than expected as in this case the difference between the two current samples is artificially large.

Assuming that this is the case why is the same effect not seen at the smaller electrode? Differences in the diffusion patterns of the electroactive species to each of the electrode surfaces and slow electron transfer kinetics can be used to explain this observation. The differences in the diffusion patterns at the two electrodes will be considered first.

It has already been established that the diffusion layer thickness ( $d$ ) is determined by the relationship  $d = (\pi Dt)^{1/2}$  and is independent of the electrode radius (Section 2.4.5). Under the experimental conditions used for this study  $d = 1.06 \times 10^{-5} \text{ m}$  and is assumed to be equal at both electrodes as both sets of experiments were carried out under the same conditions. For the microelectrode of radius  $4.46 \mu\text{m}$  the diffusion layer thickness is of the same order of magnitude as the electrode diameter. On the other hand for the electrode of radius  $24.32 \mu\text{m}$  the diffusion layer thickness is smaller than the electrode diameter by a factor of five. This leads to a difference in the diffusion patterns to the electrode surfaces [1,10]. At the larger electrode planar diffusion to the electrode surface occurs and the response approaches that of electrodes of conventional size i.e. a

steady state current is not reached. However because the diffusion layer thickness and the electrode diameter are of the same order at the smaller electrode radial diffusion to the surface occurs. This leads to the build up of edge effects allowing the electrode to reach steady state within the pulse width.

More precisely at values of  $Dt/r^2$  greater than one, where  $r$  is the radius of the electrode,  $t$  is the electrolysis time, and  $D$  is the diffusion co-efficient of the electrolysed species (in centimetres squared per second), the current approaches steady state [3]. This is so because the dimensions of the diffusion layer under these conditions greatly exceed the dimensions of the electrode, and the volume from which molecules diffuse to support the current is relatively large. It is for this reason that the current can recover from the pulse more rapidly at the smaller electrode. In contrast at small values of  $Dt/r^2$  the current follows the behaviour expected under conditions of planar diffusion because the electrode dimensions are now larger than the diffusion layer and the current cannot recover as quickly under these conditions. For the microelectrode of radius  $4.46\mu\text{m}$  the value of  $Dt/r^2$  is 1.43 whereas for the electrode of radius  $24.32\mu\text{m}$  this value is 0.057.

To verify this theory experimentally a series of experiments were carried out in which the differential pulse waveform period was altered while all other variables were kept constant. The same experimental procedure was followed for this study at each of the electrodes and experimental conditions were identical. Table 2.3 lists the data recorded at the larger electrode and Table 2.4 lists the corresponding set of data recorded at the smaller electrode. If the assumptions made above are correct the peak current heights should increase as the differential pulse waveform period is reduced at the larger

electrode because the current has less time to recover while little or no effect should be seen at the smaller electrode.

Table 2.3: Effect of differential pulse waveform period on the peak current heights at a microelectrode of radius 24.32 $\mu$ m.

Pulse Amplitude/mV	Peak current heights in nA corresponding to different Differential Pulse Waveform Period in seconds			
	1.0	0.8	0.6	0.4
100	52.50	67.00	77.50	84.50
80	39.50	60.00	70.00	74.50
60	39.00	49.50	60.00	64.00
40	28.50	38.00	44.50	45.50
20	16.00	22.00	24.50	24.00

The obvious trend in this table of data recorded at a microelectrode of radius 24.32 $\mu$ m is that the peak current heights at any particular pulse amplitude increase as the differential pulse waveform period i.e. the time between pulse applications is reduced.

Table 2.4: Effect of the differential pulse waveform period on peak current heights at a microelectrode of radius 4.46 $\mu$ m.

Pulse Amp./mV	Peak current heights in nA corresponding to different Differential pulse waveform periods in seconds					
	1.0	0.8	0.6	0.4	0.2	0.1
100	5.30	5.20	5.15	4.95	5.45	5.75
80	4.38	4.38	4.50	4.40	4.55	4.90
60	3.23	3.35	3.45	3.48	3.45	3.70
40	2.20	1.98	2.20	2.20	2.35	2.50
20	1.03	0.95	1.00	1.03	1.05	1.15

At this smaller electrode an increase in peak current heights with decreasing differential pulse waveform periods is also observed. However the effect is less pronounced and is only clearly evident when the waveform period is reduced to 0.2 seconds.

As expected the peak current heights increased with a decrease in the differential pulse waveform period at the larger electrode while at the smaller electrode the effect is much less pronounced. These results support the theory that diffusion control is at least partly responsible for the unexpectedly large peak current heights recorded for the differential pulse method.

It was also thought that slow kinetics were contributing to the large peak current heights by inhibiting the recovery of the current on termination of a pulse. This would lead to the situation discussed above and illustrated in Figure 2.5 i.e. the current is unable to return to a state governed solely by the underlying ramp prior to the application of the next pulse. Slow electron transfer kinetics reduces the rate at which the electroactive species reacts at the electrode surface. This has the effect of reducing the concentration gradient between the electrode surface and the bulk solution. The result is a reduction in the rate of diffusion of the electroactive species to the surface which directly affects the current flowing in the external circuit. It also enhances the response, but the response may not be reproducible and so not analytically useful.

It has long been established that the rate of electron transfer for  $[\text{Fe}(\text{CN})_6]^{+}$  is sensitive to the concentration of electrolyte. Many papers have been published which provide convincing evidence that the rate of electron transfer shows a first order dependence on

the concentration of cations in solution [11,12]. The catalytic influence of the alkali metal cations on the electrode process increases in the order  $\text{Li}^+ < \text{Na}^+ < \text{K}^+$ . Peter reported that the heterogeneous redox process for the hexacyanoferrate (II)/(III) couple is first order with respect to the potassium ion concentration and that this effect was related to the association of the cation with the anion in all but very dilute solutions[13].

To investigate the effect of kinetics on the system a set of differential pulse waveform experiments were carried out at the electrode of radius  $24.32\mu\text{m}$  in different concentrations of supporting electrolyte (0.1M KCl and 1.0M KCl). The larger supporting electrolyte concentration has the effect of increasing the kinetics of the system and therefore we expect that the peak current heights should be less affected by the shortening of the differential pulse waveform period as the current should be capable of recovering more rapidly on termination of the pulse.

Table 2.5: Effect of the Differential Pulse Waveform Period on peak current heights in a solution of 5mM  $[\text{Fe}(\text{CN})_6]^{4-}$  / 1.0M KCl.

		Peak Current Heights / nA corresponding to a range of Differential Pulse Waveform Periods.			
Pulse Amplitude/mV	1.0 sec.	0.8 sec.	0.6 sec.	0.4 sec.	
100	63.5	65.0	66.0	67.5	
80	53.0	56.0	55.0	55.0	
60	43.5	44.5	44.5	43.0	
40	30.0	30.5	32.0	31.5	
20	16.5	15.5	15.5	15.5	

Table 2.6: Effect of the Differential Pulse Waveform Period on the peak current heights in a solution of 5mM  $[\text{Fe}(\text{CN})_6]^{4-}$  / 0.1M KCl.

Pulse Amplitude mV	Peak Current Heights / nA corresponding to a range of Differential Pulse Waveform Periods.			
	1.0 sec.	0.8 sec.	0.6 sec.	0.4 sec.
100	52.5	67.0	77.5	84.5
80	49.0	60.0	70.0	74.5
60	39.5	49.5	60.0	64.0
40	28.5	38.0	44.5	45.5
20	16.0	22.0	24.5	24.0

The first observation is that the corresponding peak current heights differ between the two methods indicating that there is a contribution from kinetics to the experimental output. Also at both concentrations of supporting electrolyte the peak current heights increase as the differential pulse waveform period is reduced. However, this effect is less pronounced at the larger concentration of supporting electrolyte suggesting that the current recovers more rapidly on termination of the pulse. These results support the assumption that there is a contribution to the large peak current heights from slow electron transfer kinetics. Thus the technique and the models described above would prove useful only for a reversible couple. This does not limit the method to a great extent since many enzyme linked assays use reversible couples [14].

The above models are simplified with no kinetics. However, to take kinetics into account numerical methods would have to be employed. These are not stable on account of the rapid changes in potential.

#### 2.4.7 Electroanalysis with microelectrodes using Microsoft Excel Solver

The current response obtained by the application of a linear ramp waveform to a microelectrode in a solution of ferrocyanide at a sweep rate of 10mV/sec. is shown in Fig. 2.6(♦). The height of the plateau corresponds to the limiting current ( $i_L$ ) which is proportional to the concentration of the analyte in solution. However a problem arises in the determination of  $i_L$  as only rarely is the limiting current plateau parallel to the baseline. Extrapolation of the tails of the trace and measuring the perpendicular distance between them is another option but again a problem arises if the tails are not parallel. These conditions introduce an element of subjectiveness into the determination of  $i_L$ .

By collecting and digitally storing the current response it is possible to obtain a value for concentration (C) using the complete voltammetric curve, rather than the limiting current alone. Microsoft Excel Solver provides a means of achieving this simply and effectively.

Before Microsoft Excel Solver can be used to determine unknown concentrations a spreadsheet must first be prepared which consists of a list of theoretical data and a corresponding list of experimental data. The list of experimental data is created by importing the data acquired during the experiment into the Excel spreadsheet while the list of theoretical data is created by means of a model of the system. In this case the equation representing the microelectrode response for a reversible couple is used to generate the list of theoretical data. This equation is as follows [15]:

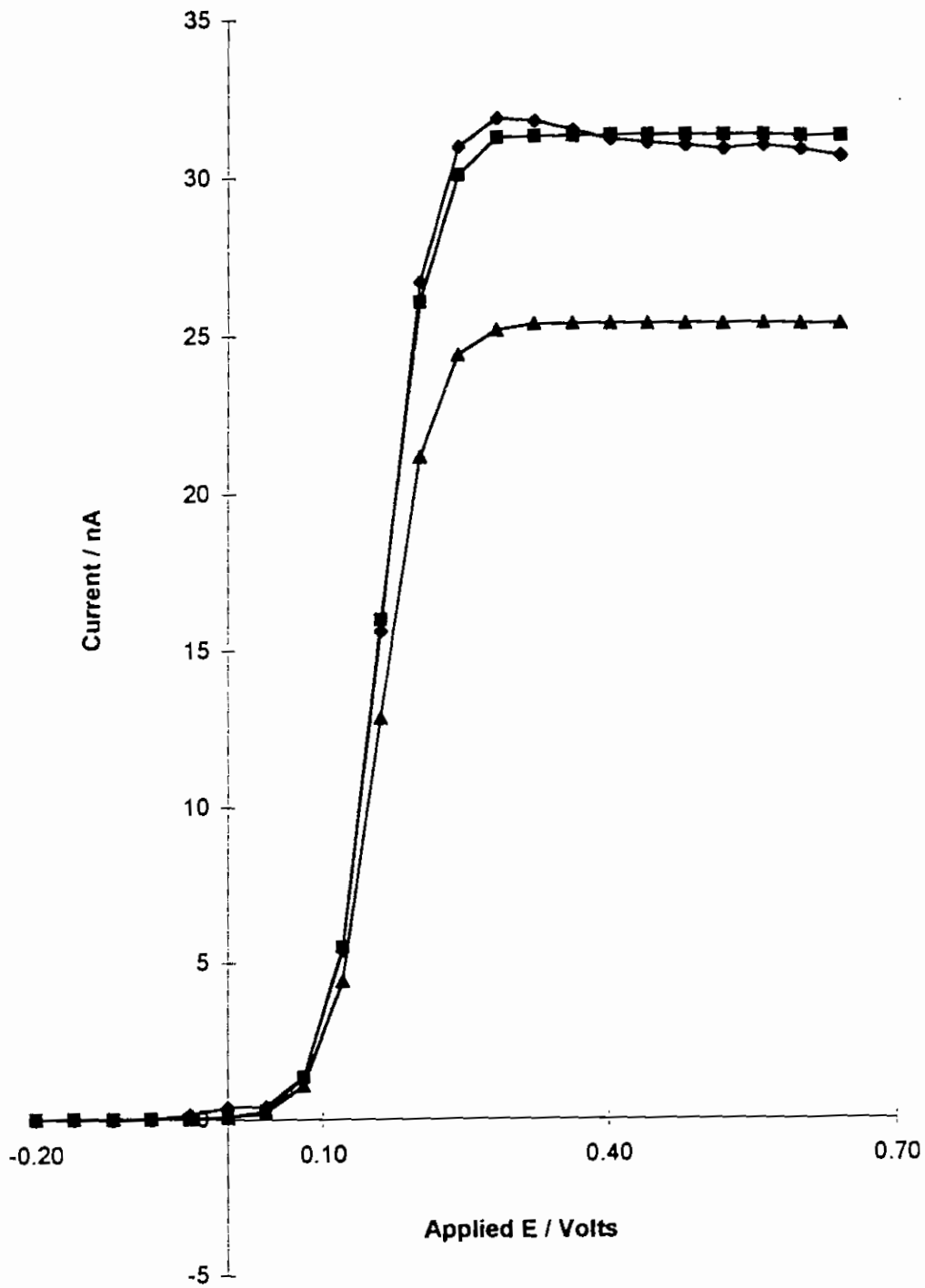


Figure 2.6. Current profiles corresponding to (♦) experimental data where microelectrode radius =  $2.53 \times 10^{-3}$  cm, sweep rate =  $10 \text{ mVs}^{-1}$ , concentration of ferrocyanide (C) is 5 mM, in 0.1M KCl (■). Theoretical data set from Figure 2.7 after the fitting process has been completed and (▲) theoretical data set from Figure 2.7 prior to activating solver where a value of  $4 \times 10^{-3}$  M was used for C.



$$i = \frac{4nFrDC}{1 + \exp\left(\frac{nF(E - E^{0'})}{RT}\right)} \quad (2.12)$$

where,  $n$  = number of electrons involved in the reaction,  $F$  = Faraday's constant,  $r$  = radius of the electrode,  $D$  = diffusion coefficient of the analyte,  $C$  = concentration of the analyte in solution,  $E$  = applied potential and  $E^{0'}$  = formal potential.

This equation describes the complete current-potential curve obtained under voltammetric conditions for a reversible system; the numerator determining the limiting current and the denominator determining the change in current as a function of potential.

The typical spreadsheet layout before fitting and a set of typical experimental parameters is given in Fig 2.7. The rows are labelled 1,2,3.... down and the columns are labelled A,B,C... across. The figures in cells A1 to E1 and A2 to B2 are experimental parameters and constants which must be entered by the student and row 3 consists of a series of labels. A typical set of experimental parameters and constants corresponding to the conditions detailed in the experimental section are included in the figure legend. Columns A and C are filled by imported experimental data for potential and current respectively while column B, the model values, are generated by entering the following equation in cell B4:-

$$=((4*SA1*SB1*SC1*SD1*SE1)/(1+EXP(SB2*(A4-SA2))))$$

Figure 2.7: Typical layout of the Excel Spreadsheet prior to activating Solver. Typical values for experimental parameters and constants are as follows:  $n=1$ ,  $F= 96487 \text{ C mole}^{-1}$ ,  $r = 2.53 \times 10^{-3} \text{ cm}$ ,  $D = 6.5 \times 10^{-6} \text{ cm}^2 \text{ sec}^{-1}$ ,  $C = \text{unknown}$ ,  $E^0 = 0.15 \text{ V}$ ,  $nF/RT=39.608$ . Both columns B and C are multiplied by a factor of  $10^9$  to improve the quality of the fitting process.

n	F	r	D	C
$E^0$	$nF/RT$			
Applied E	Model	Data	Residuals <sup>2</sup>	SSR
-2.00E-01	1.67E-05	0.00E+00	2.78E-10	425.1851778
-1.60E-01	8.13E-05	0.00E+00	6.60E-09	
-1.20E-01	0.00039617	-3.30E-02	1.12E-03	
-8.00E-02	0.001931596	0.00E+00	3.73E-06	
-4.00E-02	0.009415637	1.33E-01	1.53E-02	
0.00E+00	0.045844507	3.67E-01	1.03E-01	
4.00E-02	0.221982956	4.00E-01	3.17E-02	
8.00E-02	1.046903188	1.33E+00	8.01E-02	
1.20E-01	4.401216425	5.40E+00	9.98E-01	
1.60E-01	12.83551429	1.56E+01	7.64E+00	
2.00E-01	21.14652325	2.67E+01	3.08E+01	
2.40E-01	24.38466483	3.10E+01	4.38E+01	
2.80E-01	25.17528862	3.19E+01	4.52E+01	
3.20E-01	25.37865481	3.18E+01	4.12E+01	
3.60E-01	25.38581218	3.15E+01	3.74E+01	
4.00E-01	25.38728057	3.12E+01	3.38E+01	
4.40E-01	25.38758174	3.11E+01	3.26E+01	
4.80E-01	25.3876435	3.10E+01	3.15E+01	
5.20E-01	25.38765617	3.09E+01	3.04E+01	
5.60E-01	25.3876435	3.10E+01	3.15E+01	
6.00E-01	25.38765877	3.09E+01	3.04E+01	
6.40E-01	25.3876593	3.07E+01	2.82E+01	

The column of data is then created using the **Edit**→**Fill**→**Down** command. Column D contains a list of the square of the residuals between each pair of model and experimental current data points and the number in cell E4 is the sum of squared residuals (SSR). This is the value which Solver will attempt to minimise during the curve fitting process. Either a single variable,  $C$ , or two variables,  $C$  and  $E^{0'}$  can be optimised during this operation. Once these columns of data have been generated Solver is activated. This procedure is described in previous publications [16].

With microelectrodes the currents involved tend to be quite small, typically nanoamps. Original attempts to fit the experimental and theoretical data sets for these experiments gave unsatisfactory results, Solver failing to fit the data sets perhaps because it was unable to process the small numbers involved. To overcome this problem both the theoretical and experimental data sets were multiplied by a factor of  $10^9$ . This enhanced the performance of the curve fitting to an acceptable level. On further investigation it was found that Solver was unable to function when the value of the sum of squared residuals (SSR) fell below  $2 \times 10^{-9}$ .

Figure 2.6 shows the current profiles corresponding to the experimental data in Figure 2.7, the current profile produced by the model before fitting with an initial guess by eye of the value of  $C$  of  $4 \times 10^{-6}$  moles  $\text{cm}^{-3}$  and the current profile returned by the model on completion of the fitting process. For the reason outlined above both the theoretical and experimental data sets were multiplied by a factor of  $10^9$  before activation of Solver. In this example both  $C$  and  $E^{0'}$  are variable parameters. From the answer report it was

seen that the SSR was reduced from 425.18 to 3.37 and that a value for C of  $4.94 \times 10^{-6} \text{M}$  was returned. This is a recovery of 98.8% on a standard concentration of  $5.00 \times 10^{-6} \text{M}$   $[\text{Fe}(\text{CN})_6]^{4-}$ . The constraints which were applied to the operation of the fitting process were chosen to prevent Solver from returning a negative value for concentration or formal potential.

To test the validity of this technique a series of solutions of known concentration were prepared and analysed using this method. Table 2.8 contains the nominal concentrations of the standard solutions (C) and the concentrations returned by Solver (C').

Table 2.8: Comparison of standard concentration values with those returned by Solver. The percentage recovery calculated as  $\frac{\text{Value returned by Solver}}{\text{Standard concentration}} \times 100$  is quoted in

brackets and is a measure of the correlation between the calculated and real concentrations.

Standard Concentration (C)	Value returned by Solver when only C varied (moles $\text{dm}^{-3}$ )	Value returned by Solver when both C and $E^0$ varied (moles $\text{dm}^{-3}$ )
$1 \times 10^{-2}$	$9.86 \times 10^{-3}$ (98.6)	$9.89 \times 10^{-3}$ (98.9)
$5 \times 10^{-3}$	$4.86 \times 10^{-3}$ (97.2)	$4.92 \times 10^{-3}$ (98.4)
$1 \times 10^{-3}$	$1.06 \times 10^{-3}$ (106)	$1.05 \times 10^{-3}$ (105.0)
$5 \times 10^{-4}$	$5.12 \times 10^{-4}$ (102.4)	$4.91 \times 10^{-4}$ (98.2)
$1 \times 10^{-4}$	$2.22 \times 10^{-4}$ (45.0)	$2.22 \times 10^{-4}$ (45.0)

The percentage recovery is also quoted and serves as a measure of the correlation between the data sets. It can be seen that the concentration values returned by Solver correlate well with the nominal concentrations over the range  $1 \times 10^{-2} \text{M}$  to  $5 \times 10^{-4} \text{M}$ . However at lower concentrations the correlation becomes less satisfactory. Noise,

although present in all the traces becomes a problem at lower currents as it alters the overall shape of the trace as can be seen in Fig. 2.8. Below concentrations of  $5 \times 10^{-4} \text{M}$  the experimental trace deviates from the sigmoidal shape and the model is unable to compensate for this. Obviously this greatly affects the ability of Solver to fit the experimental and theoretical data sets and therefore affects the accuracy of the results. The presence of this noise is a limitation of the potentiostat employed in this work and there appears to be no reason why lower concentrations could not be analysed with the aid of a more noise free system.

It was also found that fitting the experimental and theoretical data sets by allowing Solver to simultaneously vary the values of  $C$  and  $E^{0'}$  (the formal potential) resulted in concentration values closer to the nominal values than those obtained by varying only  $C$  as can be seen in Table 2.8. In this way the information contained in the full sigmoidal shape is employed to yield an answer rather than just the limiting current. The value of fitting the model with two variables can be clearly seen.

## **2.5 Conclusions**

In conclusion, there is good correlation between Model 2 and the numerical derivative of a linear sweep potential waveform applied to a microelectrode. A differential pulse study does not correlate as well perhaps due to slow kinetics. Model 1 will apply for

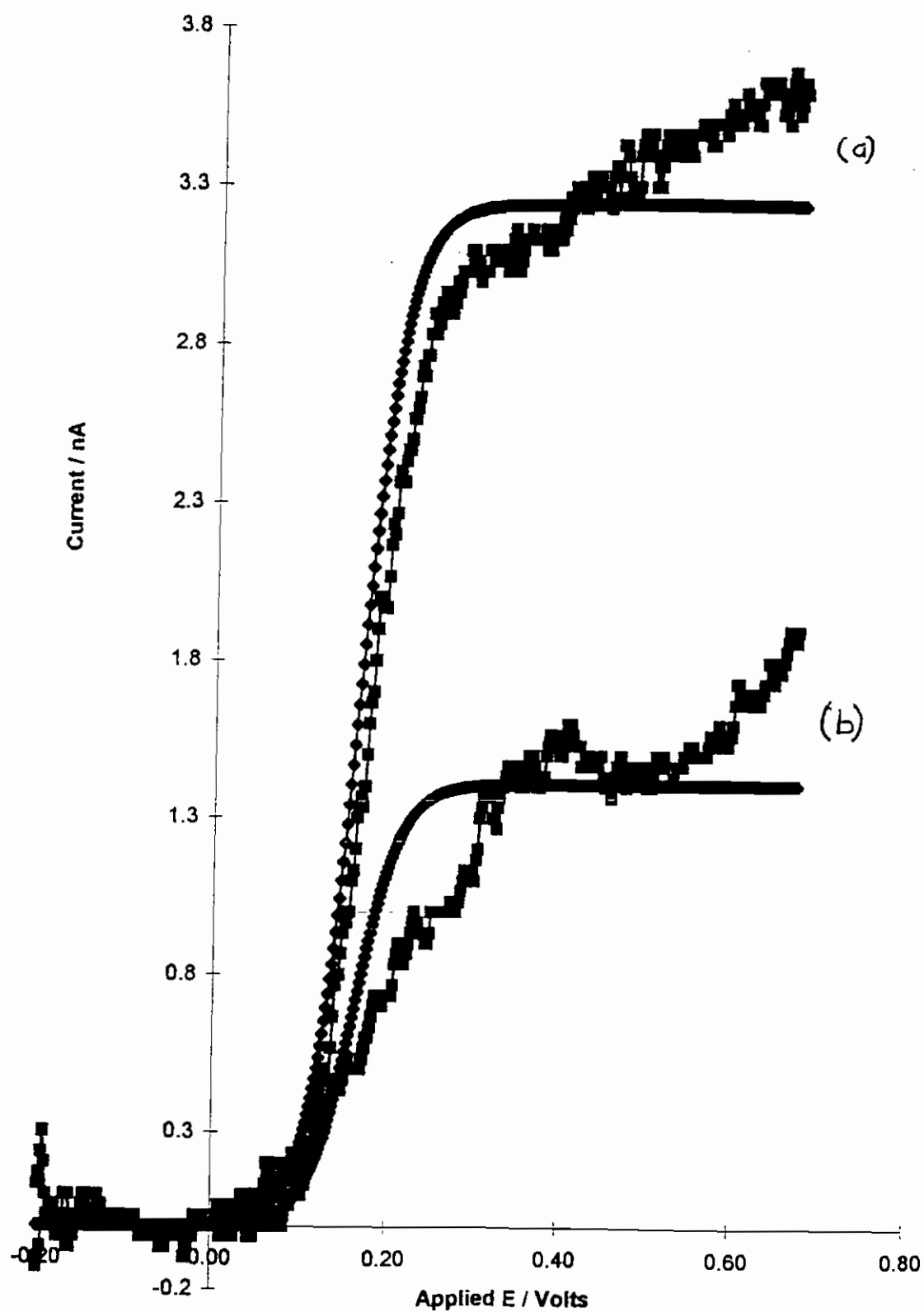


Figure 2.8 The fitting of experimental data, ( $\blacksquare$ ) to the model ( $\blacklozenge$ ) for (a)  $5 \times 10^{-4} \text{ M}$  ferrocyanide and (b) for  $1 \times 10^{-4} \text{ M}$  ferrocyanide. All other experimental conditions as in Figure 2.6

larger electrodes and further work is required to examine the effect of slow kinetics on the differential pulse response.

It is possible to use curve fitting techniques as a means of determining unknown concentrations for a reversible system to a high degree of accuracy; the limits of quantitation being governed by the presence of noise in the system. Similarly any one or a combination of the other variables in the model can be determined in a similar fashion.

## 2.6 References

1. R.M. Wightman, D.O. Wipf in *Electroanalytical Chemistry*, A.J. Bard, Ed. M.Dekker, New York, Vol. 15 (1988).
2. S. Pons, M. Fleischmann, *Anal.Chem.* **59**, 1391A, (1987).
3. R.M. Wightman, *Science*, **240**, 415, (1988).
4. A. Fitch, D.H. Evans, *J. Electroanal. Chem.* **202**, 83, (1986).
5. J.F. Cassidy, M.B. Foley, *Chemistry in Britain* **9**, 764, (1993).
6. J.A. Stamford, *J. Neurosci Methods*, **17**, 1, (1986).
7. J.B. Justice, Ed. *Voltammetry in the Neurosciences* Human Press, Clifton, NJ, (1987)
8. R.M. Wightman, L.J. May, A.C. Michael, *Anal.Chem.* **60**, 769A,(1988).
9. D.T. Sawyer, J.L. Roberts in *Experimental Electrochemistry for Chemists*, Wiley, New York, p.77, (1974)
10. M. Fleischmann, S. Pons, D. Rolison, P.P. Schmidt, *Ultramicroelectrodes*, Datatech Science, Morganton, NC, (1987)
11. A.C. Wahl, *Z. Elektrochem.*, **64**, 90, (1960).
12. M. Shporer, G. Ron, A. Loewenstein, G. Navon, *Inorg.Chem.*, **4**, (1965), 361
13. L.M.Peter, W.Durr, P.Bindra and H.Gerisher, *J.Electroanal. Chem.* **71**, 31, (1976)
14. J.F. Cassidy, C. Clinton, W. Breen, R. Foster, E. O' Donoghue, *Analyst*, **118**, 415, (1993).
15. A.J. Bard; L.R. Faulkner, *Electrochemical Methods-Fundamentals and Applications* Pg 159 Wiley: New York (1980).
15. D. Diamond, *Spreadsheet Applications in Chemistry using Microsoft Excel*; Wiley: New York, (1997).



## Chapter 3

### *Differential Pulse Voltammetry at a Rotating Disk Electrode*

#### 3.1 Introduction

Until the middle of the 1940's, theoretical electrochemistry developed primarily as the electrochemistry of the mercury electrode. Then in 1942 Levich [1] found from his study of convective diffusion in moving media that an electrode in the form of a rotating disk exhibits a unique combination of advantageous factors. These include the possibility of exact calculation of the diffusion flow, the uniform accessibility of the surface with respect to diffusion, and a steady state regime. These advantages suggested that the rotating disk electrode had the potential to become a valuable tool for electrochemical investigations.

Soon after Levich's discovery Siver and Kabanov [2] succeeded in using the RDE experimentally and demonstrated that the calculated values of limiting currents were in good agreement with the experimental values. By the 1970s 100-200 papers were being published annually reporting results obtained using the RDE method. The method has been applied to the mechanism and kinetic characteristics of electrode reactions, to the study of homogeneous chemical reactions involved in electrochemical processes, and to measuring the diffusion coefficients and the concentrations of solutes[3-5]. The

technique is widely used in electroanalytical chemistry since a variety of electrode reactions taking place in a wide potential range may be studied for analytical purposes.

Another advantage that this technique has over those involving mercury electrodes is that both anodic and cathodic reactions may be studied by choosing an appropriate metal. The RDE also has the advantage over mercury electrodes of being able to determine higher electrochemical rate constants. Furthermore modulated rotation rates have been used.

One drawback however, is that the sigmoidal response of the R.D.E. can sometimes be rather difficult to interpret, especially at low analyte concentrations. One way to solve this problem is to apply a differential pulse waveform to the R.D.E., which converts the sigmoidal response to a peaked voltammogram. This makes the signal easier to interpret, but also introduces additional theoretical considerations [6]. The aim of this work is to characterise the response obtained from applying a differential pulse waveform to an R.D.E., in a solution of a reversible electrochemical system; namely potassium ferrocyanide.

### 3.2 Theory

A differential pulse waveform, which is effectively a ramp potential waveform on top of which a series of pulses of width  $\delta$ , which are separated by a time interval,  $\tau$ , are applied to a rotating disk electrode in a solution of a reversible couple, namely  $[\text{Fe}(\text{CN})_6]^{3-/4-}$ .

Two straightforward models of the current response are proposed here. Model 1 assumes that the current subsequent to the pulse dominates, while Model 2 assumes that the pulse width is sufficiently long to allow a steady-state current to exist during the pulse width.

#### Model 1

A differential pulse waveform of pulse width  $\delta$ , where the interval between pulses is  $\tau$ , is applied to a rotating disk electrode. The resulting differential current,  $\partial i$ , is a combination of the current sampled before the pulse,  $i_2$ , and just before the end of the pulse;  $i_1 + i_3$ . The differential current for a reduction process is;

$$\partial i = i_1 + i_3 - i_2 \quad 3.1$$

where the current associated with the pulse,  $i_1$ , is taken to be independent of the underlying current;

$$i_1 = \frac{nFA\sqrt{DC}}{\sqrt{\pi\delta}} \left[ \frac{(1-\sigma^2)\epsilon_1}{(1+\epsilon_1)(1+\sigma^2\epsilon_1)} \right] \quad 3.2$$

where

$$\sigma^2 = \exp\left(\frac{-nF\Delta E}{RT}\right) \quad 3.3$$

and

$$\varepsilon_1 = \exp\left(\frac{-nF(E_1 - E^0)}{RT}\right) \quad 3.4$$

where  $\Delta E$  = pulse amplitude,  $E_1$  is the potential before the pulse is applied and all the other symbols have their usual meaning.

The current before the pulse is applied,  $i_2$ , depends on  $E_1$  and is represented as follows;

$$i_2 = \frac{0.62nFAD^{2/3}\omega^{1/2}\nu^{-1/6}C}{(1 + \varepsilon_1)} \quad 3.5$$

and the current at the end of time  $\delta$ , if the pulse were not applied would be;

$$i_3 = \frac{0.62nFAD^{2/3}\omega^{1/2}\nu^{-1/6}C}{(1 + \varepsilon_2)} \quad 3.6$$

where

$$\varepsilon_2 = \exp\left(\frac{-nF(E_2 - E^0)}{RT}\right) \quad 3.7$$

where  $E_2$  is the potential magnitude at time  $\delta$  after the time when the voltage is  $E_1$  without the pulse being applied. The contribution of the current from the pulse is  $i_1$ .  $\partial i$  is plotted against  $E_1 + \Delta E$ , where  $E_1$  is the base potential.

### Model 2

For a pulse width,  $\delta$ , of 55 msec and when  $D = 6.5 \times 10^{-6} \text{ cm}^2 \text{ sec}^{-1}$  [7] the diffusion layer thickness  $d_1$ , where  $d_1 \cong (\pi D t)^{1/2}$ , is  $1.06 \times 10^{-3} \text{ cm}$ . From R.D.E. theory [8], the effective diffusion layer thickness,  $d_2 = 1.61 D^{1/3} \omega^{-1/2} \nu^{1/6}$  and at  $f = 2000 \text{ rpm}$   $d_2 = 0.96 \times 10^{-3} \text{ cm}$ . Therefore a steady state response can arise within the timescale of the pulse width. The resulting differential pulse current,  $\partial i'$ , is as follows;

$$\partial i' = i_4 - i_2 \quad 3.8$$

where

$$i_4 = \frac{0.62 n F A D^{2/3} \omega^{1/2} \nu^{-1/6} C}{(1 + \varepsilon_3)} \quad 3.9$$

$$\text{where } \varepsilon_3 = \exp \left( \frac{-nF(E_2 + \Delta E - E^0)}{RT} \right) \quad 3.10$$

$\partial i'$  is plotted against  $E_1 + \Delta E/2$ .

An important aspect of equations 3.1 and 3.8 is that the differential currents in each case are directly related to the concentration of substrate.

### 3.3 Experimental

All experiments were carried out using an Edt potentiostat Model ECP 100, and at room temperature. A J.J.Lloyd X-Y chart recorder Model PL3 was used to chart the response and an EG&G Parc M394 system was used to digitally acquire the signals. A three electrode one compartment system was used where the working electrode was a platinum disk rotated using a Metrohm 628-10 system; the reference was a saturated calomel electrode and the auxiliary was a carbon rod. All chemicals used were of reagent grade and all solutions were prepared using de-ionised water. All solutions were degassed for at least 10 minutes prior to analysis and a positive nitrogen pressure was maintained above the cell during analysis. The cell was blackened to minimise exposure of the ferrocyanide solution to light. The electrode area was determined from limiting current measurements. The simulations were calculated using a computer program written in Microsoft EXCEL.

### 3.4 Results and Discussion

#### 3.4.1 Determination of the active electrochemical area of the electrode

From the limiting currents recorded at rotation rates in the range 500 RPM to 3000 RPM in a solution of 1mM  $[\text{Fe}(\text{CN})_6]^{4-}/0.1\text{M KCl}$ , taking  $D = 6.5 \times 10^{-6} \text{cm}^2 \text{sec}^{-1}$  [7],  $\nu = 0.01 \text{cm}^2 \text{sec}^{-1}$  the electrode area was determined from a plot of  $i_L$  against  $\omega^{1/2}$  to be

0.0703cm<sup>2</sup> (correlation coefficient =0.9993). On occasion during the experimental work it was deemed necessary to polish the electrode surface. This required that the electrode area be re-determined. However after polishing with 1µm alumina it was found that the electrode area was consistently 0.0703 ± 0.0005cm<sup>2</sup>.

### 3.4.2 Characterisation of RDE response to a differential pulse waveform

Figures 3.1 and 3.2 show the experimental differential pulse voltammograms at a rotating disk electrode as a function of pulse amplitude ( $\Delta E$ ) and rotation rate ( $\omega$ ) respectively. It can be seen that the peak current heights increase with increasing pulse amplitude and to a smaller extent with rotation rate. Pulse widths at half height were found to be constant over the range of pulse amplitudes and rotation rates studied. Varying the differential pulse waveform period was found to affect the peak current heights and this observation will be discussed in a later section.

It can be seen that the background signal varies with pulse amplitude perhaps due to double layer charging. It is clear that analytically useful information can be taken from these plots.

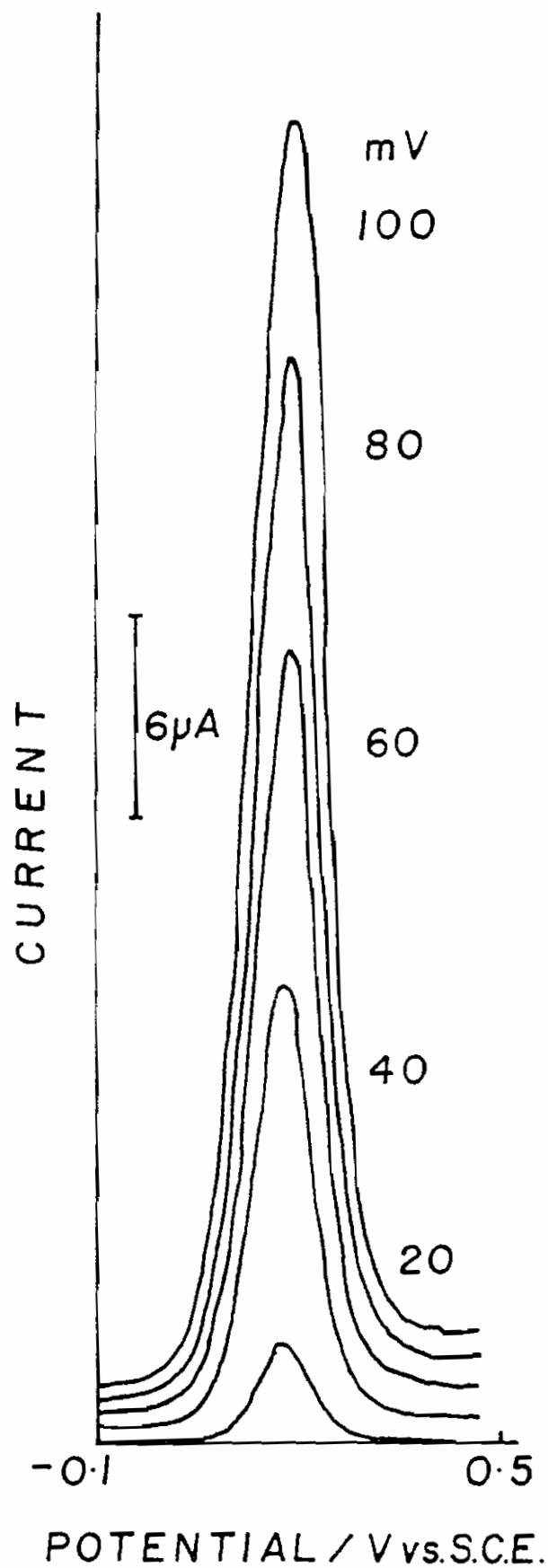


Fig. 3.1 Effect of pulse amplitude on the DPRDE response for  $1 \text{ mM } [\text{Fe}(\text{CN})_6]^{4-}$  in aqueous  $1.0 \text{ M KCl}$ . Platinum disk electrode area =  $0.0703 \text{ cm}^2$ , scan rate =  $10 \text{ mV sec}^{-1}$ , rotation rate =  $1000 \text{ RPM}$ , DPWP =  $0.50 \text{ secs.}$ , pulse amplitude =  $55 \text{ msec.}$  Pulse amplitudes are indicated in the figure.



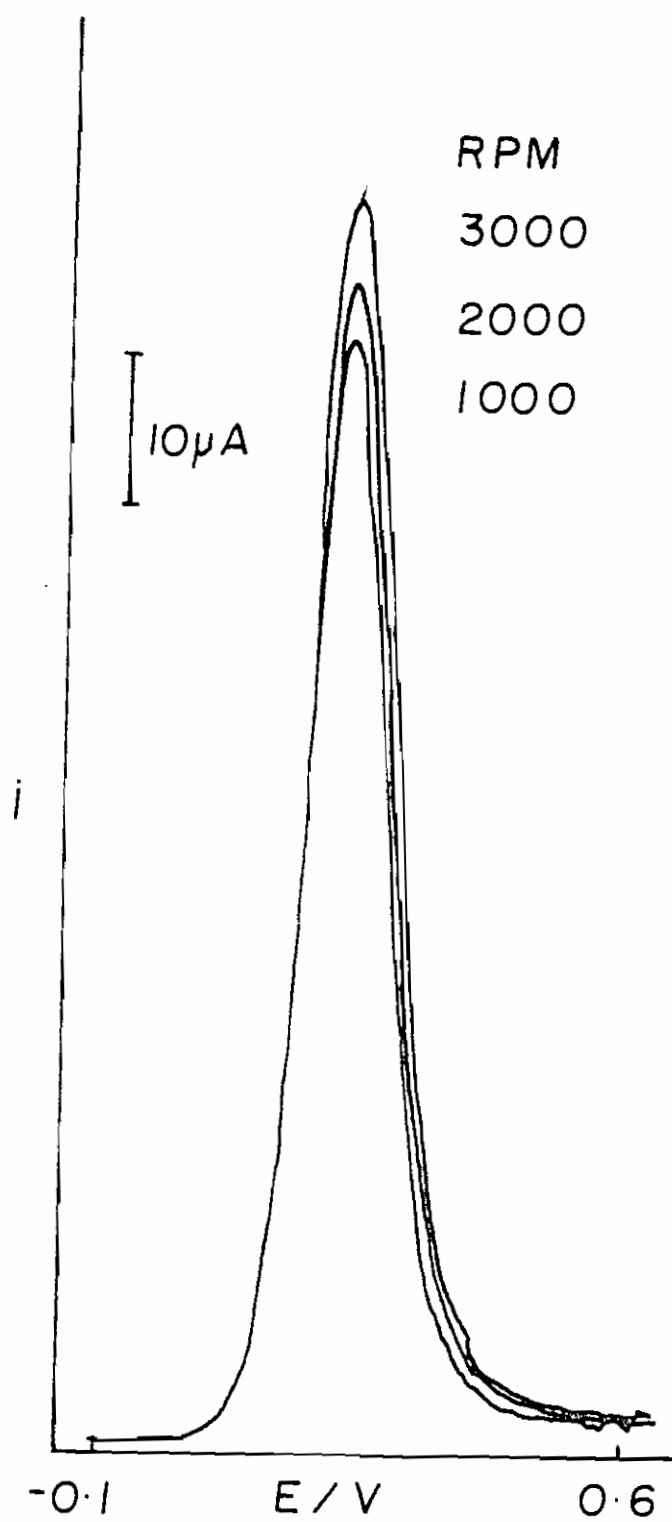


Fig. 3.2 Effect of the rotation rate on the DPRDE response for  $5 \text{mM } [\text{Fe}(\text{CN})_6]^{4-}$  in aqueous  $1.0 \text{M KCl}$ . Pulse amplitude =  $50 \text{ mV}$ . Conditions as in Fig. 3.1. Rotation rates are indicated in the figure.

### 3.4.3 Generation of theoretical data set for comparison with experimental results

Simulations of the two models discussed in section 3.2 were carried out by inputting the equations in Microsoft EXCEL and plotting the differential current ( $\partial i$ ) as a function of applied potential (E). Figure 3.3 is typical of the traces produced by these simulations. The example given is a simulation of Model 2 at pulse amplitudes in the range 20mV to 100mV at 1000 RPM and is typical of the response obtained. On comparing this simulation with the experimental traces of Figures 3.1 and 3.2 it is apparent that not only do they follow the same trends that were observed in the experimental traces but also the peak current heights and pulse widths at half heights are similar. A more quantitative comparison of the correlation between the models and experimental traces is given in the following sections.

The numerical derivative of the current response produced by applying a linear ramp waveform to the system was also determined. This was trivial requiring only a basic potentiostat and waveform generator, a data acquisition unit and a personal computer with relevant software, namely Microsoft EXCEL. This technique also produced a peaked response as expected and its merits with respect to the other techniques and theoretical treatments mentioned will be discussed in this chapter.

The ideal sigmoidal response produced by the application of a linear ramp waveform under steady state conditions is characterised by the following equation[8]:

$$i = \frac{0.62nFACD^{\frac{2}{3}}\omega^{\frac{1}{3}}\nu^{-\frac{1}{6}}}{1 - \exp\left[\frac{nF(E - E^{\circ'})}{RT}\right]} \quad (3.11)$$

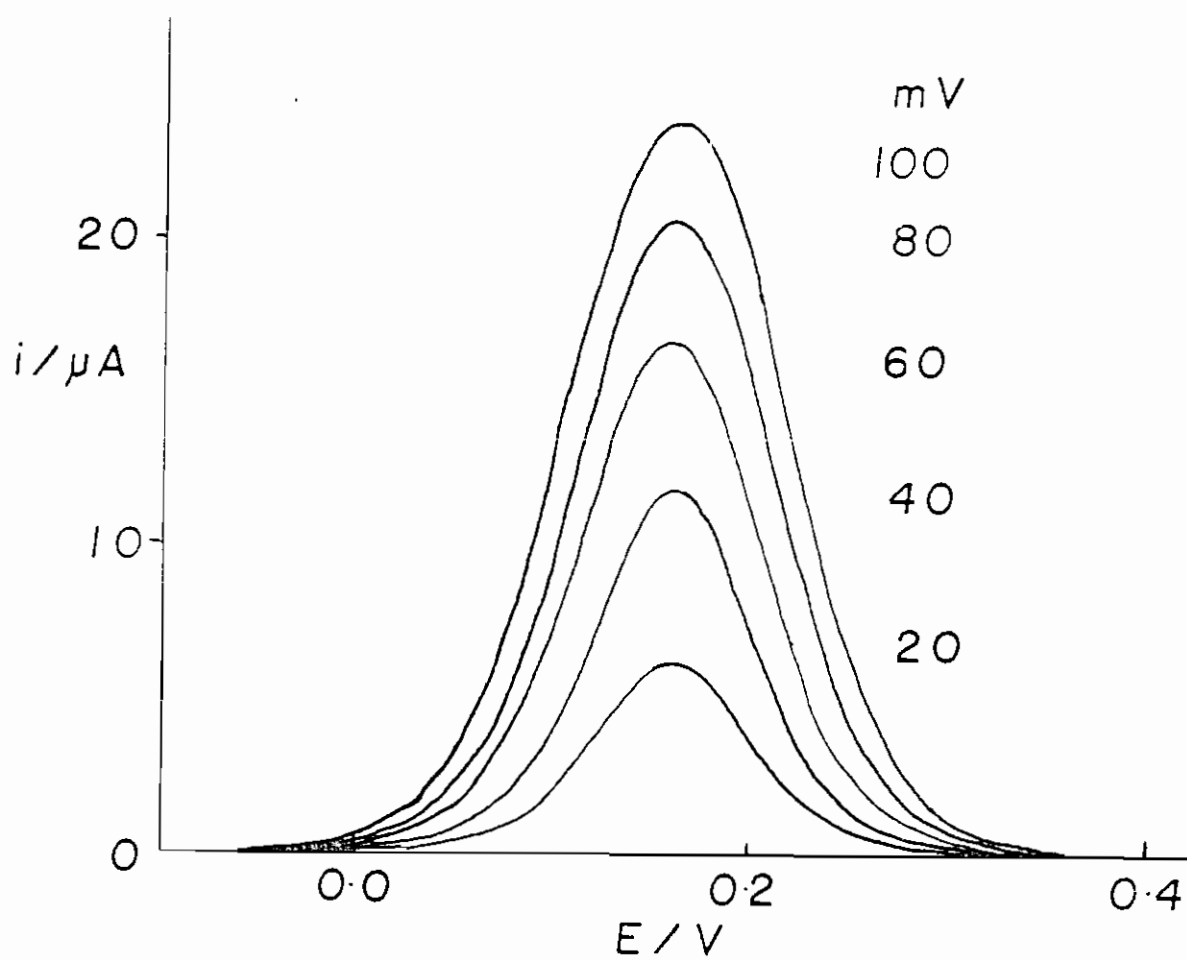


Fig. 3.3 Simulated DPRDE response from Model 2.  $E' = 0.16$  V, diffusion coefficient =  $6.32 \times 10^{-6} \text{cm}^2 \text{sec}^{-1}$ , kinematic viscosity =  $0.01 \text{cm}^2 \text{sec}^{-1}$ . Conditions as in Fig. 3.1.

It was therefore assumed that the derivative of this equation with respect to the applied potential would describe the ideal differential response. This equation takes the form;

$$\frac{di}{dE} = \frac{-0.62nFAD^{\frac{2}{3}}\omega^{\frac{1}{2}}\nu^{-\frac{1}{6}}C \exp\left(\frac{nF(E - E^{0'})}{RT}\right) \frac{nF}{RT}}{\left[1 + \exp\left(\frac{nF(E - E^{0'})}{RT}\right)\right]^2} \quad (3.12)$$

A simulation of this equation was carried out in EXCEL and by assuming that  $dE$  equals  $\Delta E$  it was possible to determine a set of theoretical peak current heights for a range of pulse amplitudes by this method. The effect of varying the rotation rate on the simulations was also studied and the results obtained are displayed in Tables 3.1, 3.2 and 3.3. Also contained in these tables are the peak current heights returned by the various methods mentioned above. A detailed discussion of the relevance, correlation and relative strengths of these methods is given below.

Table 3.1: Comparison of the experimental (columns 2 and 3) and theoretical results obtained for a differential pulse study at a platinum RDE rotating at 1000RPM. 1mM  $[\text{Fe}(\text{CN})_6]^{4-}/1\text{M KCl}$ , sweep rate =  $10\text{mV sec}^{-1}$ , electrode area  $0.0703\text{cm}^2$ , pulse amplitudes and differential pulse waveform periods are shown in the table. DPWP = Differential Pulse Waveform Period.

Peak Current Heights in $\mu\text{A}$						
Pulse Ampl. mV	D.P. Study DPWP=0.5s	D.P. Study DPWP=1.0s	Model 1	Model 2	Numerical Derivative	Simulation of eqn. 3.12
100	39.80	36.80	31.11	23.39	21.82	30.86
80	31.40	30.40	27.14	20.95	18.86	23.77
60	24.10	22.4	22.00	17.00	15.57	18.51
40	15.6	14.6	15.61	11.90	11.02	12.34

20	5.2	5.2	8.00	6.13	5.91	6.17
----	-----	-----	------	------	------	------

Table 3.2 Comparison of the experimental and theoretical results obtained for a differential pulse study at a platinum RDE rotating at 2000RPM. Conditions as Table 3.1.

Peak Current Heights in $\mu\text{A}$						
Pulse Ampl. mV	D.P. Study DPWP=0.5s	D.P. Study DPWP=1.0s	Model 1	Model 2	Numerical Derivative	Simulation of eqn. 3.12
100	40.40	38.60	31.11	33.89	31.41	43.64
80	33.80	32.70	26.90	29.53	27.19	34.91
60	26.10	24.90	22.00	24.00	21.72	26.18
40	16.60	15.80	15.43	16.86	15.00	17.45
20	6.20	6.00	8.07	8.78	8.13	8.73

Table 3.3 Comparison of the experimental and theoretical results obtained for a differential pulse study at a platinum RDE rotating at 3000RPM. Conditions as Table 3.1.

Peak Current Heights in $\mu\text{A}$						
Pulse Ampl. mV	D.P. Study DPWP=0.5s	D.P. Study DPWP=1.0s	Model 1	Model 2	Numerical Derivative	Simulation of eqn. 3.12
100	43.80	42.60	31.43	41.78	36.90	51.47
80	36.60	35.60	26.88	35.62	32.07	42.76
60	28.10	27.00	21.90	29.29	25.69	32.07
40	17.80	17.20	15.70	20.80	18.28	21.38
20	7.00	6.20	8.10	10.76	9.66	10.69

Table 3.4: Comparison of the experimental and theoretical results obtained for a differential pulse study at a platinum RDE rotating at 1000RPM. 1mM  $[\text{Fe}(\text{CN})_6]^{4-}$  /0.1M KCl, sweep rate = 10mV sec<sup>-1</sup>, electrode area 0.0703cm<sup>2</sup>, pulse amplitudes and differential pulse waveform periods are shown in the table.

Pulse Ampl. mV	Peak Current Heights in $\mu\text{A}$					
	D.P. Study DPWP=0.5s	D.P. Study DPWP=1.0s	Model 1	Model 2	Numerical Derivative	Simulation of eqn. 3.12
100	31.40	28.80	31.66	24.44	19.32	31.45
80	24.20	23.40	27.38	21.43	16.59	25.15
60	18.40	17.60	22.18	17.23	13.18	18.87
40	11.80	10.80	15.70	12.25	9.32	12.57
20	4.60	4.20	8.14	6.36	4.89	6.29

Table 3.5 Comparison of the experimental and theoretical results obtained for a differential pulse study at a platinum RDE rotating at 2000RPM. Conditions as

Table 3.4.

Pulse Ampl. mV	Peak Current Heights in $\mu\text{A}$					
	D.P. Study DPWP=0.5s	D.P. Study DPWP=1.0s	Model 1	Model 2	Numerical Derivative	Simulation of eqn. 3.12
100	30.40	30.10	31.67	34.72	24.05	44.47
80	25.00	23.80	27.38	30.00	20.36	35.57
60	19.00	17.40	22.40	24.60	15.95	26.68
40	11.80	11.20	15.71	17.14	10.95	17.78
20	4.80	4.20	8.21	9.00	5.71	8.56

Table 3.6 Comparison of the experimental and theoretical results obtained for a differential pulse study at a platinum RDE rotating at 3000RPM. Conditions as Table 3.4.

Pulse Ampl. mV	Peak Current Heights in $\mu\text{A}$					
	D.P. Study DPWP=0.5s	D.P.Study DPWP=1.0s	Model 1	Model 2	Numerical Derivative	Simulation of eqn. 3.12
100	32.70	31.00	31.78	42.14	27.38	54.45
80	26.50	24.40	27.19	36.25	23.21	43.57
60	20.20	17.80	22.14	29.76	18.10	31.47
40	12.50	11.00	15.90	23.20	12.38	21.78
20	4.80	4.20	8.28	10.95	6.66	10.89

#### 3.4.4 Evaluation of correlation between experimental and theoretical data

On comparing columns 2 and 3 of Tables 3.1-3.6 it is apparent that the magnitude of the differential pulse waveform period ( $\delta-\tau$ ) (DPWP) affects the magnitude of the peak current heights returned by the application of a differential pulse waveform to the system as all other experimental parameters were constant for these two data sets. The peak current heights are consistently higher at the shorter (DPWP). This can be explained by slow electron transfer kinetics inhibiting the recovery of the current after the pulse to such an extent that the current due to a pulse contains a contribution from the previous pulse. This effect would obviously be more pronounced at shorter DPWPs.

On inspection of the peak current heights returned by Model 1 it can be seen that the peak current heights returned are independent of rotation rate. This is because this model is based on the assumption that the current associated with the pulse ( $i_1$ ) dominates the response. On consulting eqn.3.2 it can be seen that  $i_1$  is independent of rotation rate ( $\omega$ ). Therefore this model is not suitable for this system as the experimental peak current heights vary with rotation rate.

The peak current heights returned by Model 2 follow the same trend as those returned experimentally, the peak current heights increasing both with rotation rate and pulse amplitude. However the magnitude of the peak current heights returned by this model fail to correlate well with those returned by applying a differential pulse waveform to the system, the experimental values being consistently larger than those predicted by the model. This can again be explained by a contribution to the experimental output from slow electron transfer kinetics which is not taken into account in the model.

However the peak current heights returned by Model 2 correlate very reasonably with those returned by the numerical derivative method over the complete range of pulse amplitudes and rotation rates studied at a concentration of  $KCl = 1.0M$ . The fact that these sets of data do not correlate as well at the lower concentration of electrolyte is evidence for the presence of slow electron transfer kinetics since it has been established that the rate of electron transfer in the ferri/ferrocyanide system shows a first order dependence on the concentration of cations in solution [9,10]. Slow kinetics affect the rate of current increase in the sigmoidal response which has the effect of reducing the peak current heights returned by the numerical derivative. At a concentration of



electrolyte of 1.0M the kinetics are fast and do not inhibit the rate of current increase in the sigmoidal curve and in this case Model 2 can be used to characterise the response as was found in Chapter 2.

The simulations of eqn. 3.12 fails to correlate with any of the data sets over the complete range of pulse amplitudes and rotation rates studied. However at a concentration of KCl = 1.0M the peak current heights returned by this simulation correlate well with those predicted by model 2 in the range 20-60mV. The fact that the correlation is not as satisfactory at larger pulse amplitudes is an indication that the assumption that  $\partial E = \Delta E$  is not quite justified.

#### 3.4.5 Determination of limits of detection and limits of quantitation.

Figure 3.4 shows the differential pulse response at ferrocyanide concentrations in the range  $1 \times 10^{-6} \text{M}$  to  $1 \times 10^{-4} \text{M}$ . It can be seen that the background current takes the form of a U-shaped curve and a peak can be seen at concentrations as low as  $5 \times 10^{-5} \text{M}$ . Peak current heights were determined for ferrocyanide concentrations in the range  $2 \times 10^{-4} \text{M}$  to  $10 \times 10^{-4} \text{M}$  and a graph of concentration against peak current height was plotted. This plot yielded a straight line of slope = 0.0491, intercept =  $6.349 \times 10^{-7}$  and standard deviation about the regression line =  $3.770 \times 10^{-7}$ . Taking the intercept to be the signal corresponding to the blank ( $S_b$ ) and the standard deviation about the regression line to be the standard deviation about the blank ( $\sigma_b$ ) the limits of detection and limit of

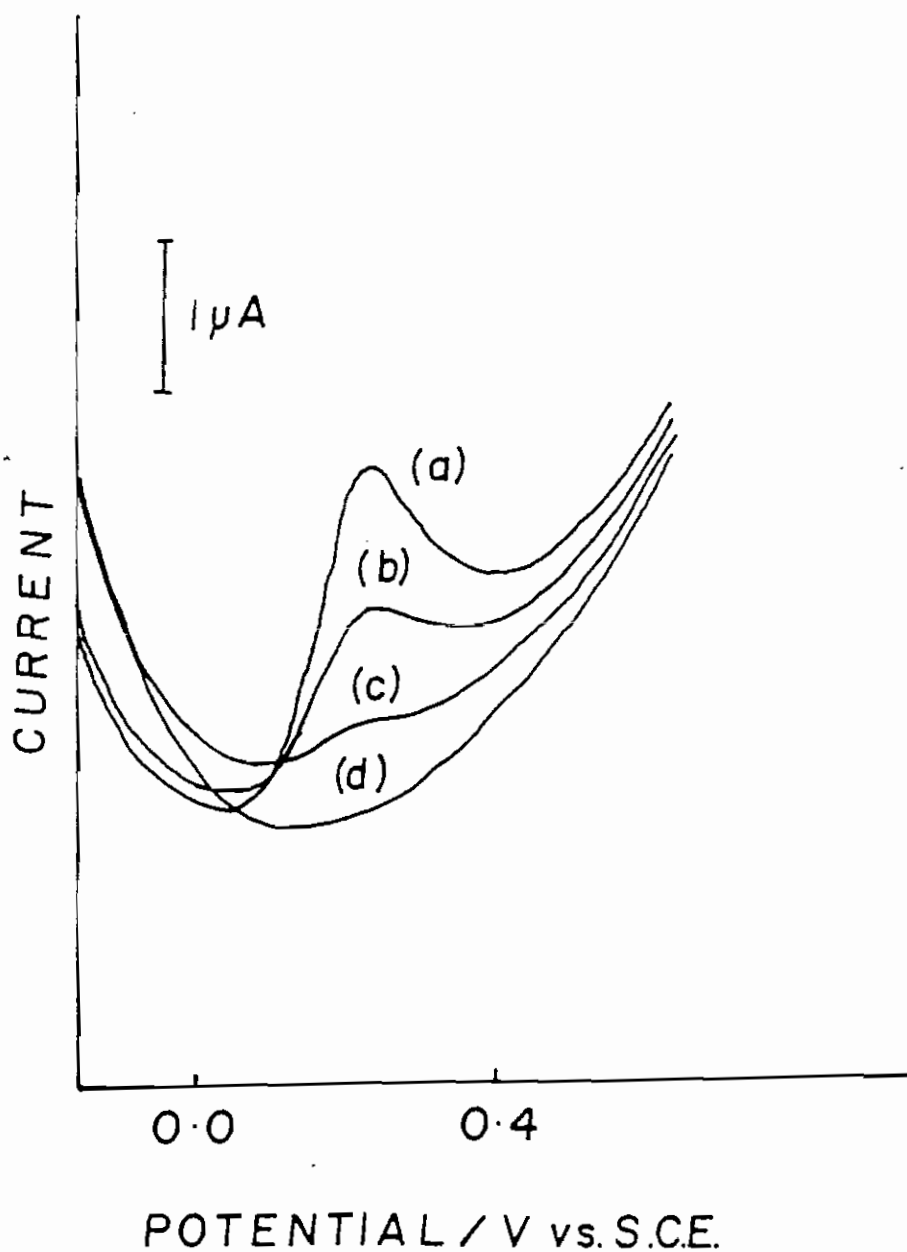


Fig. 3.4 Differential pulse response at low concentrations. Supporting electrolyte = 1.0 M KCl, pulse amplitude = 100 mV, DPWP = 0.50 secs., rotation rate = 1000 RPM, scan rate = 10 mV sec<sup>-1</sup>, pulse width = 55 msec. [Fe(CN)<sub>6</sub>]<sup>4-</sup> concentrations are as follows: (a) = 1 × 10<sup>-4</sup> M. (b) = 5 × 10<sup>-5</sup> M. (c) = 1 × 10<sup>-5</sup> M. (d) = 0 M (1.0 M KCl).

quantitation were found to be  $2.30 \times 10^{-5} \text{M}$  and  $7.68 \times 10^{-5} \text{M}$  respectively, where  $\text{LOD} = S_b + 3\sigma_b$  and  $\text{LOQ} = S_b + 10\sigma_b$ .

#### 3.4.6 Detailed study of the background current

From Figures 3.5 to 3.7 it can be seen that the background current takes the form of a U-shaped curve. It was decided to investigate this background current further to see if it would yield information about the point of zero charge.

Characterisation of this current profile consisted of monitoring changes in the overall shape of the curve as a function of pulse amplitude ( $\Delta E$ ), differential pulse waveform period (DPWP), frequency of revolution of the electrode ( $\omega$ ) and electrolyte concentration (C) at both platinum and silver electrodes because although this behaviour was originally observed at platinum similar behaviour was seen at silver.

Figure 3.5 shows the behaviour of the background current as a function of pulse amplitudes. It is immediately obvious that the U-shaped behaviour is more pronounced at the larger pulse amplitudes while the position of the minimum of current is unaffected by changes in pulse amplitude. The fact that each trace initiates from a different point is puzzling as prior to initiating the potential sweep the cell potential should be constant

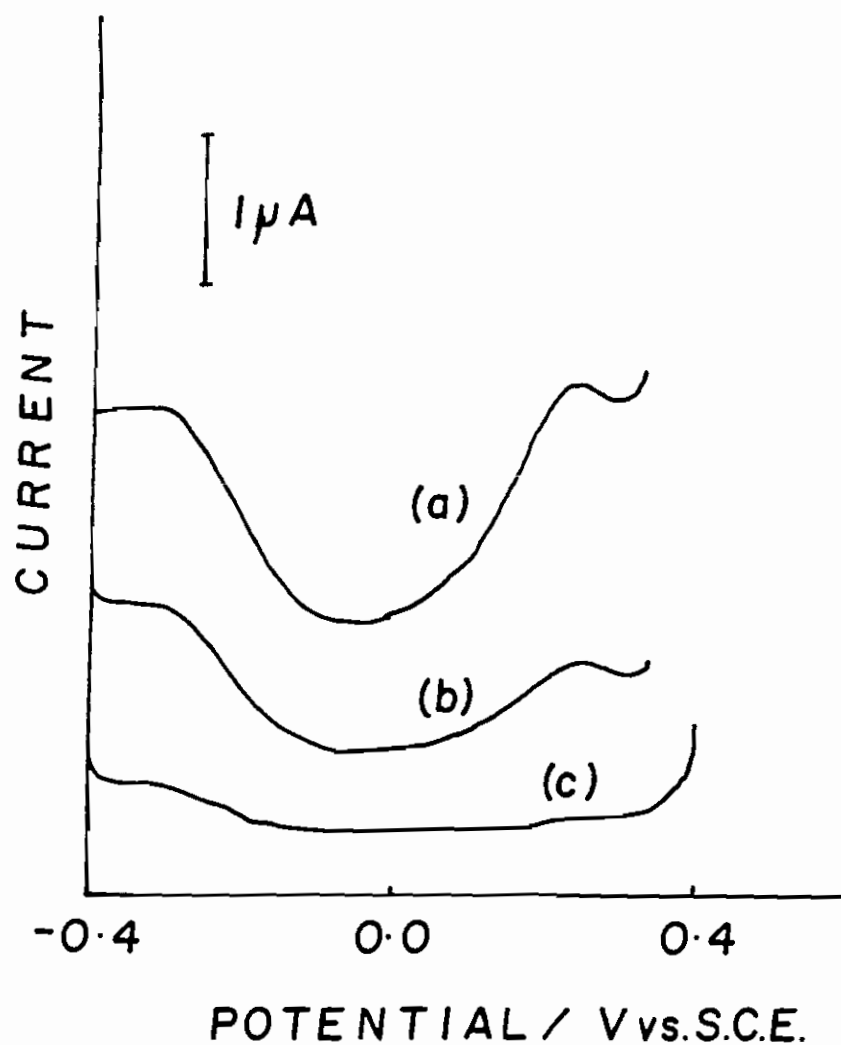


Fig. 3.5 Effect of pulse amplitude on the U-shaped curve. 0.1 M KCl at a silver electrode, DPWP = 0.50 secs., rotation rate = 3000 RPM, scan rate =  $10 \text{ mV sec}^{-1}$ , pulse width = 55 msec. Pulse amplitudes are as follows: (a) = 100 mV, (b) = 60 mV, (c) = 20 mV.

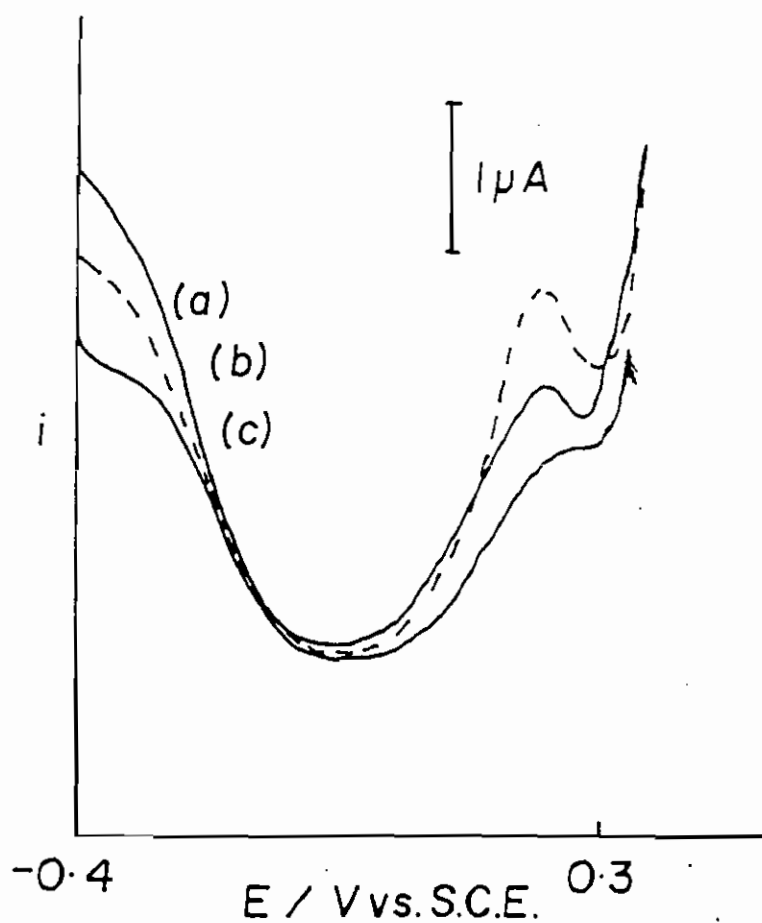


Figure 3.6 Effect of rotation rate on the U shaped curve at a silver electrode. Pulse amplitude = 100 mV. Other conditions as in Figure 3.5. rotation rates are as follows(a) 3000 RPM, (b) = 200 RPM, (c) = 100 RPM.

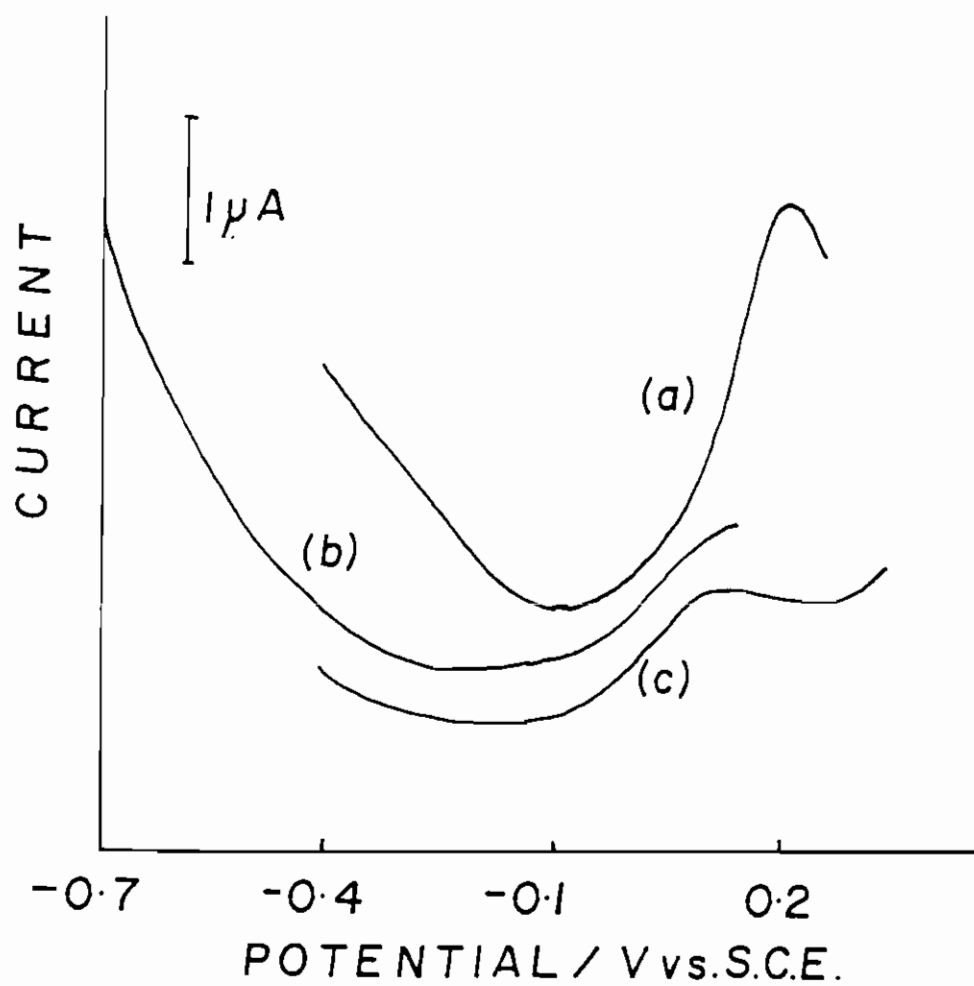


Figure 3.7 The effect of the electrolyte concentration on the U shaped curve at a silver electrode. Pulse amplitude = 100 mV. Other conditions as in Figure 3.5. (a) = 0.1M KCl, (b) = 0.01 M KCl, and (c) = 0.0001 M KCl.

and independent of the magnitude of the pulse amplitude. It can only be assumed that the potentiostat is applying pulses before the sweep is initiated. This could not be confirmed on consulting the manual.

Changes in the differential pulse waveform period (DPWP) were found to have little affect on the overall shape of the background current. Traces were recorded with differential pulse waveform periods in the range 0.1 sec to 1.0 sec. The position of the minimum of current was unaffected by changes in the DPWP and only slight differences in the tails of the curves were observed, the curves corresponding to low values of DPWP reaching higher current magnitudes.

The effect of changing the rotation rate of the electrode was found to be similar to that observed for the DPWP study with the position of the minimum of current being unaffected while the current magnitudes reached by the tails were larger at the higher rotation rates (Fig.3.6). This increase in current could be due to the diffusion layer thickness approaching that of the double layer as the rotation rate is increased and hence affecting the rate of mass transport to the electrode. However this is very unlikely as the double layer thickness in a solution of 0.1M KCl is of the order of 200 angstroms while the diffusion layer thickness at the largest rotation rate, 3000RPM is of the order of 0.80 micrometers. The variations in the current magnitudes in the region of the tails is more likely to be due to the formation of AgCl during the course of the experiment.

Changing the concentration of the KCl solution was found to affect both the position of the minimum of current and the current magnitudes in the region of the tails as shown in

Figure 3.7. On decreasing the concentration of KCl from 0.1M to 0.01M the position of the minimum of current shifted in the negative direction by approximately 80mV. Only approximate values are given for this shift as the minimum of current tended to occur over a potential range and not at a clear defined point. The range over which the minimum of current occurred was found to increase as the concentration of KCl was reduced, i.e. the U-shaped curve became broader at lower concentrations. This shift with changes in concentration is similar to the behaviour on which the Esin-Markov effect is based and the investigation of this link is discussed later in this chapter.

Further investigation of this curiously shaped background current was carried out to determine if the minima corresponded to the potential of zero charge (PZC). The potential of zero charge is a fundamental reference potential in studies of electrified interfaces. Though the absolute potential difference across an electrode-electrolyte interface cannot be measured it is possible to measure the cell potential at which the charge on the polarisable electrode is zero. At this point the electrode is at the same potential as the solution.

A method based on surface tension measurements is used to determine the PZC for liquid metals. These methods are known as electrocapillary methods. Unfortunately it is not possible to determine a value for the PZC at solid electrodes by this method and the available methods are quite complex and require considerable effort. Therefore the potential of the U-shaped background as the basis of a method of determining PZC at solid electrodes warranted further investigation.



A literature search yielded a set of systems for which PZC values were quoted for specific solution compositions at specified electrode materials. The fact that only a platinum or silver electrode was available restricted the search to systems in which these metals were used. Table 3.7 is a summary of the values taken from the literature.

Table 3.7: Summary of literature values quoted for PZC.

Solution Composition	Electrode Material	PZC (Vs SCE)
0.5M Na <sub>2</sub> SO <sub>4</sub> + 0.01M NaOH	Pt	-0.49 [11]
0.5M Na <sub>2</sub> SO <sub>4</sub> + 0.005M H <sub>2</sub> SO <sub>4</sub>	Pt	-0.04 [11]
5x10 <sup>-4</sup> M H <sub>2</sub> SO <sub>4</sub> + 1.5x10 <sup>-3</sup> M Na <sub>2</sub> SO <sub>4</sub>	Pt	+0.37 [12]
0.01M KCl	Pt	+0.24 [13]
0.1M KCl	Ag	-0.90 [14]

Solutions with the compositions listed were prepared and current profiles were recorded at the appropriate electrode. Based on the characterisation of the U-shaped curve discussed above a pulse amplitude of 100mV and a rotation rate of 3000rpm were used during this study to maximise the U-shaped nature of the curves.

Fig.3.8 is the trace obtained when recording the differential pulse response of a platinum rotating disk electrode in a solution of 0.5M Na<sub>2</sub>SO<sub>4</sub>/0.01M NaOH. The minimum of current occurs at -0.50V which corresponds to the value of the PZC given in the literature (see Table 3.4). This indicated a link between the U-shaped curve and the PZC. On recording current profiles for the remaining solution compositions from the table it was found that in each case a minimum of current occurred at the potential at which the PZC was quoted in the literature. This proved promising and had obvious potential as the basis of a technique for determining the PZC at solid electrodes, a

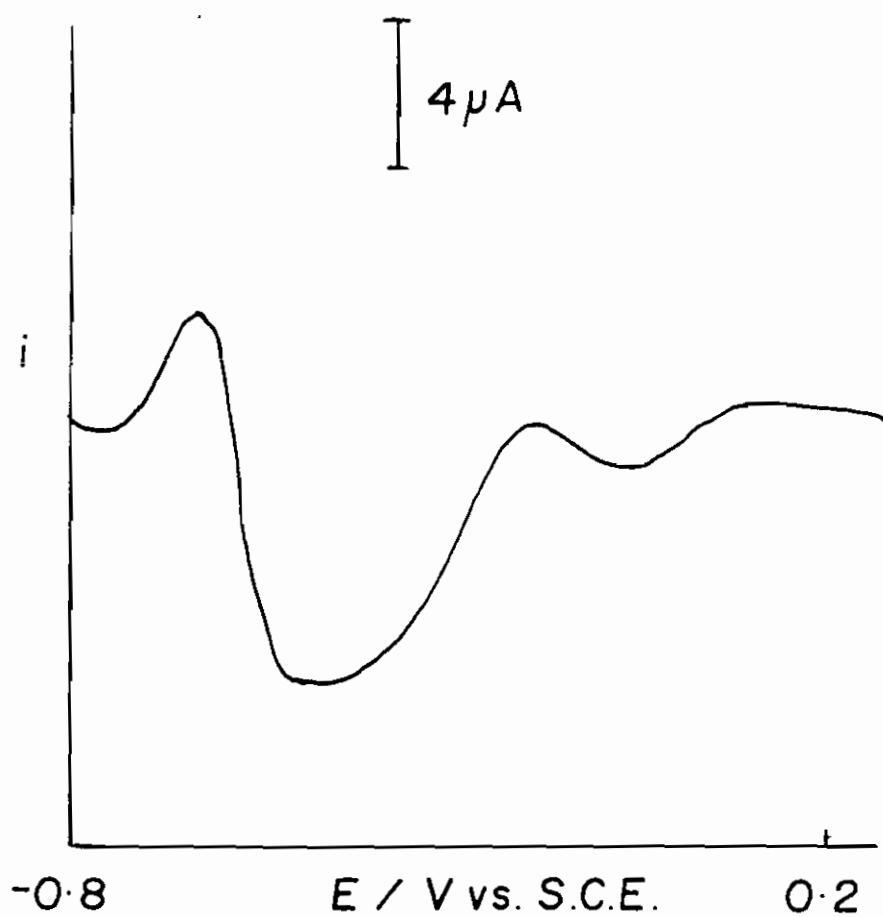


Fig. 3.8 0.5 M  $\text{Na}_2\text{SO}_4$ /0.01 M NaOH at a platinum disk electrode of area = 0.0703  $\text{cm}^2$ . Pulse amplitude = 100 mV, DPWP = 0.50 secs., rotation rate = 3000 RPM, scan rate = 10  $\text{mV sec}^{-1}$ , pulse width = 55 msec.

method which was less complex than traditional methods. However on further investigation of the systems over a wider range of applied potentials it was found that similar U-shaped curves occurred at different potentials as shown in Fig. 3.9. Furthermore in some cases the minimum of current value at these points was less than the minimum at the literature value of PZC. This introduces an uncertainty into the ability of this method to locate the pzc. Another problem arose in determining the exact potential at which the minimum of current occurred because in some cases the minimum occurred over a potential range rather than at a well defined potential.

Having ruled out the use of this U-shaped background curve as a reliable method of determining the PZC it was decided to investigate whether it could be used to observe the Esin-Markov effect. The Esin-Markov effect is used as an indicator of specific adsorption and is based on the fact that a shift occurs in the PZC when the electrolyte concentration is altered. Specific adsorption of anions is indicated by a negative shift in the PZC whereas specific cationic adsorption is revealed by positive shifts. Nonspecific adsorption provides no mechanism for a dependence of the electrode potential on the concentration of electrolyte so the Esin-Markov effect is absent for these systems.

Table 3.8 contains a list of PZC values as a function of electrolyte concentration for NaCl and NaF at mercury [15]. In the case of NaCl the value for PZC varies with concentration indicating the presence of specific adsorption whereas for NaF only a relatively small shift is present indicating that F<sup>-</sup> is not specifically adsorbed.

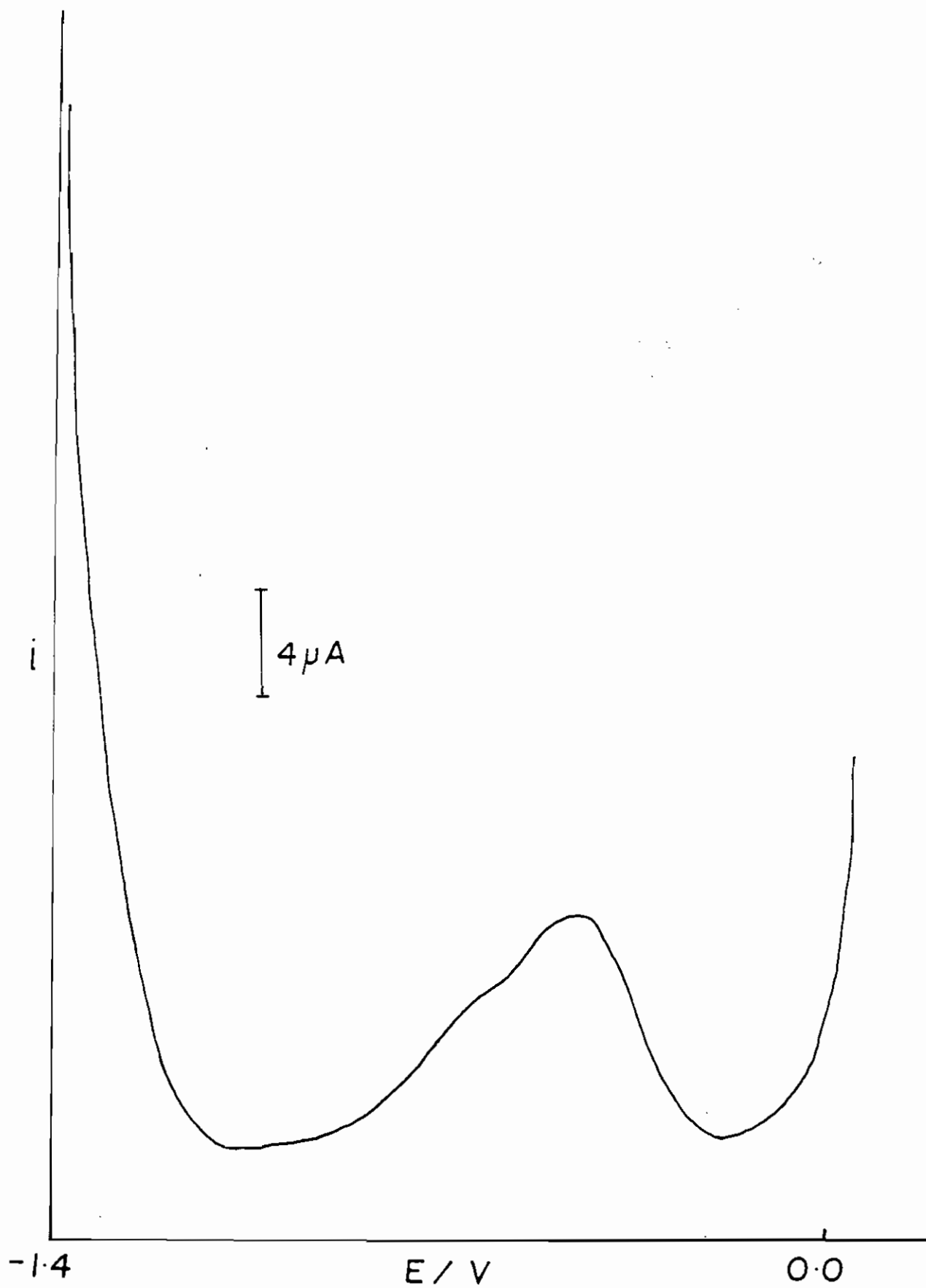


Fig. 3.9 0.1 M KCl at a silver electrode. Pulse amplitude = 100 mV, DPWP = 0.50 secs., rotation rate = 3000 RPM, scan rate = 10 mV sec<sup>-1</sup>, pulse width = 55 msec.

Table 3.8 Variation of PZC with electrolyte concentration [15].

Electrolyte	Concentration / M	PZC / Volts vs SCE
NaF	0.01	-0.480
NaF	0.001	-0.482
NaCl	1.0	-0.556
NaCl	0.1	-0.505

To investigate whether the U-shaped background could be used as an indicator of specific adsorption solutions of NaCl and NaF were prepared over the range of concentrations listed in Table 3.8. Fig. 3.10 is the trace corresponding to (a) 0.01M NaCl and (b) 0.001M NaCl. Although the minimum of current occurs in the region of the literature value given in Table 3.8 it occurs over a range of approximately 50mV. This makes it difficult to determine with confidence whether the position of the minimum is shifted by the change in concentration of the electrolyte and it is impossible to quantify this shift. Attempts were made to study NaF but a deposit was formed on the electrode surface preventing the collection of meaningful data.

A study was carried out to determine whether the position of the minimum of current was affected by the addition of alcohol to the system. Stenin et al [16] found that the adsorption of organic compounds with an alcohol group at a platinum electrode caused the PZC to shift in the positive direction. Figure 3.11 is an attempt to reproduce this work and shows the affect of 1ml additions of methanol to a solution of  $1 \times 10^{-3} \text{M H}_2\text{SO}_4$  +  $3 \times 10^{-3} \text{M Na}_2\text{SO}_4$ . Although the position of the minimum appears to shift towards more negative potentials as the concentration of methanol increases it is impossible to

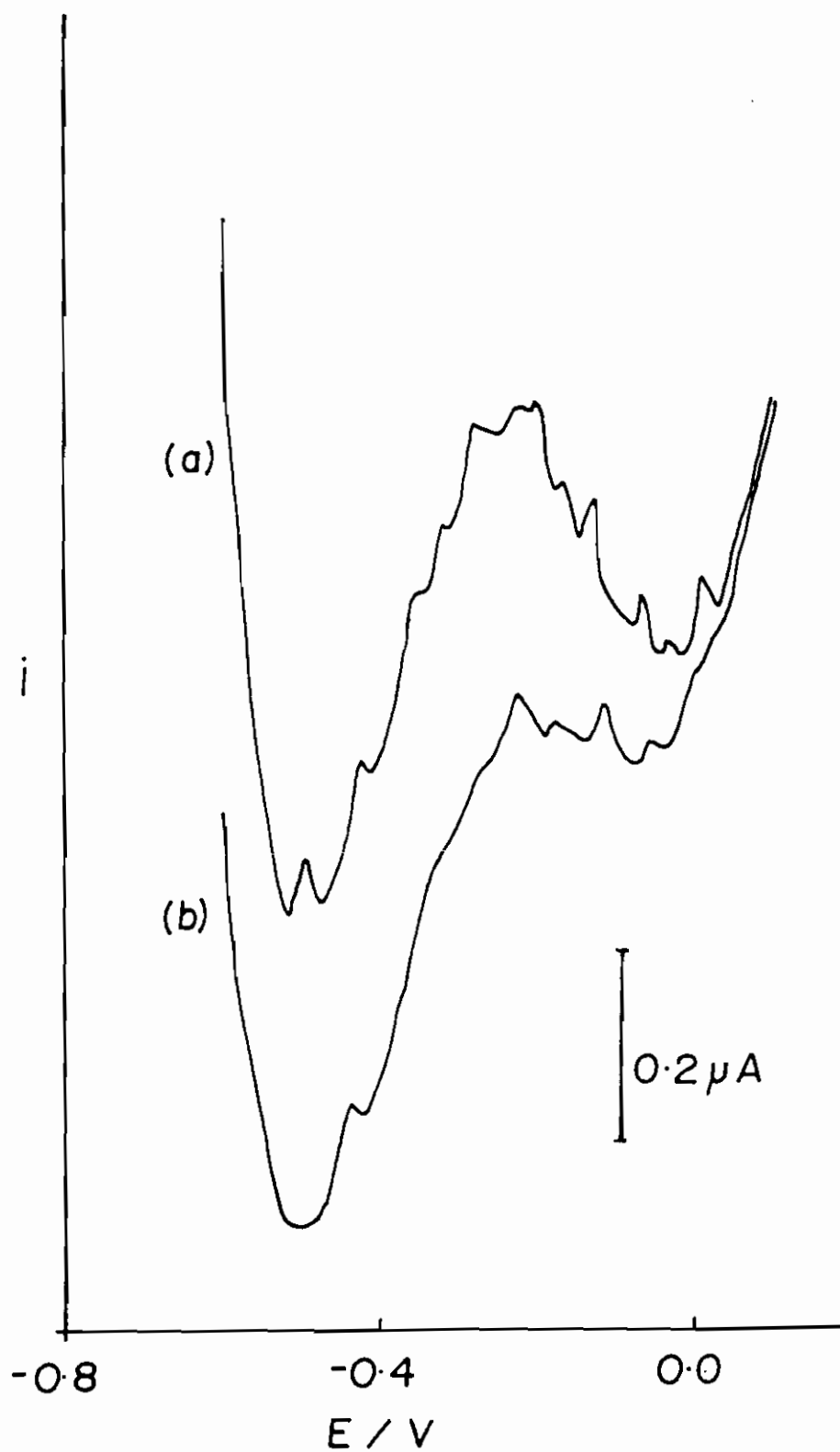


Fig. 3.10 Investigation of the Esin-Markov effect. (a) = 0.01M NaCl, (b) = 0.001 M NaCl. Platinum electrode area =  $0.0703 \text{ cm}^2$ , pulse amplitude = 100 mV, DPWP = 0.50 secs., rotation rate = 3000 RPM, scan rate =  $10 \text{ mV sec}^{-1}$ , pulse width = 55 msec.

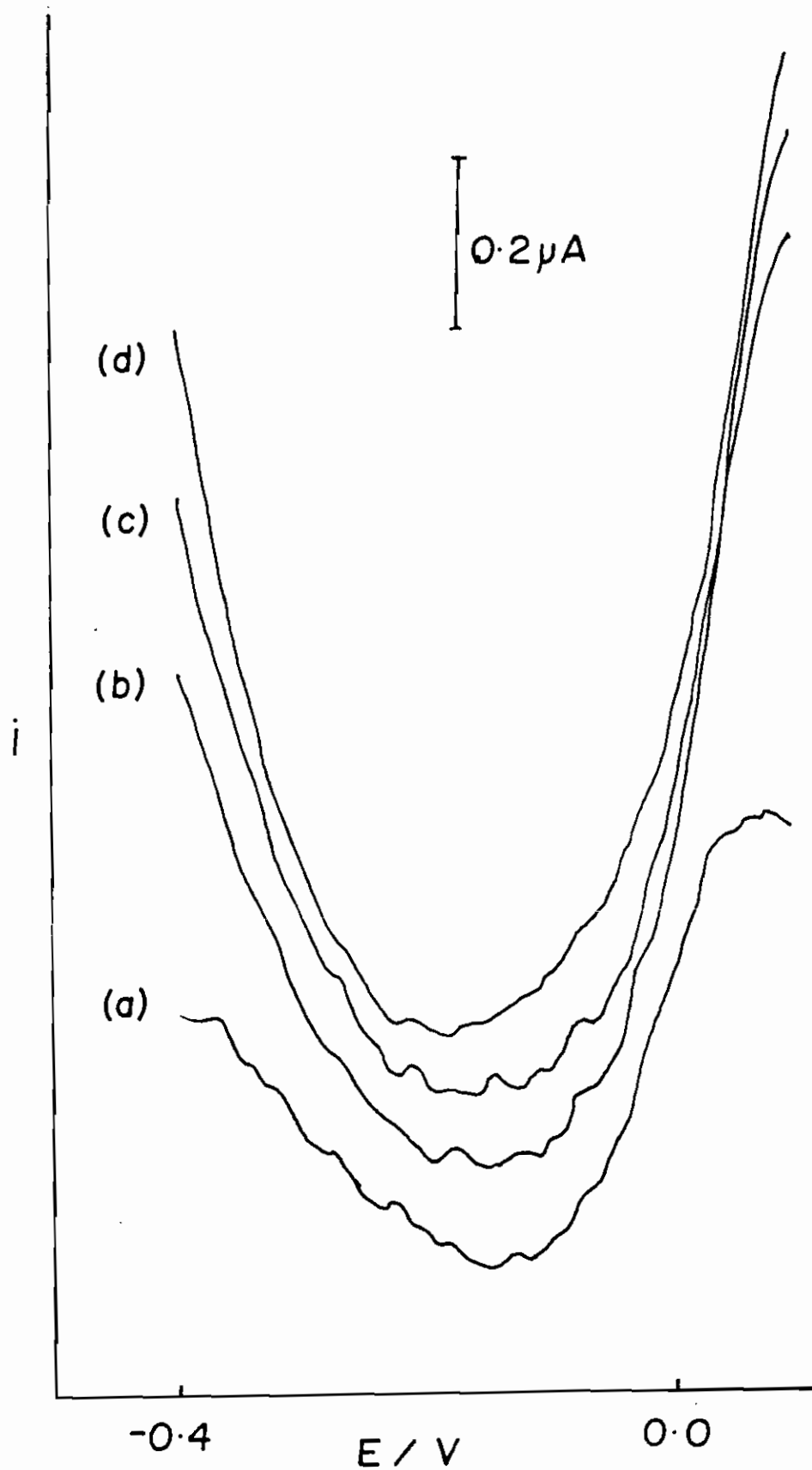


Fig. 3.11 Effect of the addition of alcohol on the U-shaped curve. (a) 0.01M KCl. (b) 1 ml of methanol added. (c) 2 mls of methanol added and (d) 10 mls of methanol added to 50 mls of  $1 \times 10^{-3}$  M  $\text{H}_2\text{SO}_4$  +  $3 \times 10^{-3}$  M  $\text{Na}_2\text{SO}_4$  at a platinum electrode of area  $0.0703 \text{ cm}^2$ . Pulse amplitude = 100 mV, DPWP = 0.50 secs., rotation rate = 3000 RPM, scan rate =  $10 \text{ mV sec}^{-1}$ , pulse width = 55 msec.

quantify this shift due to the broadness of the U-shaped curve. Also this shift is not consistent with the data recorded at mercury and can only be explained by differences in the nature of the metals. Once again the broad nature of the U-shaped curve limits its application.

### 3.5 Conclusions

The peaked response produced by the application of a differential pulse waveform to a rotating disk electrode was characterised. Peak current heights returned by Model 2 correlated satisfactorily with those returned by the numerical derivative of a solution of ferrocyanide in 1.0M KCl. Peak current heights returned by this method at lower concentration of KCl failed to correlate as well due to slow kinetics. Slow kinetics also explain the deviation of the peak current heights returned by the application of a differential pulse waveform to a solution of ferrocyanide in KCl from those returned by Model 2. Model 1 was found to be inappropriate for modelling of this system as it failed to reflect the effect of rotation rate on peak current heights. The analytical technique was found to have a limit of detection of  $2.30 \times 10^{-5} \text{M}$  and a limit of quantitation of  $7.68 \times 10^{-5} \text{M}$ . The U-shaped background current was investigated and it was found that the minimum of current occurred at the PZC for a number of systems. However the use of this technique as a means of determining PZC values was ruled out due to the presence of similar minima over the potential range studied. These minima were also studied to determine whether they exhibited the Esin-Markov effect or were



affected by the addition of alcohols. In both cases it was found that due to their broad nature it was difficult to determine whether or not a shift occurred in the minima therefore ruling out their potential as a means of studying these effects.

### 3.6 References

1. V.G. Levich, *Physicochemical Hydrodynamics*, Prentice Hall, Englewood Cliffs, New Jersey, (1962).
2. Yu G. Siver, B.N. Kabanov, *Zh. Fiz. Khim.*, **22**, 53, (1948)
3. G. Lalande and G. Faubert, *J. Power Sources*, **61**, 227, (1996)
4. S.M. Golabi and J.B. Raoof, *J. Electroanal. Chem.*, **416**, 75, (1996).
5. Q. Wu and M. Maskus, *Anal. Chem.*, **68**, 3688, (1996).
6. J.E. Anderson, A.M. Bond and R.D. Jones, *Anal. Chem.*, **53**, 1016, (1981).
7. D.T. Sawyer and J.L. Roberts, *Experimental Electrochemistry for Chemists*, Wiley, New York, (1974), p.77.
8. A.J. Bard and L.R. Faulkner, *Electrochemical Methods - Fundamentals and Applications*, Wiley, New York, (1980), pp. 283-299.
9. A.C. Wahl, *Z. Elektrochem.*, **64**, 90, (1960).
10. M. Shporer, G. Ron, A. Loewenstein, G. Navon, *Inorg.Chem.*, **4**, 361, (1965).
11. A.N. Frumkin, O.A. Petri in *Comprehensive Treatise of Electrochemistry*, Plenum Press, New York, (1980), pp. 228.
12. A.N. Frumkin, O.A. Petri in *Comprehensive Treatise of Electrochemistry*, Plenum Press, New York, (1980), pp. 237.
13. A.N. Frumkin, O.A. Petri in *Comprehensive Treatise of Electrochemistry*, Plenum Press, New York, (1980), pp. 252.
14. R.L. Garrell, K.D. Beer, *Spectrochim. Acta.*, **43B**, 617-628, (1988).

15. D.C. Grahame, Chem. Rev., **41**, 441, (1947).

16. V.F. Stenin, G.Ya Tsyachnaya, B.I. Podlovchanko, V.E. Kazarinov,  
Electrokhimiya, **7**, 1384-1388, (1971).

## Chapter 4

### **Comparison and critical evaluation of the relative suitability of Graphite Furnace Atomic Absorption Spectroscopy and Anodic Stripping Voltammetry techniques for the determination of lead in potable water.**

#### 4.1 Introduction

Electrochemical methods have been used for the analysis of heavy metals in a wide range of matrices. The most commonly used method is anodic stripping voltammetry (ASV) [1,2]. However the use of electrochemical techniques for heavy metal analysis has not been exceedingly widespread. Atomic spectroscopic methods have generally been favoured over electroanalytical methods, for instance a method for the determination of lead and cadmium in air based on ASV, developed by National Institute of Occupational Health and Safety (NIOSH) researchers, was published in 1977 [3]. However, this method did not appear in the 1984 version of the NIOSH manual of Analytical Methods [4], having been substituted by atomic spectroscopic methods.

So why did ASV lose favour and be overtaken by atomic spectroscopic methods? At that time the spectroscopic methods were believed to be more user-friendly and offered

higher sample throughput rates. Also the ASV technique was based around the hanging mercury drop electrode (HMDE) which required the use of mercury, an environmentally unfriendly metal and gave less than satisfactory recoveries and %RSD values.

However the fact remained that ASV techniques were very suitable for the determination of heavy metals and widespread research was carried out in this area which led to some interesting variations of the technique, widening the scope of applications and overcoming some of the undesirable aspects of the technique. Mercury film electrodes were developed which replaced the numerous drops of mercury required for HMDE with a single mercury film of thickness of the order of 100 angstroms. Original anodic stripping voltammetry techniques specific to a certain metal such as cadmium [5], lead [6] and thallium [7] were replaced by techniques capable of multielement trace analysis [8]. However there were a number of difficulties associated with this procedure, for instance difficulties arose when attempting to determine copper and zinc simultaneously due to the formation of intermetallic species between these two metals [1]. Fortunately procedures to overcome these problems have been developed [9]. Detection limits for heavy metals using ASV are generally in the range  $10^{-8}$  to  $10^{-10}$ M, allowing for trace element determinations in a variety of sample types. The advent of differential pulse anodic stripping voltammetry (DPASV) further improved both the precision and detection limits (as low as  $5 \times 10^{-12}$  M) of these techniques. These stripping techniques are capable of direct analysis, that is they do not require any concentration steps or sample pretreatment therefore minimising the use of reagents. The ability to be species sensitive i.e. the ability to differentiate the various

forms of a given trace metal in solution is another interesting capability of these techniques since knowledge of the chemical state of trace metals in solution is important for understanding their transport, toxicity and reactivity in natural waters. This contrasts anodic stripping voltammetry with graphite furnace atomic absorption spectrometry (GFAAS) which yields total metal analysis.

Is it time for anodic stripping methods to retake the place it lost in the early 1980s as the preferred method for trace heavy metal analysis or have developments in spectroscopic methods outweighed those made in the electrochemical techniques? To answer this question it was decided to choose a system which would be analysed by both DPASV and GFAAS techniques. Every aspect of the methods would then be critically evaluated and compared.

Lead analysis in potable water was chosen as the system on which the comparison was to be based for a number of reasons. Firstly potable water is arguably the most frequently analysed matrix for heavy metals and a new directive from the EU (Council Directive 98/83/EC of 3 November 1998 on the quality of water intended for human consumption) is to be introduced which reduces the maximum permissible levels of lead in potable water from 50ppb to 10ppb. This requires adjustments to current analysis procedures as presently lead levels below 10ppb are only quantified as "<10ppb".

## 4.2 Theory

### 4.2.1 Anodic Stripping Voltammetry

Essentially anodic stripping voltammetry is a two-step technique. The first, or deposition step, involves the electrolytic deposition of a small portion of the metal ions from solution into a mercury electrode as a preconcentration step. This is followed by the stripping step, which involves the dissolution or stripping of the metals from the electrode.

Most frequently the preconcentration is done by cathodic deposition at a controlled potential which is at least 200 mV more negative than the reduction potential of the element(s) to be determined. The metal ions reach the electrode surface by diffusion and convection which in this case is forced by rotation of the electrode or stirring of the solution. They are subsequently reduced and concentrated as amalgams in the mercury. Concentration of metals in the amalgam is usually 100-1000 times the concentration of the ions in solution which results in a 0.5 to 5% decrease in the bulk concentration of the metal ions [10]. Because the electrolysis is not exhaustive the deposition conditions must be reproducible.

Oxygen must be removed prior to the deposition step because of its chemical reactivity. It may oxidise the metals in the amalgam and hydroxide ions formed during the

reduction of oxygen in neutral or basic media may precipitate metal ions in the vicinity of the working electrode.

Following the pre-selected time of the deposition step rotation of the electrode or stirring of the solution is terminated and a pre-selected rest period is allowed before commencing the stripping step. As the forced convection is stopped the deposition current drops almost to zero and a uniform concentration distribution is established very rapidly (after about 2 seconds in film electrodes and 30 seconds for the hanging mercury drop electrode) [11]. The rest period also ensures that the stripping step occurs in quiescent solution. However during the rest period electrodeposition continues, facilitated by diffusion transport. This results in a non-zero intercept in the peak current versus deposition time plot.

Following the rest period the potential is scanned anodically either linearly or in a differential pulse ramp. The latter is more sensitive since it discriminates the faradaic current over the double layer charging current. During this scan the amalgamated metals are stripped out of the electrode in an order that is a function of their standard potentials. They are oxidised and give rise to anodic peak currents which can be measured.

The resultant current-potential profile provides the analytical information of interest. The peak potential of each metal is a characteristic of that metal and is related to the standard potential of its redox couple and can therefore be used for qualitative identification. The peak current height is proportional to the concentration of the



corresponding metal ion and the concentration can be determined by standard addition or by means of a calibration curve.

The most popular working electrodes for stripping analysis are the hanging mercury drop and the thin mercury film electrode. The hanging mercury drop is formed at the tip of a capillary or microsyringe while the thin film electrode is formed by electrolytically plating mercury from a  $\text{Hg}^{2+}$  solution onto the surface of a carbon substrate. The resulting film is usually less than 100 angstroms thick.

#### 4.2.2 Graphite Furnace Atomic Absorption Spectroscopy.

The basis of atomic absorption spectrometry is the resonance absorption of UV/Visible light by neutral metal species in gaseous form. If polychromatic light is transmitted through a gas with metals in their atomic states, radiation at very specific wavelengths from this light is absorbed.

A hollow-cathode lamp comprising the element to be determined as the cathode generates emission radiation characteristic of the element as a result of an electrical glow discharge. The analytical sample which is in a gaseous state and the atoms of which absorb in the region of the resonance line, is located in the atomiser in the path of the beam. The neutral atoms can be suspended in a flame or as a vapour in a graphite tube. The intensity of the emission radiation from the source reaching the detector is weakened in the process. Spectral lines which are not absorbed are not weakened. The weakening of the resonance line is recorded by the detector and finally it is printed out in the form of the inverse spectrum. The loss in intensity of the primary light or absorbance is proportional to the population of neutral metal atoms in the graphite tube.

A typical AAS instrument consists of a hollow cathode lamp for producing the characteristic emission radiation, a device for background correction, an atomiser unit, a detector and recorder assembly and an inert gas supply.

Applying several hundreds of volts to the hollow cathode lamp causes a glow discharge which leads to the generation of the emission spectrum of a particular element. Background correction is necessary to compensate for reductions in the intensity of the emission spectrum of interest caused by processes other than absorption by the atomic cloud. A graphite tube (Fig. 4.1) placed horizontally in the light beam can be used as the atomiser unit. These tubes are generally 28 mm long, 8mm wide with an internal diameter of 6mm. The tube interior is coated with pyrolytic graphite. Electrodes at the ends of the tube are connected to a low voltage high current supply capable of delivering 3.6 kW to the tube walls and temperatures of 3000 K can be achieved. Samples are introduced through a small orifice in the top of the tube by a micro syringe. The graphite tube is then subjected to a temperature program which produces an atomic cloud of the metal in the path of the hollow cathode lamp beam. The individual steps of this temperature program consist of drying the sample, ashing and atomisation. Drying is normally done at temperatures of approximately 100<sup>0</sup>C and its function is to evaporate any solvent or extremely volatile matrix components. Ashing is conducted at a pre-determined intermediate temperature determined by the element to be analysed and the matrix involved. During ashing matrix components are volatilised any fats and oils present are pyrolysed. During the atomisation step the analyte dissociates and the atoms volatilise creating the atomic cloud responsible for the absorption.

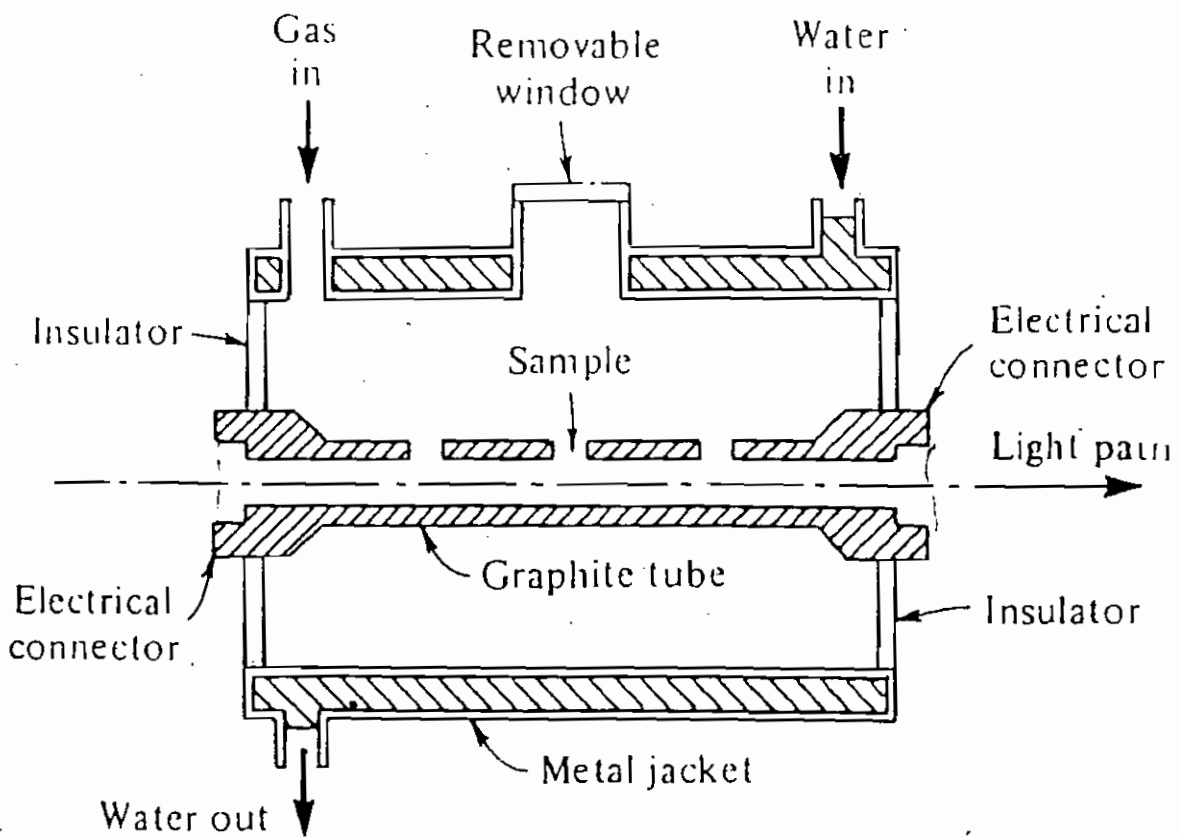


Fig. 4.1 Schematic diagram of a graphite tube atomiser unit.

The absorption signal is recorded by the detector as a reduction in the intensity at the characteristic wavelength of the hollow cathode lamp beam followed by appropriate amplification and conversion.

## **4.3 Experimental**

### 4.3.1 Instrumentation

An Edt Model ECP 100 polarograph was used for the optimisation and validation of the DPASV method and a J.J. Lloyd X-Y chart recorder Model PL3 was used to chart the response. An EG&G Model 394 Polarographic analyser and Model 303A SMDE were also used during the validation. A three electrode one compartment system was used where the reference was a saturated calomel electrode and the auxiliary was a carbon rod. The working electrode consisted of a glassy carbon disk, 3mm in diameter embedded in a Teflon rod of diameter 10mm which was rotated by a Metrohm 628-10 system.

Spectroscopic determinations were carried out using a Varian SpectrAA-200 atomic absorption spectrometer with a GTA-96 graphite tube atomiser and autosampler. Background correction was achieved by means of a deuterium discharge lamp. Pyrolytically coated graphite furnace tubes were employed. The instruments were controlled and the data processed by SpectrAA software on a Targa PC.

### 4.3.2 Reagents

The water used both for preparing solutions and rinsing labware was first distilled by passing through a Buchi F210 distilling apparatus before deionising in an Elgastat UHQ deioniser. 1000ppm lead standards were supplied by Riedel-de-Haen and low lead nitric acid (<0.005ppm) supplied by BDH was used to acidify all solutions.

### 4.3.3 Labware selection and cleaning

Polypropylene (PP) volumetric flasks were used throughout this work. Glassware being avoided because of the possibility of metals being leached into solutions and PVC, PMMA and PS being avoided because of the possibility of contamination from cadmium, copper, lead, tin and titanium [12]. These PP flasks were firstly degreased in a laboratory dish washer before acid washing with acidified (5% HNO<sub>3</sub>) distilled and deionised water. These flasks were then rinsed with distilled and deionised water before being inverted and allowed to dry. The electrochemical cells were of polyethylene and were also initially degreased in a laboratory dish washer. These cells were filled with 6M nitric acid and allowed to stand for at least one hour before rinsing thoroughly with distilled and deionised water prior to introduction of the first solution. The cells and electrodes were rinsed thoroughly with distilled and deionised water between samples to avoid contamination.

#### 4.3.4 Sample preparation

Five working lead standards (2, 4, 6, 8, 10 ppb) were prepared by appropriate dilution of the stock 1000ppm lead solution with acidified (1% v/v HNO<sub>3</sub>) distilled and deionised water. Approximately 1mM solutions of Hg<sup>++</sup> were prepared by dissolving 0.0856g of Hg(NO<sub>3</sub>)<sub>2</sub>·H<sub>2</sub>O in 250 mls of acidified (1% v/v HNO<sub>3</sub>) distilled and deionised water.

#### 4.3.5 Sample collection

250ml polyethylene bottles were used for the collection of water samples. These bottles were initially degreased in a laboratory dishwasher before rinsing with distilled and deionised water. Each bottle was then filled with distilled and deionised water which had been acidified to pH 1 with low lead nitric acid and allowed to stand for one week before rinsing with distilled and deionised water. At the point of sampling the potable water was allowed to flow for one minute from the tap before sampling. The bottle was also rinsed with the water it was to contain. On collection the water sample was acidified to 0.1% with low lead nitric acid and on arrival in the laboratory was further acidified to 1%.

#### 4.4 Comparison of DPASV and GFAAS methods for the determination of lead in potable water

To facilitate a comprehensive comparison of the suitability of these techniques for the routine analysis of lead levels in potable waters it was decided to optimise each method before assessing its performance under each of the following headings:

- |                 |                           |
|-----------------|---------------------------|
| (1) Linearity   | (5) Limit of Detection    |
| (2) Accuracy    | (6) Limit of Quantitation |
| (3) Precision   | (7) Stability             |
| (4) Specificity | (8) Robustness            |

A typical validation protocol specifying acceptance criteria for each of these headings is contained in Appendix A. Firstly, the performance of each method will be tested against this protocol and then by comparing the performance of the two techniques under each of these headings an informed decision will be made as to which technique is most suited to the routine analysis of lead in potable water.

##### 4.4.1 Lead analysis in potable water by DPASV

Thin mercury film electrodes were preferred to the dropping mercury electrode for the practical reason that they consume considerably less mercury, a thin film of mercury

being required for analysis of a large number of samples compared to a continuous stream of mercury drops for the dropping mercury electrode or one drop of mercury per sample for the hanging mercury drop electrode. It is difficult to justify using larger volumes of a toxic substance than necessary for any analysis system, especially when the system involves environmental analysis.

There are two possible methods for the formation of this thin mercury film. The first involves preplating a thin mercury film from a solution of a mercury salt, this film then being used repeatedly for the analysis of a large number of samples. The alternative method involves formation of the film *in situ*. This is achieved by adding a small concentration of mercury nitrate to each sample solution and simultaneously depositing the mercury film and the metals to be measured. The *in situ* method has been shown to yield better selectivity and reproducibility than the preplating method [13], however it was decided to initially adopt the preplating approach in an attempt to reduce the volume of mercury consumed.

The original conditions adopted for this method were arrived at from a literature survey carried out prior to commencing any experimental determinations. These initial conditions are listed in Table 4.1.



Table 4.1 Original conditions for the analysis of lead in potable water by DPASV

Mercury Film Formation:

Mercury films were deposited onto a glassy carbon electrode from a solution of 5mM Hg(NO<sub>3</sub>)<sub>2</sub> in 5% HNO<sub>3</sub> at a potential of -0.80V vs SCE for 20 secs. while the electrode was rotated at 3000 rpm.

Analysis of samples:

Deposition potential	$E_{dep}$	-0.70V vs SCE
Final potential	$E_f$	-0.20V vs SCE
Deposition time	$t_{dep}$	300 secs.
Rest time	$t_{rest}$	90 secs
Scan rate	$v$	10 mV sec <sup>-1</sup>
Pulse amplitude	$\Delta E$	100 mV
Differential pulse waveform period	DPWP	0.50 secs.
Rotation rate	$\omega$	1000 rpm

All samples were degassed by bubbling with nitrogen for at least 15 minutes prior to analysis and a nitrogen atmosphere was maintained above the electrochemical cell during analysis.

#### 4.4.1.1 Optimisation of lead analysis in potable water by DPASV

Initial investigations carried out on lead standards at concentrations below 10 ppb using these initial conditions showed that it was possible to obtain reproducible results (Fig. 4.2) with good precision and accuracy with a limit of detection of 0.16 ppb and a limit of quantitation of 0.536 ppb. However the analysis time for each sample was 420 seconds. An analysis time of this magnitude may be acceptable when analysing a number of different metals in a single sample simultaneously but is not practical when a single element is to be analysed.

Acceptable precision and accuracy having already been achieved, optimisation of this method primarily involved reduction of the analysis time.

The preconcentration time (300 s.) is the most significant time consuming step of the analysis. Although a degassing time of 15 minutes is required this is not a rate determining step as samples can be degassed in a separate apparatus while analysis is being carried out. Shortening of the deposition time can be achieved by increasing the magnitude of the signal produced per unit concentration. Increasing the signal per unit concentration will require less analyte in the mercury film to produce a detectable signal and hence the deposition time may be reduced. Ideally the baseline should be smooth in the region of the analyte peak to improve the sensitivity of the method. However, although distilled and deionised water was used to prepare all standards and the cells

were rinsed thoroughly with ultrapure water prior to analysis, the blank was found to contain a small peak at the potential where the lead stripping peak is known to occur.

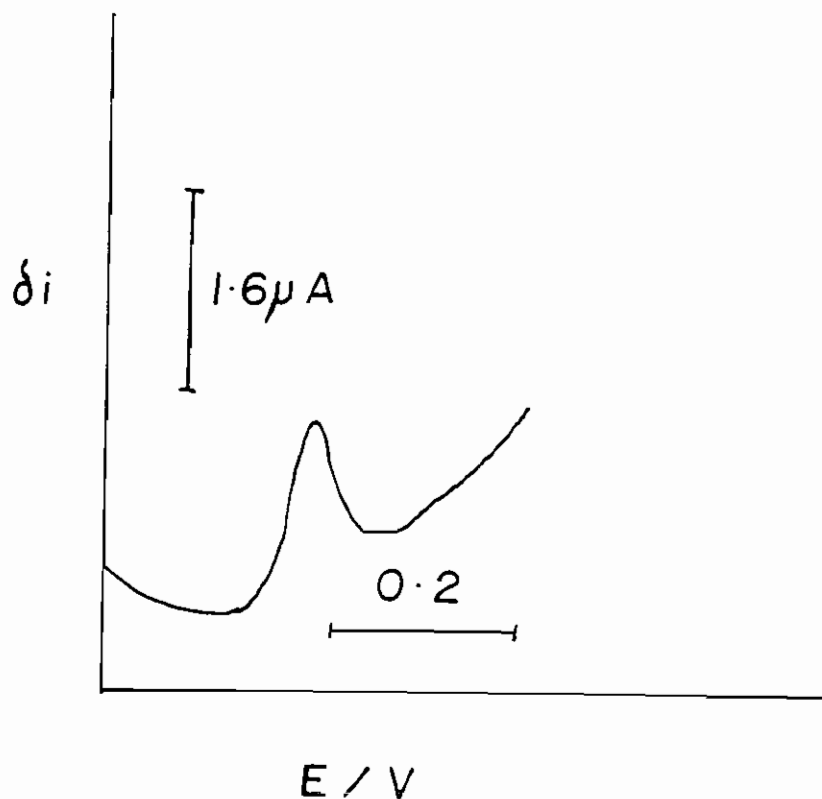


Fig. 4.2 Reproducibility of the current response. Shown are five replicate analyses of a 2 ppb standard. Conditions as outlined in Table 4.1

The presence of this peak considerably reduces the ability of this technique to reliably detect lower concentrations and consequently raises the limit of detection.

At first it was thought that this background peak was due to contamination of the blank during preparation. However precautions taken to avoid contamination of the blank failed to eliminate this background peak. On consulting the literature it was found that filling the electrochemical cell with 6M HNO<sub>3</sub> for at least one hour prior to analysis reduces the presence of background peaks in the blank by leaching traces of metals which may have adsorbed onto the cell walls during previous analyses [14].

Also the low lead nitric acid used to acidify the standards although low in lead (<0.005 ppm) was not lead free and therefore contributed to the lead background peak. Originally standards were acidified to 5% with this nitric acid. An investigation to determine if the amount of acid added could be reduced therefore reducing the lead contamination found that acidification of the standards to 1% was sufficient for successful lead determinations. Acidification of the mercury solution was also reduced to 1%.

On adopting these procedures it was possible to reduce the background peak current from 1.43  $\mu$ A to 0.67  $\mu$ A.

It was also found that the sensitivity of the polarograph could be improved by manipulation of the control settings. This enabled a larger response to be obtained per

unit of lead concentration allowing the deposition time to be further reduced. However it was decided to retain the original deposition time until all other parameters had been optimised.

Depositions were carried out at potentials more negative than the original value of -0.70 V vs SCE with the expectation that the more negative potentials would cause the metal to deposit at a higher rate. Deposition potentials in the range -0.80 V to -1.20V were investigated. Slight increases in the peak current heights for a fixed lead concentration were observed at the more negative deposition potentials. However the original deposition potential of -0.70V was retained because decreasing the deposition potential by 100mV adds 10 seconds to the analysis time at a sweep rate of 10mV sec<sup>-1</sup>. The original deposition potential of -0.70V vs SCE was retained.

Attempts to increase the sweep rate from the original 10 mV sec<sup>-1</sup> proved unsuccessful, peak shape and return to baseline deteriorating with increasing sweep rate. This is most probably due to the ramp potential changing considerably within the pulse width at the larger sweep rates. The original sweep rate of 10 mV sec<sup>-1</sup> was retained.

Generally the best sensitivity is found at the larger pulse amplitudes but the peak resolution is improved when small amplitudes are used [15]. As expected the peak current height increased with pulse amplitude and the value of 100mV used in the initial conditions (the maximum achievable by the polarograph) was adopted.

Peak current heights increased with rotation rate as expected and the maximum rotation rate obtainable with the Metrohm 628-10 system, 3000 rpm was adopted for the final method.

Combination of these improvements to the original method parameters allowed the deposition time to be reduced from 300 seconds to 150 seconds. It was also found that the rest period could be reduced from 90 s. to 10 s. without a loss in peak current heights or reproducibility.

At this stage optimisation of the method parameters is complete (Table 4.2) with an overall reduction in analysis time from 420 seconds to 200 seconds without loss of accuracy or precision. The amount of suprapure acid required for sample preparation was also reduced by a factor of 5. Fig. 4.3 is a typical calibration recorded under these optimised conditions.

Finally it was considered a worthwhile exercise to attempt to reduce the quantities of mercury required by the method. Originally the mercury film was deposited from a solution of 5mM  $\text{Hg}(\text{NO}_3)_2$  in 1%  $\text{HNO}_3$ . It was found that a 1mM solution of  $\text{Hg}(\text{NO}_3)_2$  in 1%  $\text{HNO}_3$  was equally efficient for film formation.

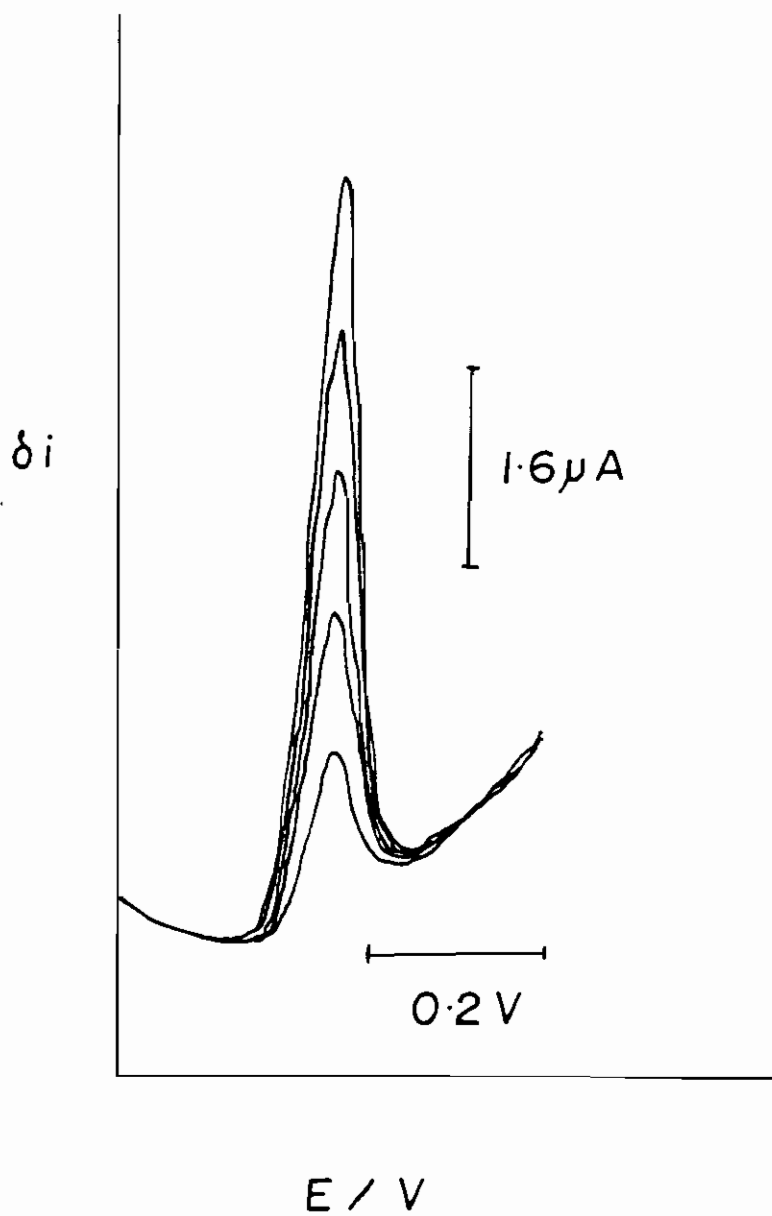


Figure 4.3 Calibration curve for lead with concentrations of 2, 4, 6, 8 and 10 ppb recorded under the optimized conditions listed in table 4.2.

Table 4.2 Optimised DPASV parameters for the analysis of lead in potable water

Mercury Film Formation:

Mercury films were deposited from a solution of  $\approx 1\text{mM Hg(NO}_3)_2$  in 1%  $\text{HNO}_3$  at a potential of  $-0.80\text{V vs SCE}$  for 20 secs. while the electrode was rotated at 3000 rpm.

Analysis of samples:

Deposition potential	$E_{\text{dep}}$	$-0.70\text{V vs SCE}$
Final potential	$E_f$	$-0.30\text{V vs SCE}$
Deposition time	$t_{\text{dep}}$	150 secs.
Rest time	$t_{\text{rest}}$	10 secs
Scan rate	$v$	$10\text{ mV sec}^{-1}$
Pulse amplitude	$\Delta E$	100 mV
Differential pulse waveform period	DPWP	0.50 secs.
Rotation rate	$\omega$	3000 rpm



#### 4.4.1.2 Evaluation of the performance of the DPASV method for the analysis of lead in potable water

##### 4.4.1.2.1 Calibration Curve Linearity

A correlation coefficient of  $0.9995 \pm 3.2 \times 10^{-4}$  was obtained for a series of ten concentrations with an average intercept of  $0.054\mu\text{A}$  compared to the  $4.88\mu\text{A}$  returned for a 10 ppb standard. A plot of response factor against concentration indicated that a linear response is obtained over this concentration range.

##### 4.4.1.2.2 Accuracy

Tables 4.3(a) and 4.3(b) detail the percentage recoveries for ten 4 ppb samples and ten 8 ppb samples respectively. Compiling these results gives an average recovery of  $94.13 \pm 11.82\%$  for the 4 ppb standards and  $96.37 \pm 6.07\%$  for the 8 ppb standards.

A t-test was carried out on the results in Table 4.4. The value of t calculated from the experimental data returned for ten independent analyses of an 8 ppb standard (Table 4.4) was 0.768 which is smaller than the value of 2.26 taken from the tables, with 95% confidence and 9 degrees of freedom. This indicates that the method is accurate.

Table 4.3(a): % Recoveries for “unknown” 4 ppb lead samples. All samples prepared as outlined in section 4.3.4 and analysed according to the parameters optimised in section 4.4.1.1

Sample no.	[Pb] / ppb	% Recovery
4a	3.42	85.80
4b	3.68	92.37
4c	3.71	93.22
4d	3.49	87.60
4e	4.43	111.19
4f	3.90	97.89
4g	3.31	83.08
4h	3.92	98.39
4i	3.08	77.31
4j	4.56	114.46

Table 4.3(b): % Recoveries for “unknown” 8 ppb lead samples. All samples prepared as outlined in section 4.3.4 and analysed according to the parameters optimised in section 4.4.1.1

Sample no.	[Pb] /ppb	% Recovery
8a	8.17	102.95
8b	7.48	94.25
8c	6.94	87.45
8d	8.62	108.56
8e	7.71	97.15
8f	7.22	90.97
8g	7.47	94.13
8h	7.84	98.79
8i	7.35	92.59
8j	7.69	96.90

Table 4.4 Concentrations returned for ten independent analyses of an 8 ppb lead standard. All samples prepared as outlined in section 4.3.4 and analysed according to the parameters optimised in section 4.4.1.1

Determination no.	[Pb] / ppb
1	8.174
2	7.482
3	6.948
4	8.612
5	7.710
6	7.220
7	7.475
8	7.844
9	7.348
10	7.691

#### 4.4.1.2.3 Precision

##### 4.4.1.2.3(a) Intra-assay precision

The results obtained for ten independently prepared samples of the same lead concentration (8 ppb) which were analysed using the previously optimised method parameters are listed in Table 4.5. These results yield a % RSD value of 4.07%.

Table 4.5 Response obtained for ten independently prepared 8 ppb standards. Samples prepared as outlined in section 4.3.4 and analysed according to the parameters optimised in section 4.4.1.1

Sample no.	Peak current height / $\mu\text{A}$
8a	1.935
8b	1.826
8c	1.742
8d	2.004
8e	1.862
8f	1.785
8g	1.825
8h	1.883
8i	1.805
8j	1.859

#### 4.4.1.2.3(b) Instrument precision

Table 4.6 lists the peak current heights returned for 10 replicate analyses of an 8 ppb standard.

Table 4.6 Response obtained for repeat analysis of an 8 ppb standard solution. Samples prepared as outlined in section 4.3.4 and analysed according to the parameters optimised in section 4.4.1.1

Sample no.	Peak current ht/ $\mu\text{A}$
8a	1.921
8b	1.896
8c	1.915
8d	1.892
8e	1.914
8f	1.841
8g	1.891
8h	1.920
8i	1.882
8j	1.848

These results yield a % RSD value of 1.504 % .

#### 4.4.1.2.4 Specificity

The magnitude and shape of the lead peak was unchanged by the presence of the metals specified in Table 4.7. These metals were chosen as they are the most likely to be present in potable water samples. The final concentration of each metal corresponds to the National Limit Value (NLV) for Ireland which specifies the maximum permissible

levels of these metals in water intended for human consumption in the Irish Republic.

Also it was found that the lead peak was clearly resolved from all other metal peaks.

Table 4.7 Concentrations of metals to be added to a 10 ppb lead solution during the specificity study.

Metal	Conc. in test soln./ppb
Iron	200
Zinc	5000
Tin	1000
Copper	3000

#### 4.4.1.2.5 LOD & LOQ

The Limit of Detection (LOD) and Limit of Quantitation (LOQ) were calculated from a regression method as follows. Five lead standards of concentrations 2, 4, 6, 8, 10 ppb were analysed and a graph of peak current height vs concentration was plotted in Excel. The “Data Analysis” function in Excel was then used to determine exact values for the intercept and standard error about the regression line. Taking the intercept to represent the part of the total signal that is due to the blank ( $S_b$ ) and the standard error about the regression line to represent the standard deviation of the blank measurements ( $\sigma$ ) the LOD and LOQ were determined from the following;

$$\text{LOD} = S_b + 3\sigma$$

$$\text{LOQ} = S_b + 10\sigma$$

By this method the LOD and LOQ were found to be 0.113 ppb and 0.375 ppb respectively.

#### 4.4.1.2.6 Stability

Sample solutions collected were found to be stable from time of collection to completion of this study, a period of approximately two weeks. Standard solutions were also found to be stable for a period of over 24 hours, fresh standards being prepared daily. The mercury nitrate solution was found to be stable for a period extending to a number of weeks.

### 4.4.2 Lead analysis in potable water by GFAAS

#### 4.4.2.1 Optimisation of lead analysis in potable water by GFAAS

Lead can be analysed at a number of atomic wavelengths, some of which are listed in Table 4.6. The more commonly used resonance lines are 217.0 nm and 283.3 nm. The 217.0 nm line is considerably more sensitive than the 283.3 nm line. However the 283.3 nm line was chosen for this system because it delivers adequate sensitivity and is less prone to non-atomic interference than the 217.0 nm line.

The initial furnace temperature program was based on the instrument cookbook for lead determination by GFAAS which is shown in Fig. 4.4.

Table 4.8 Common resonance lines for lead in order of decreasing sensitivity. [16].

Resonance Line	Wavelength (nm)
1	217.0
2	283.3
3	261.4
4	368.4
5	364.0

The simplest form of a graphite furnace temperature program will consist of three stages, drying, ashing and atomisation. Argon flows through the tube for the first two stages and not for the third. It is important to choose the drying stage carefully as inadequate drying of the sample leads to poor precision. The optimum ashing temperature is one which is sufficiently high to degrade the sample matrix without causing atomisation of the sample and the optimum atomisation temperature is the lowest temperature giving the maximum absorbance and lowest %RSD. The duration of each stage and the temperature ramps between stages need to be considered also.



Fig. 4.4: Instrument cookbook for the determination of lead.

<Pb> Atomic No. 82

Wavelength <nm>	Slit <nm>	Conc. <μg/l> for 0.2 Abs.	Lamp Intensity
283.3	0.5	27	100
217.0	1.0	14	20
261.4	0.5	1120	30

*PERFORMANCE DATA*

Maximum Ash Temperature	<°C>	600
Maximum Atomize Temperature	<°C>	2100

*RECOMMENDED CHEMICAL MODIFIERS*

Orthophosphoric acid <1000μg/mL>

Ammonium dihydrogen orthophosphate <5mg/mL>

EDTA, citrate, oxalate <0.5 – 1.0 % v/v>

Palladium solution <500 – 2000 μg/mL> plus  
reducing agent such as ascorbic acid

Before commencing the optimisation of the method it was decided that all samples should be acidified to 1% with low lead nitric acid. This lessens the surface tension of the samples. Solutions without acid added can form rounded droplets that can “pull-up” and migrate as the capillary tip exits the graphite tube. It was also found that absorbances returned for blank solutions held in acid washed vials on the autosampler rack did not differ from those stored in unacidwashed vials indicating that contamination of samples from the vials was not a problem.

#### 4.4.2.1.1 Optimisation of drying stage

If the drying parameters are not carefully selected, satisfactory precision or reproducibility of measurements will not be obtained. In the instrument literature it was reported that with aqueous solutions the best drying conditions have been achieved by ramping to a temperature of approximately 75<sup>0</sup>C in 5 seconds and then applying a slow ramp to about 90<sup>0</sup>C [16]. In this way it is possible to dry the sample smoothly with a maximum gas flow at a temperature below the boiling point. A total dry time of between 1 and 3 seconds per microlitre of sample volume is also recommended. A sample volume of 10 microlitres was chosen because while sufficient to produce a detectable signal at 1ppb the smaller volume reduces the risk of problems arising due to the sample spilling over or spreading across the internal flat surface of the tube.

To determine the optimum drying parameters a blank, 5 ppb standard and a 10 ppb standard were initially analysed using a temperature program selected by the instrument software. A series of alterations were made to the drying stage of this program and the resulting effects on the atomic peak and % RSD were noted. Fig. 4.5 is the original temperature program (steps 1, 2 and 3 compose the drying stage) proposed by the instrument and Table 4.9 lists the alterations which were made during the course of the optimisation and the corresponding effect on the atomic peak and %RSD values.

Fig. 4.5: Temperature program proposed by SpectrAA-200 software for the analysis of lead in potable water.

Step	Temp/ <sup>o</sup> C	Time/s	Flow,L/min	Gas type	Read	Sig.store
1	85	5	3.0	Normal	No	No
2	95	40	3.0	Normal	No	No
3	120	10	3.0	Normal	No	No
4	400	5	3.0	Normal	No	No
5	400	1	3.0	Normal	No	No
6	400	2	0.0	Normal	No	Yes
7	2100	1	0.0	Normal	Yes	Yes
8	2100	2	0.0	Normal	Yes	Yes
9	2100	2	3.0	Normal	No	Yes

Table 4.8 Common resonance lines for lead in order of decreasing sensitivity. [16].

Resonance Line	Wavelength (nm)
1	217.0
2	283.3
3	261.4
4	368.4
5	364.0

The simplest form of a graphite furnace temperature program will consist of three stages, drying, ashing and atomisation. Argon flows through the tube for the first two stages and not for the third. It is important to choose the drying stage carefully as inadequate drying of the sample leads to poor precision. The optimum ashing temperature is one which is sufficiently high to degrade the sample matrix without causing atomisation of the sample and the optimum atomisation temperature is the lowest temperature giving the maximum absorbance and lowest %RSD. The duration of each stage and the temperature ramps between stages need to be considered also.

## 4.4.2.1.2

## Optimisation of ashing temperature

Because of the relatively simple nature of the sample matrix in this case it was not expected that a complicated ashing stage would be required. The instrument cookbook for lead analysis in potable water (Fig. 4.4) recommends a maximum ashing temperature of 600°C. To determine the optimum ashing temperature a blank and two standards (5ppb and 10ppb) were analysed at ashing temperatures in the range 300-600°C. The background corrected atomic peak was measured and variations in the background signal were noted. The results obtained are shown in Table 4.11.

Table 4.11 Optimisation of ashing temperature. %RSD values are quoted for two replicates

T <sub>ash</sub>	Blank			5 ppb Pb			10 ppb Pb		
	Bgnd	Abs.	RSD	Bgnd	Abs.	RSD	Bgnd	Abs.	RSD
300	0.0033	0.0003	37.3	0.0006	0.0518	2.1	0.0004	0.1068	0.7
400	0.0030	0.0002	>100	0.0000	0.0511	0.3	0.0001	0.1021	0.8
500	0.0036	0.0006	30.4	-0.0004	0.0418	35.7	-0.0003	0.1030	3.9
600	0.0031	0.0004	19.8	0.0000	0.0409	17.1	0.0003	0.1035	4.7

As expected the background absorbances were very small relative to the absorbance of the standards with the best results being observed at an ashing temperature of 400°C. Good %RSD values were also observed for this ashing temperature. Above 400°C mean absorbance values decreased sharply due to atomisation of the analyte before the “read” steps of the temperature program.

Based on these results an ashing temperature of 400°C was considered to be the optimum.

#### 4.4.2.1.3 Optimisation of atomisation temperature.

The atomisation temperature affects the sensitivity of the analysis. The optimum temperature is considered to be the lowest temperature giving the maximum absorbance and lowest %RSD, high temperatures reducing the life of the graphite tube and platform. A blank and two standards (5ppb and 10 ppb) were analysed at atomisation temperatures in the range 1800-2100°C and the results obtained are shown in Table 4.12.

Table 4.12 Optimisation of atomisation temperature.

T <sub>atom.</sub>	Blank			5 ppb Pb			10 ppb Pb		
	Bgnd	Abs.	RSD	Bgnd	Abs.	RSD	Bgnd	Abs.	RSD
1800	0.0033	0.0002	13.8	0.0002	0.0493	0.3	0.0001	0.0976	5.6

1900	0.0025	0.0010	84.8	0.0009	0.0493	0.6	0.0007	0.1039	5.3
2000	0.0031	0.0003	20.4	-0.0001	0.0520	3.0	-0.0002	0.1017	1.7
2100	0.0027	0.0010	53.8	0.0001	0.0503	5.5	0.0001	0.1059	3.2

It can be seen that the best sensitivities are achieved at atomisation temperatures of 2000°C and 2100°C. 2000°C was chosen as the optimum atomisation temperature as it returned the better % RSD values.

#### 4.4.2.1.4 Optimisation of the length of ashing time

The length of the ashing time in the original temperature program was 8 seconds. It was observed that decreasing the ashing time lead to an increase in the background absorbance and an increase in % RSD values between replicates. Increasing the length of ashing time was found to have little effect on mean absorbances or % RSD values and it was decided to retain the original duration of the ashing stage for the final temperature program.

#### 4.4.2.1.5 Optimisation of the ramp time from the ashing stage to the atomisation stage.

The original ramp rate of one second corresponded to the maximum rate of heating achievable with the GTA atomiser. Increasing the length of this stage resulted in a reduction in mean absorbances. Consequently a ramp time of 1.0 seconds between

ashing and atomisation stages was adopted for the final temperature program which is shown in full in Table 4.13.

Also the addition of burnoff or cooldown stages to the temperature program was found not to be necessary in this case

Table 4.13: Optimised graphite furnace temperature program

Step	Temp/ <sup>o</sup> C	Time/s	Flow,L/min	Gas type	Read	Sig.store
1	75	5	3.0	Normal	No	No
2	90	30	3.0	Normal	No	No
3	400	5	3.0	Normal	No	No
4	400	1	3.0	Normal	No	No
5	400	2	0.0	Normal	No	Yes
6	2000	1	0.0	Normal	Yes	Yes
7	2000	2	0.0	Normal	Yes	Yes
8	2000	2	3.0	Normal	No	Yes

Figure 4.6(a) is a typical absorbance signal for a potable water sample following the temperature program listed in Table 4.13. Figure 4.6(b) shows the calibration graph which was generated using the same temperature program.



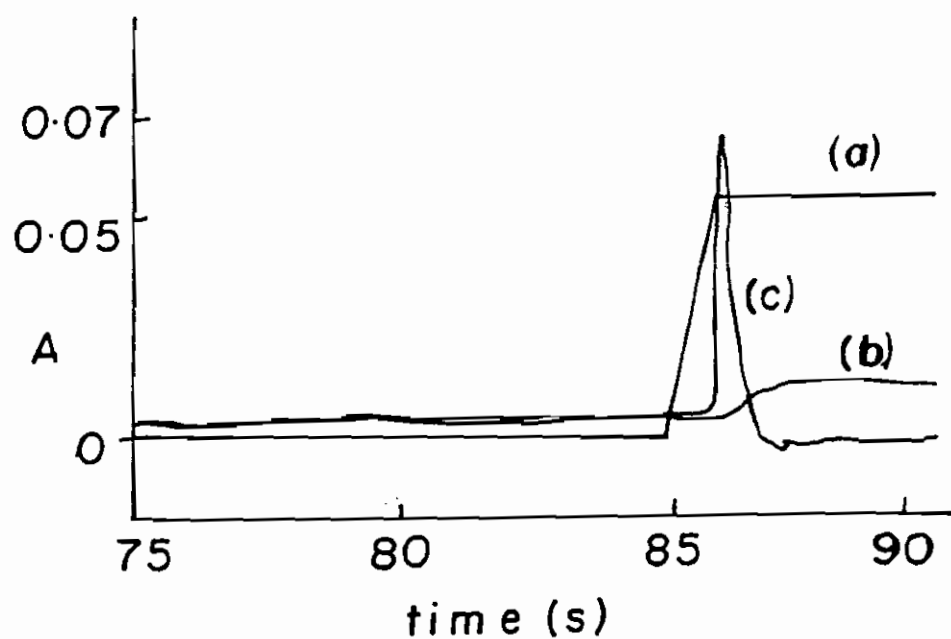


Figure 4.6(a) Absorbance signal recorded for lead in a potable water sample followed the temperature program listed in Fig 4.5. Sample was acidified to 1% with nitric acid. Injected volume = 20 $\mu$ l. (a) the temperature ramp, (b) the background sweep, (c) the absorbance peak due to the lead.

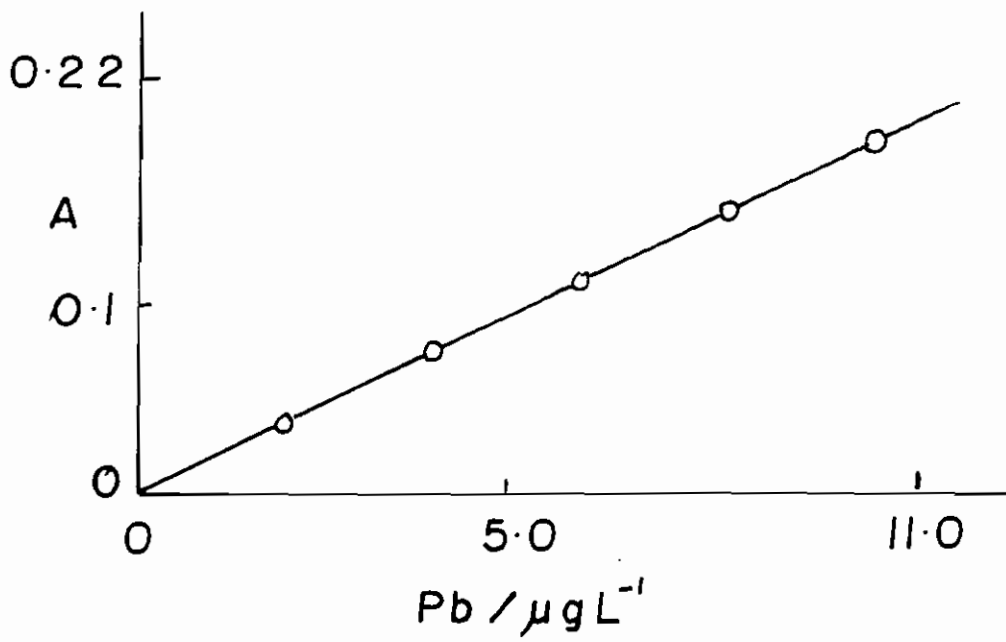


Fig. 4.6(b) Calibration graph (2-10 ppb) generated by the SpectrAA-200 software.  
Conditions as Fig. 4.5

#### 4.4.2.2 Evaluation of the performance of the GFAAS method for the analysis of lead in potable water

##### 4.4.2.2.1 Calibration Curve Linearity

A correlation coefficient of  $0.9996 \pm 1.5 \times 10^{-4}$  was obtained for a series of ten calibrations with an average intercept of 0.0007 absorbance units compared to absorbances in excess of 0.10 returned for a 10 ppb standard. A plot of Response Factor, which is ( signal-blank )/concentration plotted against concentration, against concentration also indicated a linear response over this concentration range.

##### 4.4.2.2.2 Accuracy

Tables 4.14(a) and 4.14(b) detail the percentage recoveries for ten 4 ppb samples and ten 8 ppb samples respectively.

Compiling these results gives an average recovery of 97.6 % (  $\pm$  sd = 10.4%) for the 4 ppb standards and 101.0 % (  $\pm$  sd = 1.73 %) for the 8 ppb standards.

Once again a statistical test, the t test was used to gauge the accuracy of the method for ten 8 ppb solutions. The value of t calculated from the data in Table 4.15 was 0.9699 which is smaller than the value of 2.26 taken from the tables at 95% confidence and 9 degrees of freedom. This shows that there is no bias inherent in the method.

Table 4.14(a): % Recoveries for “unknown” 4 ppb lead samples. All samples prepared as outlined in section 4.3.4 and analysed according to the parameters optimised in section 4.4.2.1.

Sample No.	[Pb] / ppb	% Recovery
4a	4.02	100.50
4b	3.95	98.75
4c	3.75	93.75
4d	3.79	94.75
4e	3.86	96.50
4f	3.81	95.25
4g	3.56	89.00
4h	5.01	125.25
4i	4.42	110.50
4j	3.99	99.75

Table 4.14(b): % Recoveries for “unknown” 8 ppb lead samples. All samples prepared as outlined in section 4.3.4 and analysed according to the parameters optimised in section 4.4.2.1.

Sample no.	[Pb] /ppb	% Recovery
8a	8.07	100.88
8b	7.94	99.25
8c	8.14	101.75
8d	8.23	102.88
8e	8.01	100.13
8f	8.24	103.00
8g	7.81	97.63
8h	8.03	100.38
8i	8.13	101.63
8j	8.22	102.75

Table 4.15 Concentrations returned for ten independent analyses of an 8 ppb lead standard. All samples prepared as outlined in section 4.3.4 and analysed according to the parameters optimised in section 4.4.2.1.

Determination no.	[Pb] / ppb
1	8.19
2	7.83
3	8.15
4	8.03
5	8.13
6	7.41
7	8.40
8	8.07
9	8.22
10	8.50

#### 4.4.2.2.3 Precision

##### 4.4.2.2.3(a) Intra-assay precision

The results obtained for ten independently prepared samples of the same lead concentration (8 ppb) which were analysed using the previously optimised method parameters are listed in Table 4.16.

The % RSD value of 1.701% (n = 10) for the absorbances returned falls within the acceptance criteria set out in the validation protocol (Appendix A).

Table 4.16 Response obtained for ten independently prepared 8 ppb standards. Samples prepared as outlined in section 4.3.4 and analysed according to the parameters optimised in section 4.4.2.1.

Sample no.	Absorbance
8a	0.1362
8b	0.1340
8c	0.1375
8d	0.1388
8e	0.1352
8f	0.1391
8g	0.1319
8h	0.1356
8i	0.1373
8j	0.1387

#### 4.4.2.2.3(b) Instrument precision

Table 4.17 lists the absorbances returned for 10 replicate analyses of an 8 ppb standard.

The % RSD value of 2.549 % ( $n = 10$ ) returned satisfies the acceptance criteria laid down in the validation protocol.

Table 4.17 Response obtained for repeat analysis of an 8 ppb standard solution. Samples prepared as outlined in section 4.3.4 and analysed according to the parameters optimised in section 4.4.2.1.

Sample no.	Absorbance
8a	0.1328
8b	0.1267
8c	0.1320
8d	0.1300
8e	0.1317
8f	0.1365
8g	0.1363
8h	0.1308
8i	0.1333
8j	0.1379

#### 4.4.2.2.4 LOD & LOQ

The Limit of Detection (LOD) and Limit of Quantitation (LOQ) were calculated from a regression method as outlined in Section 4.4.1.2.5 and values for LOD and LOQ were found to be 0.598 ppb and 1.993 ppb respectively.

Having optimised and validated these methods for the analysis of lead in potable water twenty water samples were taken from randomly selected domestic residences and analysed for lead content by each method. Comparison of the results obtained (Table 4.18) would serve as a further comparison of the methods.

On examining the results presented in Table 4.18 it can be seen that the lead concentrations returned by the two methods agree quite well although with some exceptions. It appears that the discrepancies between the methods are due to random errors. To confirm the absence of a systematic difference between the results returned by these methods ten replicate analyses of the same 8 ppb standard were carried out by each method and a paired t-test was carried out according to;

$$S_p = \sqrt{\frac{(n_1 - 1)s_1^2 + (n_2 - 1)s_2^2}{n_1 + n_2 - 2}}$$

$$t = \frac{|\bar{x}_1 - \bar{x}_2|}{s_p \sqrt{\frac{1}{n_1} + \frac{1}{n_2}}}$$

where,  $S_p$  = pooled standard deviation,  $n_1$  and  $n_2$  represent the number of determinations made by method 1 and method 2 respectively,  $s_1$  and  $s_2$  are the standard deviations of method 1 and method 2 respectively and  $\bar{x}_1$  and  $\bar{x}_2$  are the average value returned by methods 1 and 2 respectively.

The calculated value of t was 1.82 which is less than the tabulated value of 2.101 read at 95% confidence and  $n - 1$  degrees of freedom. This confirms the absence of a systematic difference between these methods.



Table 4.18 Results obtained for the analysis of lead in twenty randomly selected water samples by DPASV and GFAAS.

Sample no.	Lead Concentration / ppb	
	GFAAS	DPASV
1	3.29	5.50
2	2.36	2.38
3	3.09	
4	3.42	3.54
5	2.97	2.13
6	1.06	1.13
7	0.25	0.31
8	2.45	2.44
9	3.77	3.83
10	1.12	1.07
11	1.46	1.47
12	2.89	1.81
13	0.67	0.37
14	2.21	2.18
15	1.61	1.76
16	3.01	2.40
17	1.62	1.81
18	1.40	1.36
19	0.88	0.30
20	4.63	4.51

On comparing the results obtained for each method with the acceptance criteria laid down in the validation protocol it was found that each technique satisfied these criteria. Each of the two techniques is therefore suitable for the analysis of lead in potable water.

To determine which of these techniques was the most suitable for the routine analysis of lead in potable water would require a more detailed comparison of the results obtained. Table 4.19 contains the results obtained for each of the techniques under the headings listed in Section 4.4.

Table 4.19: Comparison of the performance of each method under the principle validation criteria.

	DPASV	GFAAS
Linearity	0.9995±3.2 x 10 <sup>-4</sup>	0.9996±1.5 x 10 <sup>-4</sup>
Accuracy (4ppb)	94.13%	97.64 %
Accuracy (8ppb)	96.37%	101.03 %
Intra-assay precision	4.07 % RSD	1.70 %
Instrument precision	1.50 % RSD	2.55 %
Specificity	Satisfactory	Satisfactory
Limit of Detection	0.113 ppb	0.598 ppb
Limit of Quantitation	0.375 ppb	1.993 ppb
Stability	Satisfactory	Satisfactory
Robustness	Satisfactory	Satisfactory

These results show that both techniques perform well under each of the principle validation criteria. GFAAS performing slightly better in terms of accuracy and intra-assay precision with DPASV having the upper hand in terms of LOD and LOQ and instrument precision.

It has been shown that a method for the analysis of lead in potable water based on differential pulse anodic stripping voltammetry performs well relative to the established method of graphite furnace atomic absorption spectroscopy under the principal validation criteria listed in Table 4.19. Both methods also satisfy the acceptance criteria laid down in the validation protocol drawn up for this system (Appendix A).

Being satisfied that the DPASV method can compete with the GFAAS method on the basis of analytical performance it is also necessary to consider some practical considerations.

#### **4.5 Practical considerations**

Possibly the most important of these considerations is cost. Metrohm have recently (1999) released a new system called the "757 Computrace" which they claim can achieve sub parts per billion limits of detection while costing only 30% of a GFAAS system and 10% of an ICP-MS system. They also point out that the running costs of their system are only a fraction of those for the spectroscopic techniques. Installation of the electrochemical system also has the advantage of not requiring any alterations to the infrastructure of the laboratory compared to the ventilation and gas delivery requirements of the spectroscopic methods.

Sample throughput is another important practical consideration. Both methods can be automated with autosamplers readily available on the market. The DPASV method validated here has an analysis time of 200 seconds compared to the 48 seconds of the GFAAS method. This allows for a larger sample throughput by the GFAAS method. At first it would appear that this gives the spectroscopic method a clear advantage, offering a sample throughput at least double that of the DPASV method. However the DPASV method has the ability to perform multi-element analysis; up to seven metals in a single sweep. Therefore if a single metal is to be analysed the graphite furnace

method offers the better sample throughput rate but for samples in which a number of metals are to be analysed the anodic stripping method offers superior sample throughput. In reality potable water samples are analysed for a number of metals including lead, copper, zinc, cadmium and mercury and it is therefore expected that the multi-element analysis capability of the anodic stripping method will in the majority of applications compensate for the long analysis time relative to the graphite furnace technique.

Stripping analysis also has the ability to determine the exact chemical nature of trace metals. This is important as knowledge of the chemical state of trace metals is important for understanding their transport, toxicity and reactivity in the environment. No such information can be obtained by spectroscopic methods.

The main limitation of stripping analysis is its restriction to about thirty metals and it therefore does not apply to as wide a range as spectroscopic techniques.

## **4.6 Conclusions**

A method for the analysis of lead in potable water based on anodic stripping voltammetry can compete favourably with the established method of graphite furnace atomic absorption spectroscopy under the principle validation criteria of calibration curve linearity, accuracy, precision, limit of detection, limit of quantitation and

specificity. The practical consideration of cost also makes the electrochemical technique an attractive alternative to the spectroscopic method for routine analysis of heavy metals in potable water. Sample throughput rates were much higher for the spectroscopic method in the study of lead analysis. However if multi-element analysis is to be carried out the sample throughput rate for the electrochemical method becomes superior to that of the spectroscopic method.

Recent advances in electrochemical instrumentation, particularly advances in automation have enabled anodic stripping voltammetry to compete with the established spectroscopic methods for routine analysis of heavy metals.

## 4.7 References

1. J. Wang, *Environ. Sci. Technol.*, **16**, 104A, (1982)
2. G.E. Bately, T.M. Florence, *Anal. Chem.*, **55**, 23, (1974)
3. NIOSH Manual of Analytical Methods, 2<sup>nd</sup> ed., D.G. Taylor (Ed.), Method no. P&CAM 191, U.S. Dept. of Health, Education & Welfare (DHEW), PHS/CDC/NIOSH, Cincinnati, OH., (1977).
4. NIOSH Manual of Analytical Methods, 3<sup>rd</sup> ed., P.M. Eller (Ed.), Method nos. 7082, 7105 and 7300. DHSS/PHS/CDC/NIOSH, Cincinnati, OH., 1984 (suppl. 1990).
5. C.W. Holmes, E.A. Slade, C.J. McLerran, *Environ. Sci. Technol.*, **8**, 255, (1974)
6. S.A. Acebal, A.L. Rebello, *Anal. Chim. Acta*, **148**, 71, (1983)
7. L.K. Hoeflich, R.J. Gale, M.L. Good, *Anal. Chem.*, **55**, 1591, (1983)
8. G. Gillian, *Talanta*, **29**, 651, (1982)
9. M.L. Abdullah, B. Reusch Berg, R. Klimek, *Anal. Chim. Acta.*, **84**, 307, (1980)
10. J. Wang, *Stripping Analysis: Principles, Instrumentation and Applications*, New York: VCH Publishers, pg 17, (1985)
11. J. Wang, *Stripping Analysis: Principles, Instrumentation and Applications*, New York: VCH Publishers, pg 22, (1985)
12. W. Fresenius, and I. Luderwald, *Environmental Research and Protection*, Springer Verlag, Berlin, p.67, (1984)
13. T.M. Florence, *J. Electroanal. Chem.*, **27**, 273, (1970)
14. R.A. Carrigan, T.C. Erwin, *Soil Sci. Soc. Amer.*, **15**, 145, (1951)
15. J. Wang, *Stripping Analysis: Principles, Instrumentation and Applications*, New York: VCH Publishers, pg. 31, (1985)
16. Varian-AA Application Note #AA-28 *Practical Operation with the GTA-95 Graphite Tube Atomiser*

## *Chapter 5*

### Determination of trace levels of lead and cadmium in seawater by DPASV and GFAAS

#### **5.1 Introduction**

Environmental pollution is becoming an increasingly important issue and receiving worldwide attention. There is a great need to monitor our living environment and protect it from further deterioration. Reliable analytical measurements of environmental samples are essential for sound decision making in issues relating to public health and improving the quality of the environment. One example is the need to monitor and control the levels of heavy metals in the seas and oceans. Heavy metals may be the most harmful pollutants because, unlike many other pollutants, they are not biodegradable and are retained in the ecosystem indefinitely.

Analysis of heavy metals content in seawater is most difficult because salinity interferes with spectrometry based on flame emission atomic absorption or graphite furnace methods. A matrix separation step is therefore required prior to analysis by graphite furnace atomic absorption spectrometry. Electrochemical methods have several advantages over graphite furnace atomic absorption for measuring heavy metals in seawaters. The instrumentation is less expensive, electrochemical techniques generally do not require a separate concentration step and the instrumentation is portable and can be adapted for shipboard use. But the question remains as to how these techniques compare under the analytical criteria of calibration curve linearity, accuracy and precision. Continuing the theme of the previous chapter, the aim of this work is to

compare a method for the analysis of lead and cadmium in seawater based on DPASV with one based on GFAAS.

## 5.2 Theory

The theoretical considerations outlined in the previous chapter are equally relevant to this study but have been omitted to avoid repetition. However the complex nature of the seawater matrix relative to potable water complicates the analysis and the following additional considerations must be taken into account.

The normal concentration of several trace elements in seawater is very low, near or slightly above the detection limit for graphite furnace atomic absorbance spectrometry. In addition, seawater has a very high dissolved salt content, approximately 3.5% salts of which the sodium chloride content is typically 80%. This matrix can cause substantial background absorbance and interfere with the analysis. Matrix modification and background correction are necessary to overcome these effects.

### 5.2.1 Matrix Modification

Sodium chloride is a stable compound and is difficult to remove during the ashing stage of the graphite furnace temperature ramp. Thus the salt remains in the graphite tube and is atomised during the atomisation stage resulting in a large background signal in the region of the analyte peak. Introduction of a chemical modifier such as ammonium oxalate dissociates the salt to form ammonium chloride and sodium oxalate, both of which are more volatile than the sodium chloride and can consequently be removed during ashing.



### 5.2.2 Background Correction

Formation of the atomic cloud can cause scatter of the resonance radiation by materials other than the analyte. This gives rise to false absorbance signals. Compensation for this false absorption is made by background correction.

Background correction is achieved by measuring the attenuation of both the resonance line and reference radiation as they traverse the atomiser. The reference radiation may be a continuum from a deuterium lamp, or Zeeman-shifted radiation from the atomic line. Attenuation of the resonance radiation intensity is attributed to both the analyte and the background, while the attenuation of the reference radiation is attributed only to the background. The correction for background absorption of the resonance line is obtained from the attenuation of the reference radiation at a wavelength very near the resonance line.

## 5.3 Experimental

The instruments and reagents used for the potable water study were also used for this work. Although repetitious the details have been listed below for clarity.

### 5.3.1 Instrumentation

An EG&G Model 394 Polarographic analyser and Model 303A SMDE were employed to control the electrochemical cell. A three electrode one compartment system was used where the reference was a saturated calomel electrode and the auxiliary was a

carbon rod. The working electrode consisted of a glassy carbon disk, 3mm in diameter embedded in a Teflon rod of diameter 10mm which was rotated by a Metrohm 628-10 system.

Spectroscopic determinations were carried out using a Varian SpectrAA-200 atomic absorption spectrometer with a GTA-96 graphite tube atomiser and autosampler. Background correction was achieved by means of a deuterium discharge lamp. Pyrolytically coated graphite furnace tubes were employed. The instruments were controlled and the data processed by a PC.

### 5.3.2 Reagents

Water which had been distilled by passing through a Buchi F210 distilling apparatus before deionising in an Elgastat UHQ deioniser was used throughout this work. 1000ppm lead and cadmium standards were supplied by Riedel-de-Haen and low lead nitric acid (<0.005ppm) supplied by BDH was used to acidify all solutions.

### 5.3.3 Labware selection and cleaning

Polypropylene(PP) volumetric flasks were used throughout this work. The use of glassware was avoided because of the possibility of metals being leached into solutions and PVC, MMA and PS being avoided because of the possibility of contamination from cadmium, copper, lead, tin and titanium [1]. These PP flasks were firstly degreased in a laboratory dish washer before acid washing with acidified (5%) distilled and deionised water. These flasks were then rinsed with distilled and deionised water before being inverted and allowed to dry. The electrochemical cells were of polyethylene and were also initially degreased in a laboratory dish washer. These cells were filled with 6M nitric acid and allowed to stand for at least one hour before rinsing thoroughly with distilled and deionised water prior to introduction of the first solution.

The cells and electrodes were rinsed thoroughly with distilled and deionised water between samples to avoid contamination.

#### 5.3.4 Sample preparation

Artificial seawater samples were prepared by dissolving 25g of NaCl (Aldrich), 3g of MgSO<sub>4</sub> (Merck) and 2g of CaSO<sub>4</sub> (Riedel-de-Haen) in 1000 cm<sup>3</sup> of distilled and deionised water. The pH of this solution was then adjusted to pH = 2 with low lead nitric acid.

Working standards of lead and cadmium were prepared by appropriate dilution of the 1000 ppm stock solutions with artificial seawater. A 100 ppm stock was prepared fresh weekly from which working standards were prepared daily.

The ammonium oxalate modifier solution was prepared by dissolving 2g of ammonium oxalate in 100 ml of distilled and deionised water.

A  $1 \times 10^{-2}$  M solution of Hg<sup>2+</sup> was prepared weekly by diluting 0.34262 grams of Hg(NO<sub>3</sub>)<sub>2</sub>·H<sub>2</sub>O (Lennox) to 100 cm<sup>3</sup> with artificial seawater solution.

#### 5.3.5 Solvent Extraction of heavy metals from artificial seawater

1.5g of ammonium pyrrolidine dithiocarbamate (Aldrich) was dissolved in 100 ml of distilled and deionised water and filtered through a Whatman 541 filter paper into a flask which was then sealed. 25 ml of this solution was then added to 500 ml of the artificial seawater sample with 150 ml of di-isobutylketone and shaken vigorously for three minutes in a separating funnel. This solution was allowed to stand for ten minutes to permit separation of the phases. The lower layer was then removed and the upper organic layer was discarded. This extraction was typically carried out five times per sample.

### 5.3.6 Disposal of waste lead and cadmium solutions

All waste solutions containing lead or cadmium were stored in 5 litre plastic containers. Sodium sulphide was then added in excess to these containers and a black precipitate of lead sulphide and cadmium sulphide was formed. These solutions were then filtered. The filtrate was found to be free of lead and cadmium contamination and was disposed of by flushing down the laboratory sink. The filter papers containing the lead and cadmium sulphides were sealed in plastic bags which were in turn sealed in a plastic sample bottle and disposed of in a landfill

## 5.4 Comparison of methods for the determination of lead and cadmium in seawater samples

The aim of this preliminary work was to compare a method for the analysis of lead and cadmium in sea water sample by DPASV with a method based on GFAAS. To allow a comprehensive comparison of the performance of these two methods they were first optimised. The performance of each method was then rigorously tested and assessed under the following headings:

- |                 |                           |
|-----------------|---------------------------|
| (1) Linearity   | (5) Limit of Detection    |
| (2) Accuracy    | (6) Limit of Quantitation |
| (3) Precision   | (7) Stability             |
| (4) Specificity | (8) Robustness            |

On completion of these studies the performance of the two methods under each of these headings will be compared.

Due to difficulties in obtaining natural seawater samples and the absence of a suitable UV digestion system it was necessary to carry out this study using artificial seawater samples prepared in the laboratory. These artificial seawater samples were prepared as outlined in section 5.3.4.

### 5.4.1 Optimisation of the analysis of lead and cadmium in sea water by DPASV

Initially the conditions for mercury film formation and sample analysis optimised during the potable water study were applied to the sea water samples. Unfortunately however these conditions proved inadequate giving noisy and irreproducible signals with the film degrading after only a small number of sweeps. On consulting the literature it was decided to adopt the 'in situ' method of film formation [2].

Earlier workers in this field such as Lund and Onshus [3] prepared in situ mercury film electrodes by spiking the seawater samples with  $2 \times 10^{-5}$ M mercury nitrate and holding the working electrode at  $-0.90$ V for 5 minutes. The result was a film which produced reproducible peak heights and resulted in good linear plots when standard additions were performed. However a fresh mercury film had to be deposited for each sample, with the electrode being cleaned and polished after each sample.

Originally this method was adopted and a study was carried out to determine if it was possible to reuse the mercury film electrode by transferring it to a fresh sample and performing a standard addition. As expected however it was not possible to obtain reproducible results in the second sample using this same film. Under these conditions sample analysis time was of the order of twenty minutes per sample assuming three standard additions. The time required between samples for the cleaning and polishing of the electrode must also be considered. An analysis time of twenty minutes may be acceptable when a large number of metals are to be analysed for simultaneously but it is unacceptable for the analysis of lead and cadmium.

A study of more recent work carried out on the determination of heavy metals by anodic stripping voltammetry revealed the work of Carra, Misiego and Zirino[2]. Instead of plating a mercury film by holding the electrode at a large negative potential these workers opted to apply a less negative potential typically  $-300$ mV versus SCE for a longer time (typically 15 minutes). The result was a mechanically stable film which could be transferred between samples and reused repeatedly.

#### 5.4.1.1 Optimisation of conditions for mercury film formation

100 ml aliquots of an artificial seawater sample, prepared as described in section 5.3.4 were made  $1 \times 10^{-4}$  M  $\text{Hg}^{2+}$  by adding 1 ml of a  $1 \times 10^{-2}$  M  $\text{Hg}^{2+}$  solution. Mercury films were plated on carbon at  $-300$  mV,  $-400$  mV and  $-500$  mV for 15 minutes. The response of each film was tested by spiking the sample with 5 ppb lead and cadmium and performing 10 replicate analyses. In each case the metals were preconcentrated at a potential of  $-1.0$  V vs SCE for 4 minutes.

The responses obtained at each film were acceptable with clearly visible peaks having good baseline separation as shown in Figure 5.1. A plating potential of  $-400$  mV was chosen as the optimum however as the peak current heights returned for lead and cadmium appeared to be most reproducible under these conditions (RSD = 1.8%). It must be noted that only very slight differences were observed in the responses produced by these films.

On reducing the plating time to 10 minutes and performing 10 replicate analyses of a sample spiked with 5 ppb lead and cadmium as above it was found that the reproducibility of the peak current heights deteriorated sharply after approximately seven sweeps. It was decided to retain the plating time of 15 minutes to yield a more stable film.

Due to the relatively long times required for the plating of a mercury film attempts were made to reuse the film by transferring it directly into a second sample on completion of the first analysis. Unfortunately however the electrode behaviour deteriorated rapidly on transferring between samples. For example in the analysis of a series of artificial seawater samples spiked with 2 ppb lead the percentage recovery for the first sample was 98.04%. On transferring the electrode to the second sample and performing an analysis by standard addition the percentage recovery fell to 83.33% and on analysis of a third sample with the same electrode the data returned yielded a standard addition plot with a correlation coefficient of 0.72.

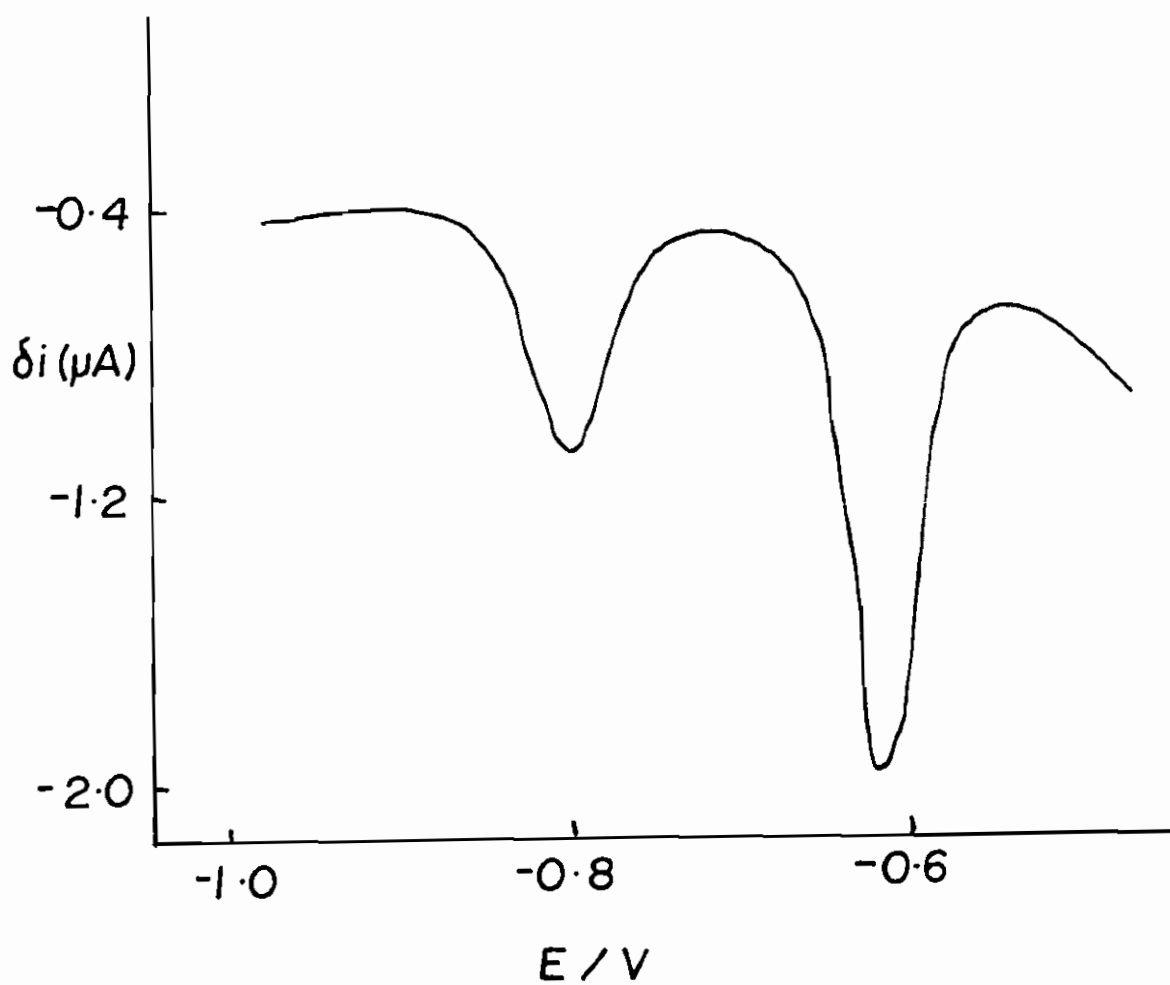


Fig. 5.1 Current response produced on applying a differential pulse anodic stripping cycle to a solution of artificial seawater spiked with 5 ppb lead and cadmium and made  $1 \times 10^{-4} \text{ M Hg}^{2+}$ . Artificial seawater prepared as outlined in Section 5.3.4, plating potential = -400 mV, plating time = 15 mins, initial stripping potential = -1.0V, final stripping potential = -0.40V. Lead and cadmium peaks occur at -0.58V and -0.86V respectively.

This sharp deterioration in performance is almost certainly due to deterioration of the mercury film caused by contact with the air and loss of potentiostatic control during transfer of the electrode between samples. The more probable reason is due to the presence of chloride. Metathesis may be an issue. It was decided to spike each sample with  $1 \times 10^{-4} \text{M Hg}^{2+}$  in an attempt to maintain the mercury film from sample to sample. On adopting this approach it was found that the film could be used for the analysis of up to six separate samples before electrode failure. However percentage recoveries deteriorated with each sample and will be discussed in Section 5.4.2.2.

#### 5.4.1.2 Optimisation of conditions for the preconcentration of lead and cadmium

Only a narrow range of potentials are available for the deposition of lead and cadmium as this potential must be more negative than  $-800 \text{ mV}$  and more positive than  $-1100 \text{ mV}$ . Cadmium is oxidised in this region of  $-800 \text{ mV}$  and hydrogen evolution can occur at potentials more negative than  $-1100 \text{ mV}$  producing bubbles at the electrode surface which destroy the mercury film. Taking these points into consideration a deposition potential of  $-1000 \text{ mV}$  was chosen.

A preconcentration time of four minutes was chosen for the initial investigations. The shortest possible time giving quantifiable peak current heights for both lead and cadmium is considered the optimum preconcentration time. It appears therefore that choosing relatively large standard additions of say  $10 \text{ ppb}$  would allow a significant decrease in the preconcentration times required. However it was decided to employ standard additions of  $2 \text{ ppb}$  because although this approach requires longer preconcentration times it yields a more accurate result as any errors contained in the experimental data are less exaggerated in the standard additions plot than those returned for the larger standard additions.

It was found that a preconcentration time of 180 seconds was sufficient to produce quantifiable signals for samples following a standard addition of  $2 \text{ ppb}$  lead and



cadmium. A preconcentration time of 180 seconds was therefore chosen as the optimum for this method.

A rest period of 10 seconds between the termination of electrode rotation and the commencement of the potential sweep was found to be sufficient and was therefore adopted for the final method.

As expected a combination of the maximum rotation rate of 3000 rpm and the maximum pulse amplitude of 100 mV resulted in the largest peak current heights obtainable for a number of solutions of differing lead and cadmium concentrations and were adopted as the optimum conditions for the method.

At this stage the method for the determination of lead and cadmium in seawater samples by DPASV had been optimised. The optimised parameters are listed in Figure 5.2.

Fig. 5.2 Optimised parameters for the determination of lead and cadmium in seawater by

#### DPASV

##### Mercury Film Formation

Mercury films were deposited by spiking the samples with  $1 \times 10^{-4}$  M  $\text{Hg}^{2+}$  and holding the electrode at  $-400\text{mV}$  for 15 minutes while the electrode was rotated at 3000 rpm.

##### Analysis of samples

Deposition potential	$E_{\text{dep}}$	$-1.0\text{V}$ vs SCE
Final potential	$E_f$	$-0.40\text{V}$ vs SCE
Deposition time	$t_{\text{dep}}$	180 secs.
Rest time	$t_{\text{rest}}$	10 secs
Scan rate	$v$	$10 \text{ mV sec}^{-1}$
Pulse amplitude	$\Delta E$	100 mV
Differential pulse		

waveform period	DPWP	0.50 secs.
Rotation rate	$\omega$	3000 rpm

Before proceeding to evaluate the performance of the method it was decided to investigate if the current response was affected by the presence of chloride in solution as it has been reported that thin mercury film deactivation can occur through the formation of  $\text{Hg}_2\text{Cl}_2$  by chloride in water samples.

100ml of a solution containing 50% of the chloride content of natural seawater was spiked with 10ppb lead and cadmium and three stripping cycles were carried out under the optimised conditions. When satisfied that the peak potentials were reproducible the chloride content was increased to 100% of that of natural seawater by adding 6.25ml of a 25% solution of sodium chloride and three stripping cycles were carried out. This procedure was repeated at chloride concentrations of 150% and 200% that of natural seawater and the results obtained are listed in Table 5.1.

Table 5.1 Effect of chloride concentration on peak potentials

% Cl <sup>-</sup>	Peak Potential ( $E_p$ )	
	Cadmium	Lead
50	-0.794	-0.604
100	-0.812	-0.612
150	-0.816	-0.616
200	-0.820	-0.620

There is a definite shift towards negative potentials with increasing chloride content. However this shift is unlikely to affect the resolution of the lead and cadmium peaks.

## 5.4.2 Evaluation of the performance of the DPASV method for the analysis of lead and cadmium in seawater.

### 5.4.2.1 Standard Addition Curve linearity

Correlation coefficients of  $0.999415 \pm 0.00077$  (n=13) and  $0.99685 \pm 0.002432$  (n=10) were returned for lead and cadmium respectively for a series of 13 standard addition analyses performed on artificial seawater samples. These standard addition analyses consisted of 3 separate additions of 2ppb lead and cadmium. However three of the analyses failed to yield data suitable for plotting a standard addition graph for cadmium. Also a number of the standard addition plots for cadmium yielded positive intercepts on the x-axis. Thus while levels of 1 ppb can be easily seen in potable water, the presence of high chloride concentrations prohibits such low concentrations to be easily seen in seawater by DPASV.

### 5.4.2.2 Accuracy

Adopting the approach of spiking each sample with  $1 \times 10^{-4}$  M  $\text{Hg}^{2+}$  the accuracy of the method was accessed by analysing six 100 ml aliquots of an artificial seawater sample which had been spiked with 1 ppb lead and cadmium.

The following percentage recoveries were returned for the analysis of six artificial seawater samples spiked with 1 ppb lead and cadmium using a single mercury film which was plated in the first sample.

Table 5.2 % Recoveries recorded for the analysis of artificial seawater samples spiked with 1 ppb lead and cadmium. Each sample was spiked with  $1 \times 10^{-4}$  M  $\text{Hg}^{2+}$ . Experimental conditions as outlined in Fig. 5.2

Sample No.	% Recovery:- Pb	% Recovery:- Cd
1	98.28	—
2	97.08	84.74
3	95.24	148.15
4	78.73	49.36
5	72.92	68.37
6	76.58	71.94

It is immediately obvious that the accuracy deteriorates with increasing use of the mercury film. On attempting to perform analysis on a seventh sample it was not possible to obtain an analytically useful signal. On visually inspecting the electrode it was clear that the mercury film has degraded. A percentage recovery could not be calculated for the cadmium content in sample 1 as the standard addition plot gave a positive intercept on the x-axis. It is immediately obvious that the percentage recoveries for lead are better than those for cadmium. Attempts to account for this fact will be made in a later section. Average percentage recoveries of  $86.638 \pm 9.413$  and  $84.64 \pm 37.615$  were recorded for lead and cadmium respectively.

#### 5.4.2.3 Precision

The precision study was carried out under two headings, instrument precision and intra-assay precision. To access instrument precision ten repeated measurements were

recorded on an artificial seawater sample containing 2 ppb lead and cadmium. The sample was spiked with  $1 \times 10^{-4}$  M  $\text{Hg}^{2+}$  and the mercury film deposited under the optimised conditions. Ten preconcentration and stripping cycles were then performed on the same sample and the peak current heights and peak potentials were recorded. Table 5.3 contains the results returned.

Table 5.3 Peak potentials and peak current heights returned for ten replicate analyses of an artificial seawater sample containing 2 ppb lead and cadmium. Conditions as outlined in section 5.4.1

Stripping Cycle	Pb		Cd	
	Peak Potential / V	Peak Current Height / $\mu\text{A}$	Peak Potential / V	Peak Current Height / $\mu\text{A}$
1	-0.616	4.394	-0.824	0.989
2	-0.616	4.448	-0.824	0.939
3	-0.616	4.411	-0.824	0.948
4	-0.612	4.564	-0.820	0.966
5	-0.612	4.552	-0.820	0.966
6	-0.612	4.571	-0.820	0.979
7	-0.612	4.534	-0.820	0.977
8	-0.608	4.693	-0.816	0.987
9	-0.608	4.696	-0.816	0.982
10	-0.608	4.640	-0.816	0.985

% RSD values of 2.37% and 1.75% were returned for lead and cadmium peak current heights respectively. Peak potentials varied only slightly and this can be explained by the small number of data points collected in the region of the peak maximum.

Intra-assay precision was assessed by analysing a series of six 100ml aliquots of an artificial seawater sample which had been spiked with 2 ppb lead and cadmium. Each aliquot was spiked with  $1 \times 10^{-4}$  M  $\text{Hg}^{2+}$ . The mercury film was plated in the first sample and was reused in the remaining five samples. A series of three standard additions of 2 ppb lead and cadmium was carried out on each sample and the results obtained are contained in Table 5.4.

Table 5.4 Results obtained for six independent analyses of a seawater sample containing 2ppb lead and cadmium.

Sample No.	Concentration of metal in sample / ppb	
	Lead	Cadmium
1	2.24	—
2	2.06	2.36
3	2.10	1.35
4	2.75	3.94
5	2.48	—
6	2.31	2.78

% RSD values of 11.10% and 41.11% were returned for lead (n = 6) and cadmium (n = 4) respectively. Cadmium concentrations in samples 1 and 5 could not be determined as the standard addition plots yielded positive intercepts on the x-axis. There appears to be a positive bias in the determination of the lead concentrations.

#### 5.4.2.4 Specificity

The specificity of the method was studied by plating a mercury film in a solution of artificial seawater containing 2 ppb of both lead and cadmium. A series of three preconcentration and stripping cycles were performed to ensure that the response was reproducible. A series of other metals likely to be present in natural seawater samples including copper, zinc, magnesium, chromium, iron and nickel were systematically added to this solution to give a final concentration of 10ppb. After each addition a preconcentration and stripping cycle was carried out and the response was compared to

that which was obtained before the addition of these metals. As expected no extra peaks appeared in the output as the formal potentials of these metals do not fall in the range of voltages over which the stripping cycle is recorded. Also no alterations in the positions or shapes of the lead and cadmium peaks was observed on addition of these metals. However a slight decrease was observed in the magnitude of the peak current heights of both lead and cadmium attributed to dilution of the samples on addition of aliquots of solutions.

#### 5.4.2.5 Limit of Detection and Limit of Quantitation

The LOD and LOQ were calculated by a regression method as outlined in Section 4.4.1.2.5. The LOD for lead was estimated as 0.34 ppb. Due to the poor linearity of the standard addition plots for cadmium it was not possible to arrive at a value for its LOD. It is expected that the LOD for lead could be lowered by employing a longer preconcentration time. A LOQ of 0.58 ppb was calculated for lead. A LOQ could not be calculated for cadmium.

#### 5.4.2.6 Stability

100 ppm stock solutions of lead and cadmium were prepared fresh weekly, dilutions only being carried out prior to analysis. The  $\text{Hg}^{2+}$  solution was found to be stable over a number of weeks.

#### 5.4.3 Optimisation of the analysis of lead and cadmium in seawater by GFAAS

Figure 5.3 and Figure 5.4 are the cookbook parameters for lead and cadmium determination by GFAAS respectively, as given by the SpectrAA-200 software. The initial conditions adopted for each method are based on these guidelines.

In the case of both metals all attempts were made to develop a method in which determinations could be made by wall atomisation, avoiding the need to employ pyrolytic platforms. Achieving this would greatly simplify the method and reduce the level of expertise and expense required for analysis. A method for the determination of cadmium was the first to be developed and optimised.



Figure 5.3 Cookbook for the determination of lead by GFAAS

<Pb> Atomic No. 82

Wavelength <nm>	Slit <nm>	Conc. <ug/l> for 0.2 Abs.	Lamp Intensity
283.3	0.5	27	100
217.0	1.0	14	20
261.4	0.5	1120	30

*PERFORMANCE DATA*

Maximum Ash Temperature	<°C>	600
Maximum Atomize Temperature	<°C>	2100

*RECOMMENDED CHEMICAL MODIFIERS*

Orthophosphoric acid <1000ug/mL>

Ammonum dihydrogen orthophosphate <5mg/mL>

EDTA, citrate, oxalate <0.5 – 1.0 % v/v>

Palladium solution <500 – 2000 ug/mL> plus  
reducing agent such as ascorbic acid

Figure 5.4 Cookbook for the determination of cadmium by GFAAS

<Cd> Atomic No. 48

Wavelength <nm>	Slit <nm>	Conc. <ug/l> for 0.2 Abs.	Lamp Intensity
228.8	0.5	1	40
326.1	0.5	400	100

*PERFORMANCE DATA*

Maximum Ash Temperature	<°C>	300
Maximum Atomize Temperature	<°C>	1800

*RECOMMENDED CHEMICAL MODIFIERS*

Orthophosphoric acid <500 - 2000ug/mL> plus  
reducing agent such as ascorbic acid

Monobasic Ammonium phosphate <5000 ug/mL>

The palladium chemical modifier permits the use of a higher ashing temperature. The monobasic ammonium phosphate modifier ensures a smooth peak shape and allows a maximum ashing temperature of 600°C.

#### 5.4.3.1 Optimisation of parameters for the determination of cadmium and lead in seawater by GFAAS

As stated earlier seawater has a very high dissolved solids content, about 3.5% salts of which the sodium chloride content is typically 80%. This matrix can cause substantial background and chemical interferences during analysis and must therefore be removed. Organic chemical modifiers such as ammonium oxalate have been used to reduce sodium chloride content background signals from seawater samples [4-6]. A literature survey revealed the work of Mc Kenzie and Doidge who on comparing seven matrix modifiers found that ammonium oxalate was the most efficient in reducing background signals from seawater samples [6]. Based on this work it was decided to adopt ammonium oxalate as the modifier of choice for this study. Preparation of this modifier solution is outlined in Section 5.3.4.

The Varian SpectrAA instrument offers two means of introducing the matrix modifier into the graphite tube. The modifier can either be co-injected or pre-injected. The co-inject option involves premixing the sample and modifier solutions in the autosampler capillary and introducing the total volume in a single injection. The pre-inject option involves two separate injections per sample. The required volume of modifier solution is injected first followed by a separate injection of the sample. Both approaches were investigated and the co-inject option was found to be the more effective in reducing the background signal. This option also has the advantage of requiring less time per sample.

On comparing Figures 5.5 and 5.6 the effectiveness of the modifier is obvious. The background signal (b) is almost completely removed, note the difference in absorbance scales between the two figures.

Being satisfied that effective matrix reduction had been achieved it was decided to proceed with the optimisation of the methods. Due to the complex nature of the sample matrix these methods were based on standard addition.

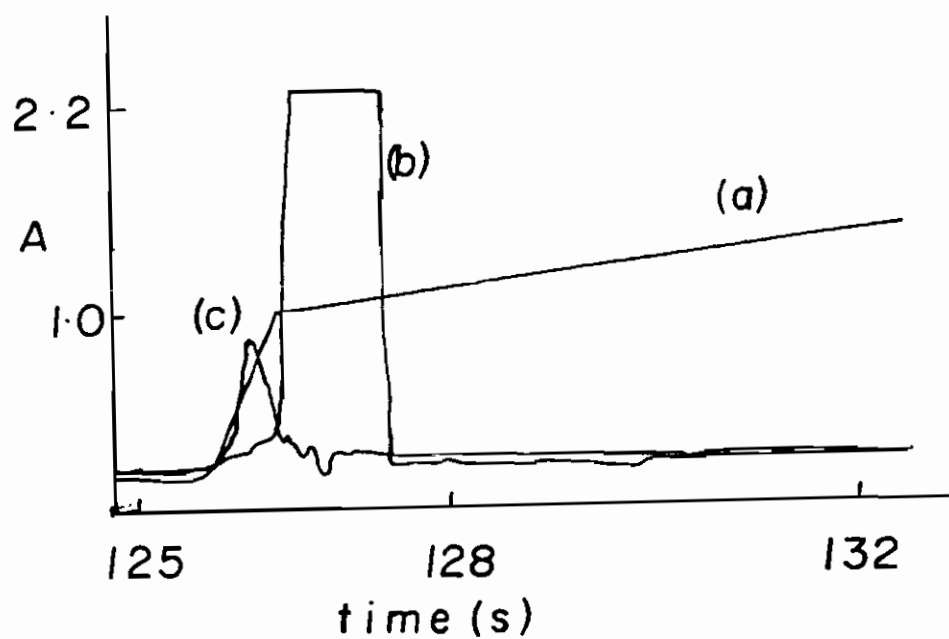


Fig.5.5 SpectrAA results display showing (a) temperature ramp, (b) background signal and (c) analyte signal for a 20 $\mu$ l injection of a 30 ppb cadmium standard in the absence of matrix modifier. Conditions as laid down in Fig. 5.4.

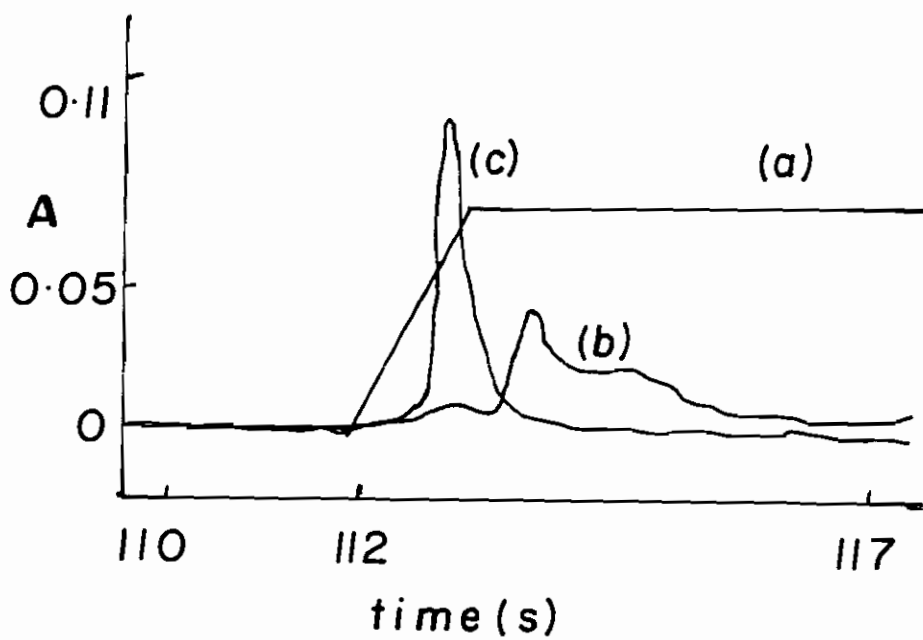


Fig. 5.6 SpectrAA results display showing (a) temperature ramp, (b) background signal and (c) analyte signal for a 20 $\mu$ l injection of a 6 ppb lead standard in the presence of 15 $\mu$ l of ammonium oxalate matrix modifier prepared as outlined in Section 5.3.4. Conditions as laid down in Fig. 5.3.

The temperature programs suggested by the SpectrAA software were adopted initially. Each individual stage of these programs could then be optimised to arrive at the final temperature programme. An artificial seawater sample prepared as outlined in section 5.3.4 was prepared and spiked with 2 ppb lead and cadmium. Three successive standard additions of 2 ppb were carried out for both lead and cadmium to test the performance of the method under these initial conditions. Very poor results were obtained yielding nonlinear standard addition plots, unacceptably large %RSD ( $> 2.5\%$ ) values and in some instances negative absorbances were returned following a standard addition.

Attempts to improve the performance of both methods included optimising the drying and ashing stages of the temperature programs to further reduce the background signal, adding a burnoff and cooldown stage to the temperature ramps to improve precision and varying the concentration of metal in the standard additions. Unfortunately however the methods still failed to produce linear standard addition plots although precision was improved (1 – 2.5 %RSD).

Examining the method in detail revealed that the source of the problem was not the instrument or temperature program employed but in the reagents used. Although AnalaR grade salts with low metal content were used for the preparation of the artificial seawater samples it was found that levels of lead and cadmium in this solution were significantly higher than those in the standard addition solutions which were diluted from 1000 ppm stock solutions with distilled and deionised water.

Taking the case of lead, the sodium chloride, magnesium sulphate and calcium sulphate salts used for the preparation of the blank solution contained lead at 0.0002%, 0.0002% and 0.0005% respectively. Although these levels of contamination may seem negligible they result in a total lead concentration of 66 ppb for a blank solution prepared as outlined in Section 5.3.4. The ammonium oxalate used to prepare the modifier solution was also contaminated by lead at 0.0001%, however as equal volumes of modifier solution are co-injected with the blank and sample solutions the resulting contributions to the absorbances cancel each other out.

Consider three standard additions of 2 ppb lead to a solution of artificial seawater. On injection of the “blank” solution the SpectrAA software records an absorbance signal equivalent to 66 ppb of lead. Following the first standard addition an absorbance signal equivalent to 68 ppb lead is recorded. Ideally the instrument could then determine the signal due to the 2 ppb standard addition by subtraction. For this to be possible the detector must be capable of accurately detecting an increase of approximately 3% in the background signal. Assuming the detection system is suitably sensitive to achieve this the poor precision would still cause problems. %RSD values between replicates were in the range 1% - 2.5%.

Consider three replicate injections of a blank artificial seawater solution (contaminated with 66 ppb lead) with a %RSD of 2.0% followed by three replicate injections of a 2 ppb standard addition (RSD = 2%). The absorbance of the blank is equivalent to a lead concentration in the range  $66 \text{ ppb} \pm 2 \%$  i.e. 64.68 – 67.32 ppb. The signal recorded on injection of the 2 ppb standard addition is  $68 \text{ ppb} \pm 2 \%$  i.e 66.64 – 69.36 ppb. Note the overlap in the concentrations ranges. This overlap explains the occurrence of negative absorbance signals on addition of standard addition solutions.

In an attempt to overcome this problem attempts were made to reduce the lead contamination of the blank by solvent extraction. The procedure adopted is outlined in Section 5.3.5. Although a reduction of almost 20% in the absorbance for lead in the blank solution was achieved it remained impossible to achieve linear calibration plots or improved precision.

## 5.6 References

1. Van Loon, J.C., in *Selected Methods of Trace Metal Analysis in Biological and Environmental Samples*, John Wiley & Sons, New York, (1985).
2. Garcia-Monco Carra, R., Sanchez-Misiego, A., Zirino, A., *Anal. Chem.*, **67**, 24, 1995.
3. Lund, W., Onshus, D., *Anal. Chim. Acta*, **86**, 109, 1976.
4. Guevemont, R. in *Organic Matrix Modifiers for Direct Graphite Furnace Atomic Adsorption Spectrophotometry*, paper 252, Pittsburgh conference on Analytical Chemistry and Applied Spectroscopy, March 9 – 13, (1981).
5. Mc Kenzie, T.N., Routh, M.W. in *A Mechanistic Approach Towards Matrix Modification in Electrothermal Atomic Absorption Spectrophotometry*, Paper 298, F.A.C.S.S. Conference, September, (1982)
6. Parker, C.R. in *Water Analysis by Atomic Absorption Spectroscopy*, Varian Techtron, (1972).



## *Appendix A*

### **Validation Protocol**

Standards/solutions must be prepared as outlined in section 4.3.4. and analysed according to the conditions optimised in sections 4.4.1.1. and 4.4.2.1. The tests must be performed according to the following procedures.

#### Calibration Curve Linearity

A series of ten calibrations in the concentration range 2 – 10 ppb lead will be carried out on independently prepared standards over a two week period. Response factors will also be calculated and a series of graphs of response factor against concentration will be plotted.

Acceptance criteria: A correlation coefficient of  $> 0.999$  for both plots and a near zero slope for the response factors vs concentration plot. The intercept on the calibration plot must be  $< 2\%$  of the instrument response for a 10 ppb lead standard.

## Accuracy

The accuracy of the method will be examined by preparing 20 solutions of known lead concentrations which will be analysed under the optimised method parameters. Also ten independent analyses of a single 8 ppb standard will be performed.

Acceptance criteria: The measured value must be within  $\pm 25\%$  of the true value at least 95% of the time [NIOSH accuracy criterion]. Also on carrying out a t-test the value of t calculated according to the following equation will be less than the tabulated value with (n-1) degrees of freedom and 95% confidence.

$$t = \frac{|\bar{X} - \beta| \sqrt{N}}{s}$$

where,  $\bar{X}$  = mean value of concentration returned,  $\beta$  = true value of concentration,  $N$  = number of solutions analysed,  $s$  = standard deviation of the concentration values returned.

## Precision

The method precision will be assessed under two headings;

- (1) Intra-assay precision
- (2) Instrument precision

To assess the intra-assay precision of the method ten samples of the same lead concentration (8 ppb) will be independently prepared and analysed using the optimised method parameters.

Instrument precision will be studied by performing replicate analyses of a sample known to contain 8 ppb lead using the optimised method parameters.

Acceptance criteria: %RSD values < 5%

## Specificity

Specificity will be studied by preparing a 10 ppb lead standard. This sample will be introduced into the cell and analysed in triplicate to ensure that the response is reproducible. This sample will then be spiked with a range of metals which are to be found in real potable water samples. Table 1 lists these metals and their final concentrations in the 10 ppb lead standard.

Acceptance criteria: Lead analyte peak remains completely resolved from and unaltered by the presence of the other metals listed in Table 1.

Table I Concentrations of metals to be added to a 10 ppb lead solution during the specificity study.

Metal	Conc. in test soln./ppb
Iron	200
Zinc	5000
Tin	1000
Copper	3000

## LOD & LOQ

The Limit of Detection (LOD) and Limit of Quantitation (LOQ) will be calculated using a regression method as follows;

Five lead standards of concentrations 2, 4, 6, 8, 10 ppb will be analysed and a graph of peak current height vs concentration will be plotted in Excel. Being satisfied that this plot meets the acceptable linearity criteria discussed above the "Data Analysis" function in Excel will be used to determine exact values for the intercept and standard error about the regression line. Taking the intercept to represent the part of the total

signal that is due to the blank ( $S_b$ ) and the standard error about the regression line to represent the standard deviation of the blank measurements ( $\sigma$ ) the LOD and LOQ will be determined from the following;

$$\text{LOD} = S_b + 3\sigma$$

$$\text{LOQ} = S_b + 10\sigma$$

This procedure will be repeated at least ten times and average values for the LOD and LOQ will be calculated.

Acceptance criteria: A LOQ less than 1 ppb for lead.

## Stability

In addition to the above acceptance criteria it is important that the sample solutions be stored in such a way that they are stable over the time period expected to elapse between sample collection and analysis. The stability of both the standard and mercury nitrate solutions must also be determined.

Acceptance criteria: Sample solutions stable over a period of at least two weeks and standard solutions stable for at least 24 hours. Mercury nitrate solution stable for at least 1 hour.

## Robustness

The robustness of the method i.e. the affect of small changes in instrument parameters or operating conditions on the response must also be assessed. Any changes resulting in a failure of the method to meet any one of the acceptance criteria must be noted and precautions taken to avoid those circumstances from arising.